

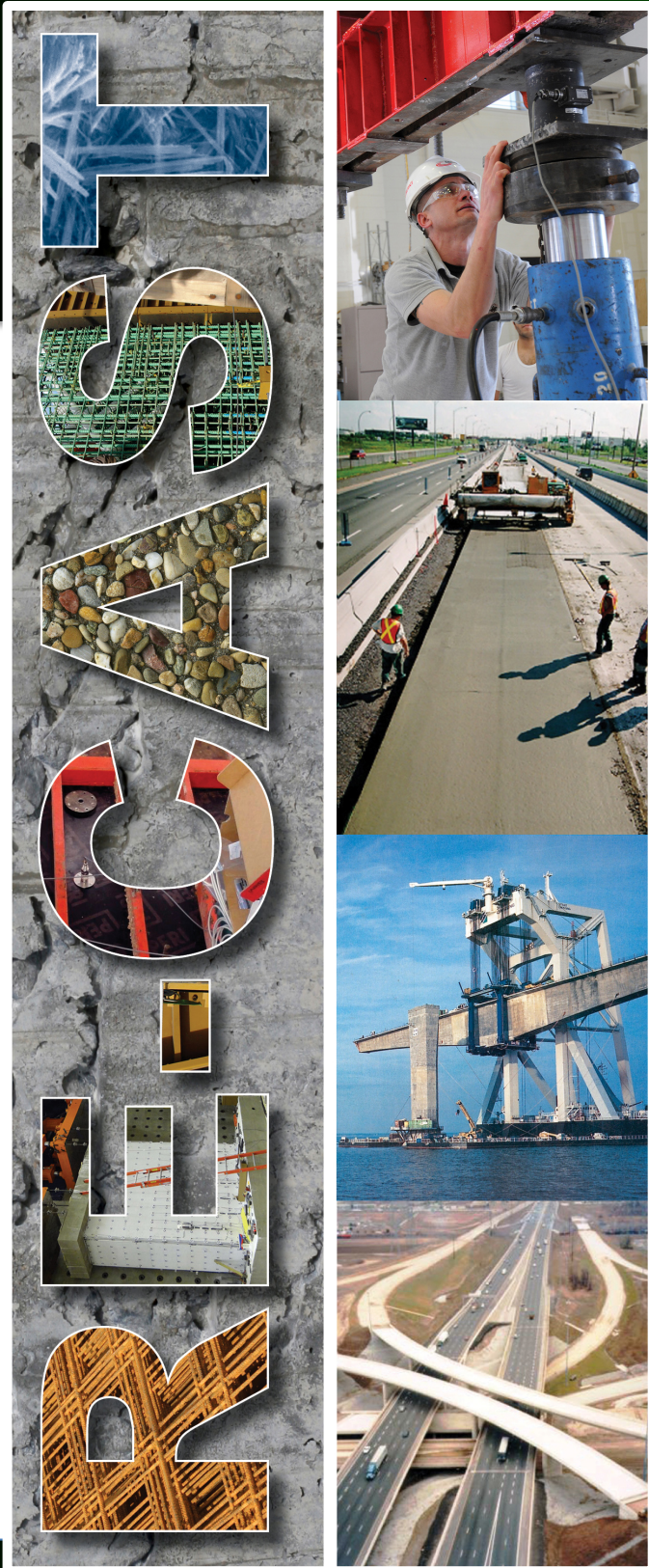
FINAL PROJECT REPORT # 00046732

GRANT: DTRT13-G-UTC45
Project Period: 6/1/2014 – 12/31/2019

Volume I: Performance of Fiber-Reinforced Self-Consolidating Concrete for Repair of Bridge Sub-Structures and Fiber Reinforced Super Workable Concrete for Infrastructure Construction

Participating Consortium Member:
Missouri University of Science and Technology
Polytechnic Institute of New York University
Rutgers, The State University of New Jersey
University of Oklahoma

Authors:
Kamal H. Khayat, Ph.D., P.Eng.
Ahmed Abdelrazik, Ph.D. Candidate



RE-CAST:
REsearch on Concrete Applications for
Sustainable Transportation
Tier 1 University Transportation Center



DISCLAIMER

The contents of this report reflect the views of the authors, who are responsible for the facts and the accuracy of the information presented herein. This document is disseminated under the sponsorship of the U.S. Department of Transportation's University Transportation Centers Program, in the interest of information exchange. The U.S. Government assumes no liability for the contents or use thereof.

TECHNICAL REPORT DOCUMENTATION PAGE

1. Report No. RECAST UTC # 00046732	2. Government Accession No.	3. Recipient's Catalog No.
4. Title and Subtitle Volume I: Performance of Fiber-Reinforced Self-Consolidating Concrete for Repair of Bridge Sub-Structures and Fiber Reinforced Super Workable Concrete for Infrastructure Construction	5. Report Date January 2020	6. Performing Organization Code:
	8. Performing Organization Report No. Project # 00046732	
7. Author(s) Kamal H. Khayat and Ahmed Abdelrazik	10. Work Unit No.	
9. Performing Organization Name and Address RE-CAST – Missouri University of Science and Technology 500 W. 16 th St., 223 ERL Rolla, MO 65409-0710	11. Contract or Grant No. USDOT: DTRT13-G-UTC45	
	13. Type of Report and Period Covered: Final Report Period: 6/1/2014 – 12/31/2019	
12. Sponsoring Agency Name and Address Office of the Assistant Secretary for Research and Technology U.S. Department of Transportation 1200 New Jersey Avenue, SE Washington, DC 20590	14. Sponsoring Agency Code:	
	15. Supplementary Notes The investigation was conducted in cooperation with the U. S. Department of Transportation.	
16. Abstract <p>The proposed research investigates the combined use of self-consolidating concrete (SCC) and fibers reinforcements to develop a novel repair material, fiber-reinforced self-consolidating concrete (FR-SCC) that can be used for the rehabilitation and strengthening of existing structures. Furthermore, the feasibility of using super workable concrete (SWC) reinforced with different types of fibers for new structural cast-in-place applications is investigated. The use of SCC matrix can greatly enhance the workability of fibrous mixtures along with incorporation of greater volume of fibers.</p> <p>SWC is a new type of flowable concrete with lower workability than SCC. Containing lower binder content can be more cost effective than SCC. SWC requires some mechanical consolidation energy to ensure proper filling of the formwork. Eight types of fibers, including a propylene synthetic fiber, five steel fibers and a hybrid steel and polypropylene synthetic fiber were investigated. Fibers were incorporated at a volume of 0.5% in FR-SCC and at 0.5% and 0.75% in FR-SWC. Two types of expansive agents (EA), Type G and Type K, were added to both concrete types to reduce shrinkage and enhance resistance to restrained shrinkage cracking. The optimized mixtures exhibited high workability, mechanical properties, and freeze/thaw durability. The incorporation of fibers with 4% Type-G EA in FR-SCC increased the 56-day flexural strength by up to 32%, and flexural toughness up to 23 times. The incorporation of 0.5% of the 1.18 in. (30-mm) hooked end steel fibers (ST1) in FR-SCC made with 4% Type-G EA increased the elapsed time to cracking determined from restrained shrinkage ring test from 16 to 20 days compared to FR-SCC made with 0.5% ST1 fibers without EA. The use of ST1 steel fibers and 4% Type-G EA decreased the 1-year drying shrinkage by 48% compared to the reference SCC mixture without any fibers and expansive agent. In case of FR-SWC, the decrease in shrinkage was 37% compared to SWC.</p> <p>In addition, 20 monolithic full-scale beams were cast using different types of concrete, including conventional vibrated concrete (CVC), fiber-reinforced conventional vibrated concrete (FR-CVC), SCC, FR-SCC, SWC and FR-SWC. Twelve reinforced concrete beams were cast using CVC to fill two thirds of the beam height. They were then filled with five different types of FR-SCC and SCC to simulate beam repair in the tension zone. Findings indicated that macro fibers can be used with FR-SCC designated for repair with fiber length ≤ 2 in. (50 mm) up to 0.5% fiber volume. Macro fibers can be used with FR-SWC designated for construction with fiber length ≤ 2.6 in. (65 mm) up to 0.75% fiber volume. Fibers had great impact on structural performance of the full-scale monolithic beams. The incorporation of 0.5% of the 1.18 in. (30-mm) hooked end steel fibers combined with 0.5 in. (13-mm) straight steel fibers at ratio 4 to 1 (STST) with 4% Type-G EA increased toughness of FR-SWC beams by 95% compared to SWC beams and by 86% in case of 0.75% 5D fibers. Repair using FR-SCC increased the flexural capacity of the beam by 6% and the toughness by 110% in case of using 0.5% ST1 fibers with 4% Type-G EA.</p>		
17. Key Words Bridge substructures; Bridge superstructures; Fiber reinforced concrete; Infrastructure; Maintenance; Performance based specifications; Self describing data. Crack resistance, Expansive agent, Fiber reinforced concrete, Flexural behavior, Macro fibers, Micro fibers, Repair, Super workable concrete.	18. Distribution Statement No restrictions. This document is available to the public.	
19. Security Classification (of this report) Unclassified	20. Security Classification (of this page) Unclassified	21. No of Pages 197



**Performance of Fiber-Reinforced Self-Consolidating
Concrete for Repair of Bridge Sub-Structures and
Fiber-Reinforced Super-Workable Concrete for
Infrastructure Construction**

Final Report

Principal Investigator (PI): Dr. Kamal H. Khayat, Ph.D., P.Eng.

Student: Ahmed Abdelrazik, PhD Candidate

ABSTRACT

The proposed research investigates the combined use of self-consolidating concrete (SCC) and fibers reinforcements to develop a novel repair material, fiber-reinforced self-consolidating concrete (FR-SCC) that can be used for the rehabilitation and strengthening of existing structures. Furthermore, the feasibility of using super workable concrete (SWC) reinforced with different types of fibers for new structural cast-in-place applications is investigated. The use of SCC matrix can greatly enhance the workability of fibrous mixtures along with incorporation of greater volume of fibers.

SWC is a new type of flowable concrete with lower workability than SCC. Containing lower binder content can be more cost effective than SCC. SWC requires some mechanical consolidation energy to ensure proper filling of the formwork. Eight types of fibers, including a propylene synthetic fiber, five steel fibers and a hybrid steel and polypropylene synthetic fiber were investigated. Fibers were incorporated at a volume of 0.5% in FR-SCC and at 0.5% and 0.75% in FR-SWC. Two types of expansive agents (EA), Type G and Type K, were added to both concrete types to reduce shrinkage and enhance resistance to restrained shrinkage cracking. The optimized mixtures exhibited high workability, mechanical properties, and freeze/thaw durability. The incorporation of fibers with 4% Type-G EA in FR-SCC increased the 56-day flexural strength by up to 32%, and flexural toughness up to 23 times. The incorporation of 0.5% of the 1.18 in. (30-mm) hooked end steel fibers (ST1) in FR-SCC made with 4% Type-G EA increased the elapsed time to cracking determined from restrained shrinkage ring test from 16 to 20 days compared to FR-SCC made with 0.5% ST1 fibers without EA. The use of ST1 steel

fibers and 4% Type-G EA decreased the 1-year drying shrinkage by 48% compared to the reference SCC mixture without any fibers and expansive agent. In case of FR-SWC, the decrease in shrinkage was 37% compared to SWC.

In addition, 20 monolithic full-scale beams were cast using different types of concrete, including conventional vibrated concrete (CVC), fiber-reinforced conventional vibrated concrete (FR-CVC), SCC, FR-SCC, SWC and FR-SWC. Twelve reinforced concrete beams were cast using CVC to fill two thirds of the beam height. They were then filled with five different types of FR-SCC and SCC to simulate beam repair in the tension zone. Findings indicated that macro fibers can be used with FR-SCC designated for repair with fiber length ≤ 2 in. (50 mm) up to 0.5% fiber volume. Macro fibers can be used with FR-SWC designated for construction with fiber length ≤ 2.6 in. (65 mm) up to 0.75% fiber volume. Fibers had great impact on structural performance of the full-scale monolithic beams. The incorporation of 0.5% of the 1.18 in. (30-mm) hooked end steel fibers combined with 0.5 in. (13-mm) straight steel fibers at ratio 4 to 1 (STST) with 4% Type-G EA increased toughness of FR-SWC beams by 95% compared to SWC beams and by 86% in case of 0.75% 5D fibers. Repair using FR-SCC increased the flexural capacity of the beam by 6% and the toughness by 110% in case of using 0.5% ST1 fibers with 4% Type-G EA.

Keywords:

Crack resistance, Expansive agent, Fiber reinforced concrete, Flexural behavior, Macro fibers, Micro fibers, Repair.

ACKNOWLEDGEMENT

The authors would like to acknowledge individuals and organizations that made this research project possible. First and foremost, the authors would like to acknowledge the financial support of the Missouri Department of Transportation (MoDOT) and the RE-CAST (REsearch on Concrete Applications for Sustainable Transportation) Tier-1 University Transportation Center (UTC) at Missouri University of Science and Technology (Missouri S&T).

The authors would like to thank the companies that provided materials required for the successful completion of this project, including BASF, Bekaert Corp, Euclid Chemical, LafargeHolcim, Pro-Perma Engineered Coatings, LLC, and Propex Concrete Systems Corp.

The cooperation and support from Ms. Abigayle Sherman and Ms Gayle Spitzmiller of the Center for Infrastructure Engineering Studies (CIES) is greatly acknowledged, as well as the assistance of Dr. Soo-Duck Hwang, Lead Scientist, and Mr. Jason Cox, Senior Research Specialist at the CIES. Valuable technical support provided by technical staff of the Department of Civil, Architectural and Environmental Engineering at Missouri S&T is deeply appreciated, Mr. Brian Swift, Mr. John Bullock, and Mr. Gary Abbott.

EXECUTIVE SUMMARY

The workability requirements for successful placement of self-consolidating concrete (SCC) necessitate that the concrete exhibits excellent deformability and proper stability to flow under its own weight through closely spaced reinforcement without segregation and blockage. The proposed research investigates the combined use of self-consolidating concrete (SCC) and fibers reinforcements to develop a novel repair materials, fiber-reinforced self-consolidating concrete (FR-SCC) that can be used for the rehabilitation and strengthening of existing structures. Furthermore, the feasibility of using super workable concrete (SWC) reinforced with different types of fibers for new structural cast-in-place applications is investigated. The use of SCC matrix can greatly enhance the workability of fibrous mixtures and incorporate greater volume of fibers.

SWC is a new type of flowable concrete with lower workability than SCC. The use of lower binder content can be more cost effective. SWC requires some mechanical consolidation during placement to ensure proper filling of the formwork. SWC is characterized by high workability in terms of filling ability, passing ability and stability; however the workability requirements are less stringent than those for SCC which can allow greater addition of fibers in fiber-reinforced super workable concrete (FR-SWC).

In this study, eight types of fibers were investigated including:

- Propylene synthetic fiber (PLP),
- Four types of hooked steel fiber (ST1), (3D), (4D), and (5D)
- Carbon fiber (CA)
- A hybrid of crimped steel fiber and polypropylene multifilament fiber (STPL)

- Micro-macro steel fibers (STST)

Fibers were incorporated at fiber volumes of 0.5% in FR-SCC and at 0.5% and 0.75% in FR-SWC. All of the investigated mixtures were tested initially for slump flow and visual stability index. Further investigation of fresh properties, mechanical properties and crack resistance were performed for selected mixtures with adequate workability. Table 1 summarizes the fresh properties of the optimized FR-SCC and FR-SWC mixtures. Table 2 reports the mechanical properties and drying shrinkage characteristics of the optimized mixtures. Table 3 presents the characteristics of the selected fibers that are referred to in Tables 1 and 2.

Table 1. Fresh properties of optimized FR-SCC and FR-SWC mixtures

Mixture	Fiber type	V _f (%)	Unit weight (pcf)	Air (%)	Slump flow (in.) 10 min / 60 min	Modified J-Ring D/a	VSI	Surface Settlement (%)	Bleeding (%)
FR-SCC 1	ST1	0.5	134.1	8	26 / 20.5	13.5	0	0.35	0.3
FR-SCC 2	STST	0.5	133.8	8	27.5 / 21	15	0	0.34	0.41
FR-SWC 1	5D	0.5	139.7	8.5	20 / 6.5	14.8	0	0.13	0
FR-SWC 2	STST	0.5	141.6	7.5	21.5 / 9	15	0	0.39	0

The overall performance evaluation using a star diagram approach was used to consider key fresh and mechanical properties and crack resistance characteristics. Mixtures that showed the highest overall performance were selected to undergo further evaluation in terms of drying shrinkage, restrained shrinkage using ring test, and freeze/thaw durability. The restrained shrinkage test was carried out to evaluate the resistance to restrained shrinkage of FR-SCC in accordance with ASTM C1581. Figure 1 shows the average strain developed in the inner steel rings for the plain SCC and three optimized

FR-SCC mixtures. Sudden drop in the compressive strain in steel ring indicates the cracking of the concrete ring.

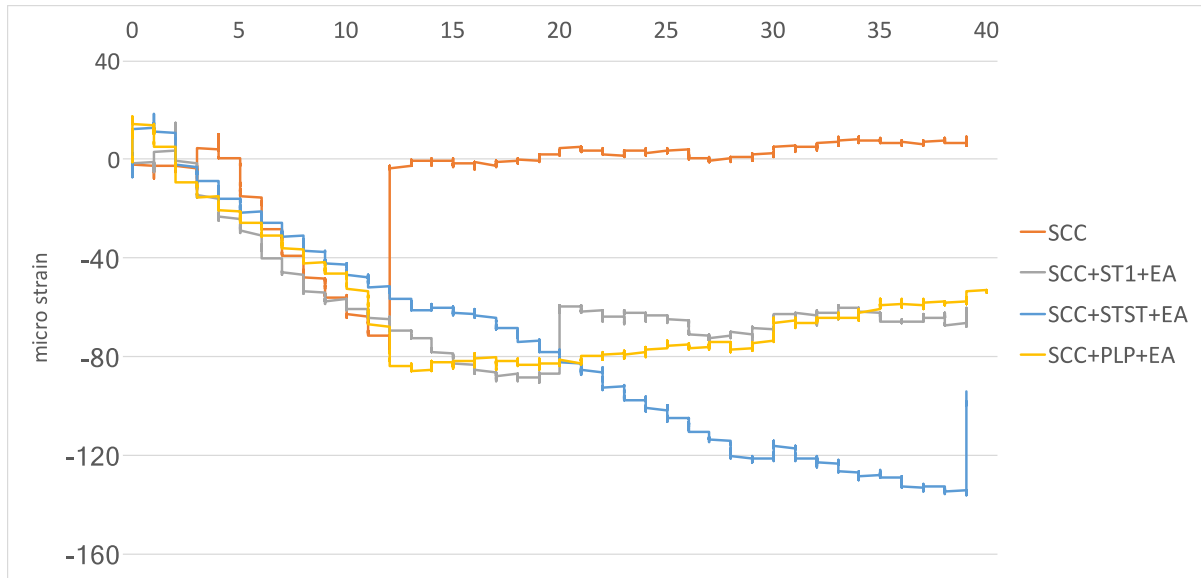
Table 2. Mechanical properties of optimized FR-SCC and FR-SWC mixtures

Mixture		FR-SCC 1	FR-SCC 2	FR-SWC 1	FR-SWC 2
Fiber Type		ST1	STST	5D	STST
V _f (%)		0.5	0.5	0.5	0.5
Compressive strength (psi)	28 days	4,560	5,090	6,060	6,050
	56 days	4,780	5,900	7,250	7,170
Splitting tensile strength (psi)	28 days	420	490	740	620
	56 days	465	570	775	690
Flexural strength (psi)	28 days	680	610	703	785
	56 days	730	670	755	840
Toughness (lb.in.)	28 days	110	95	110	130
	56 days	115	110	115	140
First crack stress (psi)	28 days	460	535	1,390	910
	56 days	490	560	1,500	980
Residual stress (psi)	28 days	325	350	930	680
	56 days	350	385	1,000	735
Elastic modulus (ksi)	28-day	3,860	3,810	3,770	4,150
	56-day	4,070	4,130	4,140	4,200
Drying shrinkage (<i>ustrain</i>)	120-day	310	400	460	450

Table 3. Characteristics of the selected fibers

	ST1	STST		5D
Material	Macro Steel	80% Macro Steel	20% Micro Steel	Macro Steel
Shape ⁽¹⁾	Hook 	Hook + 	Straight 	Hook 
Specific gravity	7.85	7.85	7.85	7.85
Length (in.)	1.18	1.18	0.51	2.36
Equivalent diameter (in.)	0.022	0.022	0.008	0.036
Aspect Ratio	80	80	65	65
Tensile strength (ksi)	160-190	160-190	160-190	170

⁽¹⁾ Figures not to scale



Mixture	Time to cracking (days)	Potential for cracking
No fibers	12.5	Moderate-high
ST1 + EA	20	Moderate-low
STST + EA	40	Low
PLP + EA	14.5	Moderate-high

Figure 1. Strain in steel ring for SCC and FR-SCC with different types of fibers (ASTM C1581)

Based on the obtained results from mechanical properties and shrinkage behavior of FR-SCC and FR-SWC, the main findings are summarized as follows:

- The incorporation of fibers with 4% Type-G EA in FR-SCC increased the 56-day flexural strength by up to 32%, and flexural toughness up to 23 times.
- The incorporation of fibers without EA in FR-SCC increased 56-day flexural strength by up to 45% and flexural toughness by up to 24 times.
- The incorporation of 0.5% STST fibers in FR-SCC with 4% Type-G EA increased the restrained shrinkage resistance (FR-SCC rings cracked after 40 days) compared to the reference SCC without any fibers and EA (SCC rings cracked after 12 days).

- The incorporation of fibers with 4% Type-G EA in FR-SWC increased 56-day flexural strength by up to 114% and flexural toughness by up to 30 times.
- Fibers decreased the elastic modulus of FR-SCC. The decrease in case of syntactic fibers was higher than that with steel fibers, where PLP fibers decreased the 56-day elastic modulus by 23%, while the decrease was by 11% in case of steel fibers.
- FR-SWC made with 3D, 4D, and STPL fibers decreased the 56-day elastic modulus by 25%, 25%, and 3%, respectively, while ST1, STST and 5D increased the 56-day elastic modulus, where STST fibers increased the elastic modulus by 4% and 16% at fiber volumes of 0.5% and 0.75%, respectively.
- The incorporation of 0.5% of the 1.18 in. (30-mm) hooked end steel fibers (ST1) in FR-SCC made with 4% Type-G EA increased the elapsed time to cracking determined from restrained shrinkage ring test from 16 to 20 days compared to FR-SCC made with 0.5% ST1 fibers without EA.
- Addition of (ST1) steel fibers in FR-SCC with 4% Type-G EA decreased 1-year shrinkage by 48% compared to the reference SCC. However this improvement was 23% for FR-SCC without EA.
- . The use of ST1 steel fibers and 4% Type-G EA decreased the 1-year drying shrinkage by 48% compared to the reference SCC mixture without any fibers and expansive agent. In case of FR-SWC, the decrease in shrinkage was 37% compared to SWC.

In total, 20 monolithic full-scale beams were cast using CVC, FR-CVC, SCC, FR-SCC, SWC and FR-SWC. For repair evaluation, twelve reinforced concrete beams were cast using CVC to the two thirds then repaired with five different types of FR-SCC and one type of SCC. Figure 2 shows the repair technique followed to simulate repair of CVC beams with FR-SCC. Figure 3 shows load-deflection curve for CVC beams that were repaired using the two optimized FR-SCC mixtures. Figure 4 shows load-deflection curve for beams cast monolithically using two optimized FR-SWC mixtures and SWC without fibers.

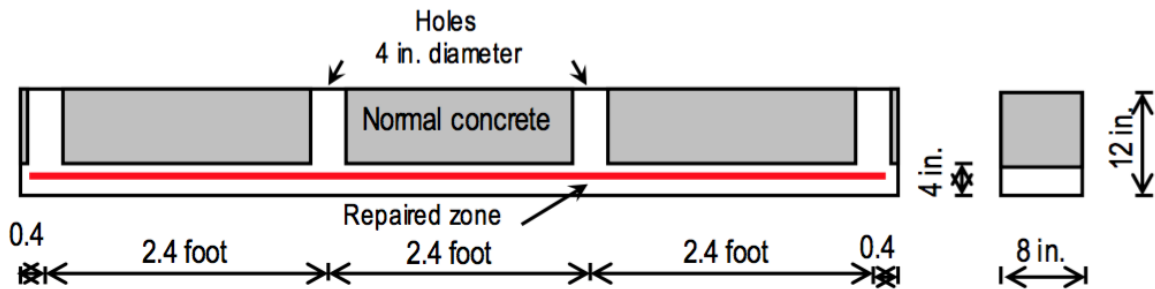


Figure 2. Repair technique of CVC beams using FR-SCC

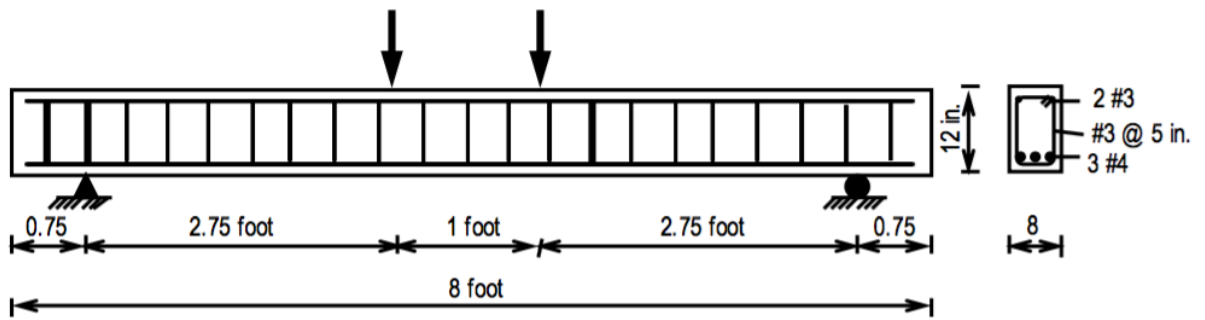
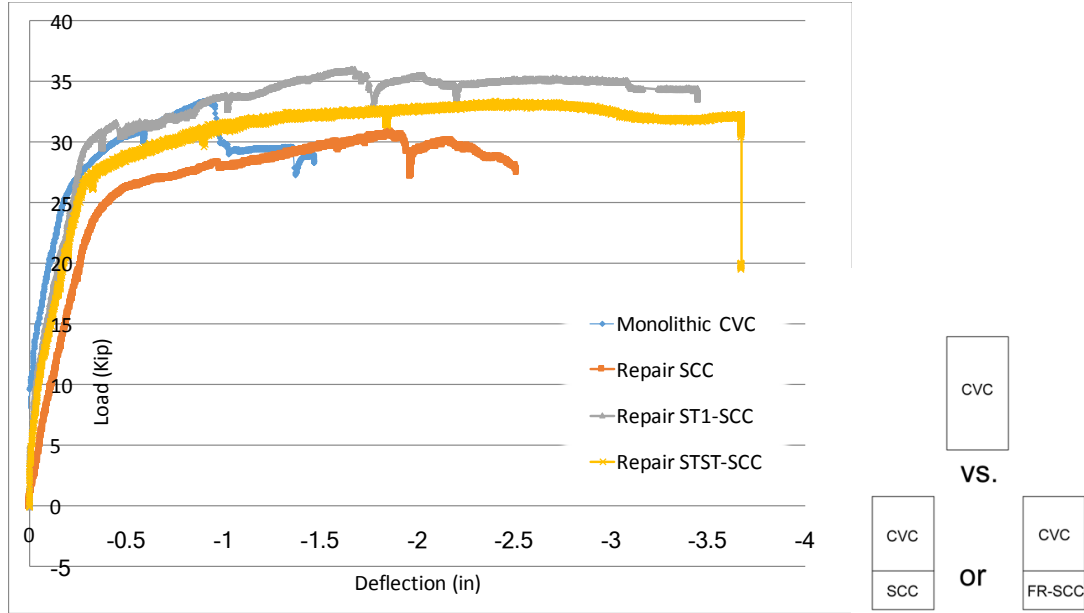


Figure 3. Load-deflection curve for CVC beams repaired using FR-SCC mixtures

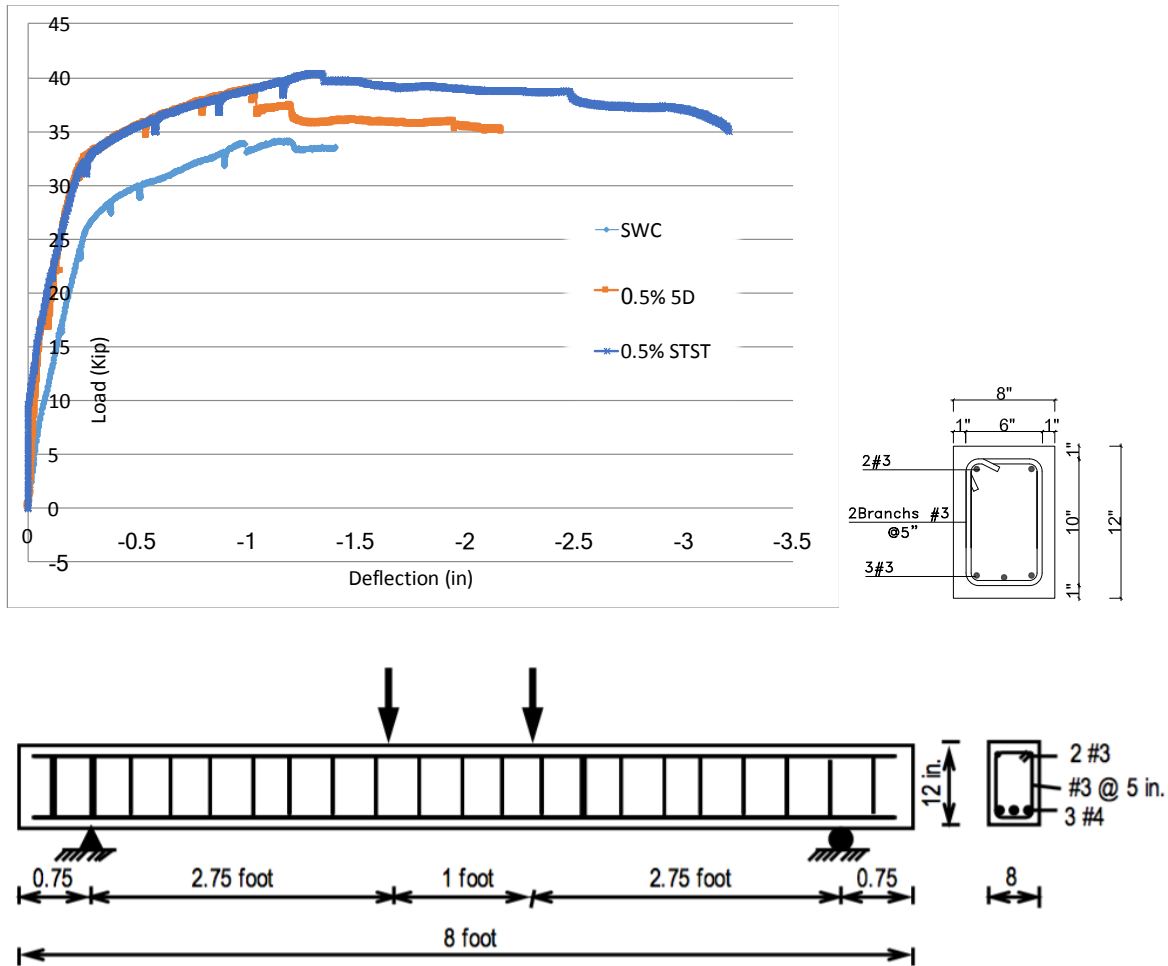


Figure 4. Load-deflection curve for FR-SWC beams

The findings from the structural performance evaluation can be summarized as follows:

- Macro fibers can be successfully used with FR-SCC designated for repair with fiber length ≤ 2 in. (50 mm) up to 0.5% fiber volume.
- Macro fibers can be successfully employed with FR-SWC designated for construction with fiber length ≤ 2.6 in. (65 mm) up to 0.75% fiber volume.
- Fibers had great impact on structural performance of the full-scale monolithic beams. The 0.5% STST with 4% Type-G EA FR-SWC mixture had 95% greater

toughness compared to SWC beams and by 86% greater toughness in case of 0.75% 5D fibers.

- The incorporation of 0.5% ST1 fibers with 4% Type-G EA increased toughness of FR-SCC beams by 90% compared to SCC beams and by 110% in case of 0.5% STST fibers.
- Repair of concrete beams using the optimized FR-SCC increased the flexural capacity of the composite concrete beam by 6% and the toughness by 110% in the case of repairing with 0.5% ST1 fibers and 4% Type-G EA.
- The repair of the beams using FR-SCC made with 0.5% ST1 fibers without EA was shown to restore 90% of the original CVC beam capacity and increased toughness by 22%.
- Repair of the beams using plain SCC was able to restore 88% of the original CVC flexural capacity and increased the toughness by 21%.

Table of Contents

ABSTRACT	iii
ACKNOWLEDGEMENT	v
EXECUTIVE SUMMARY.....	vi
1 Introduction.....	12
1.1 Project Objective	12
2 Literature review	17
2.1 General	17
2.2 Materials used for fiber-reinforced self-consolidated concrete.....	18
2.2.1 <i>Aggregates</i>	18
2.2.2 <i>Binders</i>	21
2.2.3 <i>Fibers</i>	27
2.2.4 <i>Admixtures</i>	28
2.3 Mixture proportioning of fiber-reinforced self-consolidated concrete.....	29
2.3.1 <i>Mixture proportioning of self-consolidated concrete</i>	29
2.3.2 <i>Mixture proportioning of fiber-reinforced self-consolidated concrete</i>	33
2.4 Test Methods and fresh performance of fiber-reinforced self-consolidated concrete	40
2.5 Fiber dispersion and orientation monitoring in fiber-reinforced self-consolidated concrete	50
2.6 Rheology of fiber-reinforced self-consolidated concrete	57

2.7	Mechanical properties of fiber-reinforced self-consolidated concrete	61
2.8	Shrinkage of fiber-reinforced self-consolidated concrete	65
2.8.1	<i>Drying Shrinkage</i>	67
2.9	Freeze-thaw durability of fiber-reinforced self-consolidated concrete	79
2.10	Structural performance of fiber-reinforced self-consolidated concrete structural elements	83
2.10.1	<i>Flexural performance of fiber-reinforced concrete beams</i>	84
2.10.2	<i>Flexural crack resistance of fiber-reinforced concrete beams</i>	86
2.10.3	<i>Repairing of concrete beams using fiber-reinforced self-consolidated concrete</i> ..	90
3	Experimental Program	96
3.1	Materials	96
3.1.1	<i>Binders</i>	96
3.1.2	<i>Chemical admixtures</i>	97
3.1.3	<i>Aggregates</i>	97
3.1.4	<i>Fibers</i>	98
3.2	Mixture proportioning	99
3.2.1	<i>Procedure for mixture proportioning design of FR-SCC</i>	100
3.2.2	<i>Mixing Procedure for FR-SCC and FR-SWC</i>	104
3.3	Experimental program	104
3.3.1	<i>Fresh properties and rheology</i>	110
3.3.2	<i>Mechanical properties and flexural crack resistance</i>	111
3.3.3	<i>Shrinkage</i>	114
3.3.4	<i>Freeze-thaw durability</i>	115

4	Test Results and Discussion	117
4.1	Test results of Task 2A	117
4.1.1	<i>Fresh properties</i>	118
4.1.2	<i>Mechanical properties</i>	120
4.2	Test results of Task 2B and Task 2C	124
4.2.1	<i>Fresh properties</i>	125
4.3	Mechanical properties	130
4.3.1	<i>Toughness</i>	132
4.3.2	<i>Crack resistance</i>	134
4.3.3	<i>Elastic modulus</i>	136
4.3.4	<i>Overall performance</i>	138
4.4	Test results of Task 2D	144
4.4.1	<i>Shrinkage</i>	144
4.4.2	<i>Freeze/thaw Durability</i>	147
5	Structural Performance	148
5.1	Beam design	149
5.2	Preparation of beams and instrumentation	150
5.3	Casting, sampling and curing of monolithic beams	152
5.4	Casting, sampling and curing of repaired beams	154
5.4.1	<i>Casting of substrate</i>	155
5.4.2	<i>Preparation of the intermediate surface, de-molding and curing of substrate</i>	156
5.4.3	<i>Casting of the repair</i>	156
5.5	Testing of the beams	158

5.6 Experimental program 159

 5.6.1 Task 3A: Monolithic beam flexural tests for SCC, FR-SCC, SWC and FR- SWC..... 159

5.7 Results and discussion..... 161

 5.7.1 Task 3A: Monolithic beams 161

 5.7.2 Task 3A: Monolithic beams 165

6 Conclusions..... 169

References 174

List of Figures

<i>Figure 2-1: Chemical Shrinkage at different ages [13].....</i>	<i>22</i>
<i>Figure 2-2: Compressive strength of SCC made with high contents of fly ash (FA) and slag (SL) [17]</i>	<i>23</i>
<i>Figure 2-3: Influence of FA content on compressive strength [18].....</i>	<i>24</i>
<i>Figure 2-4: Influence of FA content on absorption [18].....</i>	<i>25</i>
<i>Figure 2-5: Influence of FA on shrinkage [18].....</i>	<i>25</i>
<i>Figure 2-6: Shrinkage versus FA content at 56 days curing [18]</i>	<i>26</i>
<i>Figure 2-7: Different types of steel fibers; macro straight, crimped, 3D-hookedend, 4D-hookedend, 5D-hookedend and micro straight fibers (from left to right).....</i>	<i>27</i>
<i>Figure 2-8: Different types of syntactic fibers; polypropylene micro, polypropylene macro, polypropylene macro strand, nylon micro, poly (from left to right)</i>	<i>28</i>
<i>Figure 2-9: Schematic explanation of multi-aspect concept: (a) void content as result of maximum packing of gravel and fibers (without matrix); (b) distinction between matrix enveloping fibers and gravel matrix filling voids; and (c) model assumption and thickness of matrix layer covering fibers and gravel.....</i>	<i>34</i>
<i>Figure 2-10: Relationship between fiber factor and thickness of covering mortar before adjustment of mixture proportions (before fixation of t_{cm}).</i>	<i>36</i>
<i>Figure 2-11: Relative reduction of coarse aggregate versus increase in fiber factor to maintain initial t_{cm} of SCC mixture.....</i>	<i>37</i>
<i>Figure 2-12: Model lines for flow viscosity ratio of experimental data and aggregate spacing d_{ss} (average diameter $d_{av}=4.673$ mm) [24].....</i>	<i>39</i>
<i>Figure 2-13: Trade-off between fluidity and stability of concrete [25].....</i>	<i>42</i>
<i>Figure 2-14: V-Funnel test used to evaluate flowability through restricted section [26].....</i>	<i>43</i>
<i>Figure 2-15: Schematic of the filling capacity apparatus [26].....</i>	<i>43</i>
<i>Figure 2-16: Diagram of parameters for calculation of J-ring (Δh) value proposed by: (a) Reference [27]; and (b) modified method (Equation (26)) [28].....</i>	<i>46</i>

Figure 2-17: Slump flow variation versus fiber factor ^[28] 47

Figure 2-18: Variation in V-funnel flow time with fiber factor ^[28] 48

Figure 2-19: Variation of blocking ratio of modified L-box (one bar) with fiber factor ^[28] 49

Figure 2-20: Modified J-ring flow (ring with six or eight bars) versus fiber factor ^[28] 49

Figure 2-21: Diameter-height ratio (D/a) at center of modified J-ring test versus fiber factor ^[28] 50

Figure 2-22: X-ray pictures of cores from precast pre-stressed roof elements [29] 51

Figure 2-23: Typical Nyquist plot for plain paste and fiberreinforced composites with frequency markers (log of frequency in Hz as darkened points). [30] 53

Figure 2-24: View of the measurement device and the four-electrode arrangement 54

Figure 2-25: Experimental setup and a model configuration with flanged open-ended coaxial probe [33] 55

Figure 2-26: Layout of the magnetic probe 56

Figure 2-27: Three different orthogonal slices through a reconstructed FRC specimen from a CT-scan and 3D reconstruction of the steel fibers only [36] 56

Figure 2-28: Different fibers tested [37] 59

Figure 2-29: Properties of the fibers tested [37] 60

Figure 2-30: Consistency of a cement paste (water to cement ratio 0.4) mixed with fibers with various aspect ratios. (a) $\phi_{fr}/\alpha_m=0.18$; (b) $\phi_{fr}/\alpha_m=0.83$; (c) $\phi_{fr}/\alpha_m=1$ [37] 60

Figure 2-31: Relative yield stress as a function of the total relative packing fraction. The dashed line corresponds to the theoretical random loose packing. [37] 60

Figure 2-32: Slump flow diameter as function of fibers content ^[38] 62

Figure 2-33: Variation of blocking ratio with increasing the percentages of steel fibers ^[38] 63

Figure 2-34: Increase in residual strength with increase in fiber factor for different fiber types ^[38] 65

Figure 2-35: Divergence between predicted and modified shrinkage (MO-S 0.3% mixture) ^[44] 72

Figure 2-36: Predicted vs. measured shrinkage values determined using various models before and after modifications of the drying shrinkage models ^[44] 72

Figure 2-37: Shrinkage prediction of FR-SCC mixtures using the seven modified models ^[44] 73

Figure 2-38: Development of strains in the inner ring due to concrete contraction ^[51] 75

Figure 2-39: Time for cracking of the investigated mixtures ^[51] 75

Figure 2-40: Crack width as function of time-to-cracking for fiber-reinforced mixtures ^[51] 76

Figure 2-41: Age of first crack for all tested materials as difference with respect to plain concrete
(cracking age for plain concrete = 15 days) ^[21] 77

Figure 2-42: Maximum crack width for all tested materials relative to plain concrete (crack width for
plain concrete = 100%) ^[21] 79

Figure 2-43: Design mix and batching procedure 81

Figure 2-44: Pulse velocity for all concrete types 81

Figure 2-45: Technical properties of steel, polypropylene and glass fibers 82

Figure 2-46: Durability factors determined after freeze-thaw cycles 83

Figure 2-49: Amorphous metallic fibers used and the main characteristics ^[55] 84

Figure 2-48: Design parameters of the specimen beams ^[56] 86

Figure 2-49: Ultimate flexural capacity versus steel fiber volume dosage ^[56] 86

Figure 2-50: Four-point bending test 88

Figure 2-51: Average load-crack opening curves of the self-compacting concretes 89

Figure 2-52: Average load-deflection curves of self-compacting concretes 89

Figure 2-53: Average load-deflection curves – comparison between vibrated and self-compacting
concretes 90

Figure 2-54: 1—Schematic of composite beam specimen. (Note: Dimensions in mm; 1 mm = 0.039 in.) 91

Figure 2-55: Roughened surface of base concrete before casting repair materials 92

Figure 2-56: Beam dimensions (in mm). 93

Figure 2-57: Loading and strain-control systems (dimensions in mm) 93

Figure 2-58: Load-deflection response of control beam with: (a) beams repaired with SCC and mono- and multifilament polypropylene FR-SCC; and (b) beams repaired with hybrid and steel FR-SCC, and steel FR-SCM. 94

Figure 3-1: Testing fresh properties..... 110

Figure 3-2: Rheological properties measurement..... 111

Figure 3-3: Mechanical properties testing 112

Figure 3-4: Test setup for flexural performance of FR-SCC and FR-SWC beams..... 113

Figure 3-5: RILEM TC 162-TDF Test setup for testing Crack resistance for FR-SCC and FR-SWC (dimensions in mm) 114

Figure 4-1: Flow diameters for FR-SCC after 10 and 70 mins..... 119

Figure 4-2: Compressive strength and splitting tensile strengths of FR-SCC mixtures having 30% fly ash and different types and dosage rates of expansive agents 122

Figure 4-3: Compressive strength and splitting tensile strengths of FR-SCC mixtures having 30% fly ash and different types and dosage rates of expansive agents 123

Figure 4-4: Effect of the fiber factor on the passing ability of FR-SCC..... 127

Figure 4-5: Effect of the fiber factor on the passing ability of FR-SWC..... 127

Figure 4-6: Effect of the fiber factor on the HRWRA demand of FR-SCC..... 128

Figure 4-7: Effect of the fiber factor on the HRWRA demand of FR-SWC 128

Figure 4-8: Effect of the fiber factor on the yield stress of FR-SCC..... 129

Figure 4-9: Effect of the fiber factor on the yield stress of FR-SWC..... 129

Figure 4-10: 56-day flexural strength and flexural toughness for SCCs and FR-SCCs..... 133

Figure 4-11: 56-day flexural strength and flexural toughness for FR-SWC (left $V_f=0.5\%$, right $V_f=0.75\%$) 134

Figure 4-12: 56-day flexural crack resistance for different SCCs and FR-SCCs..... 135

Figure 4-13: 56-day flexural crack resistance for SWC and FR-SWCs..... 136

Figure 4-14: Load vs. strain for a cylinder specimen of FR-SCC..... 137

Figure 4-15: 28-day and 56-day elastic modulus for SCC and FR-SCCs 137

Figure 4-16: 28-day and 56-day elastic modulus for SWC and FR-SWCs..... 138

Figure 4-17: Star diagrams for all the SCC and FR-SCC mixtures..... 140

Figure 4-18: Area inside the star diagram for all the SCC and FR-SCC mixtures..... 141

Figure 4-19: Star diagrams for SWC and FR-SWC mixtures..... 142

Figure 4-20: Area inside the star diagram for SWC and FR-SWC mixtures..... 143

Figure 4-21: Drying shrinkage of FR-SCC and FR-SWC..... 145

Figure 4-22: Strain in steel ring for SCC and FR-SCC with or without EA..... 146

Figure 4-23: Strain in steel steel ring for SCC and FR-SCC with different types of fibers..... 146

Figure 4-24: Relative dynamic modulus of elasticity for SCC, SWC, FR-SCC and FR-SWC 147

Figure 5-1: Typical configuration of reinforcement 149

Figure 5-2: Tying rebar cages..... 151

Figure 5-3: Attaching of the strain gages to steel rebar 151

Figure 5-4: Concrete surface attached strain gages..... 152

Figure 5-5: LVDT to monitor deflection of the beam..... 152

Figure 5-6: Curing of the beams and cylinder specimens using wet burlaps..... 153

Figure 5-7: Casting points vs. supporting and loading points for repaired beams..... 154

Figure 5-8: PVC holes 155

Figure 5-9: Substrate casting (of the 2/3 upper beam height) in inverted position 155

Figure 5-10: Spraying the substrate with set retardant 156

Figure 5-11: Repairing of CVC Beams using FR-SCC..... 157

Figure 5-12: Testing of monolithic beams 158

Figure 5-13: Testing of Repaired beams..... 158

Figure 5-14: Loading points and supporting points 159

Figure 5-15: Effect of different fibers on SCC monolithic beams..... 162

Figure 5-16: Effect of different fibers on SWC monolithic beams..... 163

Figure 5-17: Effect of adding fibers to CVC, SWC and SCC monolithic beams 164

Figure 5-18: Strain in steel rebar vs. strain in concrete for SCC and FR-SCC..... 165

Figure 5-19: Repaired beam after loading up to failure 166

Figure 5-20: Monolithic CVC, monolithic FR-SCC and repaired beam using FR 167

Figure 5-21: Monolithic CVC beam vs. repaired CVC beam using SCC and different FR-SCCs..... 168

List of Tables

<i>Table 2-1: Original shrinkage models ^[44].....</i>	<i>71</i>
<i>Table 2-2: Dimensions of tested fibers and WWF.....</i>	<i>77</i>
<i>Table 3-1: Physical and chemical characteristics of cementitious materials and expansive agents.....</i>	<i>96</i>
<i>Table 3-2: Characteristics of chemical admixtures.....</i>	<i>97</i>
<i>Table 3-3: Characteristics of fibers.....</i>	<i>98</i>
<i>Table 3-4: Mixture proportions for the optimized SCC and FR-SCC.....</i>	<i>102</i>
<i>Table 3-5: Mixture proportions for the optimized SWC and FR-SWC.....</i>	<i>103</i>
<i>Table 3-6: Test parameters used to optimize FR-SCC and FR-SWC mixtures for Task 2A.....</i>	<i>105</i>
<i>Table 3-7: Mixture matrix for Task 2B.....</i>	<i>106</i>
<i>Table 3-8: Proposed concrete test methods.....</i>	<i>109</i>
<i>Table 3-9: Workability requirements for FR-SCC and FR-SWC.....</i>	<i>111</i>
<i>Table 4-1: Test parameters used to optimize FR-SCC and FR-SWC mixtures for Task 2A.....</i>	<i>117</i>
<i>Table 4-2: Fresh properties for SCC and FR-SCC.....</i>	<i>118</i>
<i>Table 4-3: Fresh properties for SWC and FR-SWC.....</i>	<i>119</i>
<i>Table 4-4: Mechanical properties for SCC and FR-SCC.....</i>	<i>120</i>
<i>Table 4-5: Mechanical properties for SWC and FR-SWC.....</i>	<i>121</i>
<i>Table 4-6: Workability requirements for FR-SCC and FR-SWC.....</i>	<i>125</i>
<i>Table 4-7: Fresh properties of SCC and FR-SCC mixtures.....</i>	<i>125</i>
<i>Table 4-8: Fresh properties of SWC and FR-SWC mixtures.....</i>	<i>126</i>
<i>Table 4-9: Hardened properties of FR-SCC.....</i>	<i>131</i>
<i>Table 4-10: Hardened properties of FR-SWC.....</i>	<i>132</i>
<i>Table 5-1: Mixture matrix for testing monolithic beams.....</i>	<i>160</i>
<i>Table 5-2: Mixture matrix for testing repaired beams.....</i>	<i>161</i>

1 Introduction

1.1 Project Objective

The purpose of the study was to investigate key engineering and structural properties of FR-SCC and fiber-reinforced super workable concrete (FR-SWC) that can be used for infrastructure repair and construction, respectively. FR-SCC is targeted for repair of sub-structure elements, while the FR-SWC is targeted for construction operations. The study was covered by three main tasks; first task included a comprehensive literature review of the research work done on FR-SCC and FR-SWC, second task focused on mixture optimization, fresh and hardened properties of SCC, FR-SCC, SWC and FR- SWC, final task was the evaluation of the structural performance of monolithic beams cast using SCC, FR-SCC, SWC and FR-SWC, furthermore is to evaluate the structural performance and the amount of flexural strength restored when CVC beams are repaired using SCC and FR-SCC.

Task 1: Literature review

The purpose of this task was to conduct a comprehensive literature review of previous experiences and research findings on the design and use of FR-SCC and FR-SWC. Detailed study about the mix design methodology of fiber-reinforced concrete and special workability test methods that can be used for FR-SCC and FR-SWC was reviewed.

The literature review focused on studies involving the hardened properties of SCC, SWC and fiber-reinforced concrete, including mechanical properties (compressive strength,

flexural strength, fracture energy, cracking resistance), structural properties (bond, shear, and flexural strengths) and durability (freeze-thaw resistance, permeability and electrical resistivity). Special attention was given to fiber dispersion and orientation monitoring in FR-SCC.

Task 2: Mix design of SCC and SWC

Task 2A: Binder optimization for SCC, FR-SCC, SWC and FR- SWC

The aim of this task was to develop and optimize the mix designs of FR-SCC and FR-SWC that exhibit superior workability and stability (both static and dynamic stability). A steel fiber (ST1-hooked end) was systematically introduced to the mixtures at a fiber volume of 0.5%. After investigating 22 mixtures in this sub-task, two mixtures of FR-SCC and two mixtures of FR-SWC were selected.

Task 2B: Selection of fiber type for FR-SCC and FR-SWC

Eight types of fibers including: propylene synthetic fiber (PLP), four types of hooked steel fiber (ST1), (3D), (4D) and (5D), carbon fiber (CA), hybrid of crimped steel fiber and polypropylene multifilament fiber (STPL), and micro-macro steel fibers (STST) were incorporated at a fiber volume of 0.5% to FR-SCC and FR-SWC and the workability of all the mixtures was primary evaluated using slump flow and VSI. Six different types of fibers were investigated with FR-SCC, only four types of fibers (ST1, STST, STPL, and PLP) showed acceptable workability. All types of fibers were investigated with FR-SWC, only six types of fibers (ST1, STST, 3D, 4D, 5D, and STPL) showed acceptable workability. Further fresh properties evaluation including modified J-Ring, surface settlement, bleeding, and rheological properties measurements was performed only for

the mixtures that showed the acceptable workability. Mechanical properties including: compressive strength, splitting tensile strength, flexural strength, toughness, modulus of elasticity, and flexural crack resistance was conducted only for the mixtures that showed acceptable workability.

Four types of fibers (ST1, STST, 5D, and STPL) showed the best fresh and hardened properties with FR-SWC, which were chosen to be incorporated to FR-SWC at a higher fiber volume of 0.75%.

Task 2C: Optimizing fiber volume for FR-SWC

Four types of fibers (ST1, STST, 5D, and STPL) were incorporated to FR-SWC at a fiber volume of 0.75%, only three types of fibers (ST1, STST, and 5D) showed acceptable workability. FR-SWC made with the acceptable three fibers at a fiber volume of 0.75% were evaluated for fresh properties and Mechanical properties.

The passing ability, stability and the HRWRA dosage to secure the required flowability were included in an overall performance evaluation of fresh properties. The mechanical properties of the optimized FR-SCC and FR-SWC mixtures were included in the overall evaluation as well. The overall performance was determined using the area of star diagram. Three FR-SCC mixtures were optimized in addition to the SCC reference and four FR-SWC mixtures were optimized besides the SWC reference. The selected FR-SCC mixtures and FR-SWC mixtures was evaluated in next tasks which included measurement of drying shrinkage, resistance to shrinkage cracking, frost durability, and structural performance.

Task 2D: Shrinkage and durability evaluation of FR-SCC and FR-SWC

Four FR-SCC mixtures and four FR-SWC mixtures beside SCC and SWC references were evaluated for drying shrinkage. Shrinkage measurements were recorded up to 365 days. Restrained shrinkage was evaluated in accordance to ASTM C1581. A ring-type test was performed. Twelve rings were cast using six different mixtures; one SWC, one SCC and four different FR-SCCs.

Three FR-SCC mixtures and three FR-SWC mixtures beside SCC and SWC references were evaluated for freeze/thaw durability. Three prismatic specimens were taken for each mixture to be tested in accordance to ASTM C666. The concrete prisms were cured first for 28 days before moving to freeze-thaw chamber for testing. Specimens were subjected to 300 freeze-thaw cycles.

Task 3: Structural performance in flexural of monolithic beams and repaired beams**Task 3A: Monolithic beam flexural tests for SCC, FR-SCC, SWC and FR- SWC**

This sub-task evaluated the flexural behavior of beam elements in order to compare conventional vibrated concrete (CVC) and those of fiber reinforced conventional vibrated concrete (FR-CVC) to fibrous mixtures of greater fluidity that necessitated low vibration energy (FR-SWC) or no mechanical consolidation (FR-SCC). 20 monolithic full scale beams were cast using CVC, FR-CVC, SCC, FR-SCC, SWC and FR-SWC. The beams were tested using four-point flexural load frame. The beams were loaded up to 3 in. deflection or a drop in the peak load by 20%. Strain in steel rebar vs. strain in concrete

surface was measured using strain gauges, also the actuator load was monitored vs. deflection for the tested beams.

Task 3B: Repaired beam flexural tests for SCC and FR-SCC

This sub-task evaluated the flexural behavior of CVC beam elements repaired with either SCC or FR-SCC. Ten Beams were cast using CVC to the two thirds and then the bottom third of each was cast using different FR-SCCs. The beams were tested using four-point flexural load frame. The beams were loaded up to 3 in. deflection, a drop in the peak load by 20% or significant delamination of the repair material, if any. Strain in steel rebar vs. strain in concrete surface was measured using strain gauges, also the actuator load was monitored vs. deflection for the tested beams.

2 Literature review

2.1 General

Reducing the micro cracks in concrete, which increases its strength is achieved by adding fibers to different types of concrete. One of the main advantages of using fibers is the partially or even completely substituting the traditional welded wire mesh reinforcement (such as shear reinforcement in beams and roof elements). This reduces the needs for manufacturing, detailing and placing the reinforcement cages and results in improved production efficiency. Furthermore, the element thickness and the structure self-weight can be also reduced, since minimum cover requirements do not hold any more. The major advantage of adding fibers into concrete is the achievement of a randomly uniform dispersion of fibers within structural elements. It has also been recently recognized that, through a suitably balanced performance of the fluid mixture fibers can be effectively aligned along the casting-flow direction. [Ferrara, 2013] [1]

Brief description of previous work performed by different researchers is summarized in this chapter, which includes:

1. Literature related to the materials used with FR-SCC.
2. Studies related to the mixture proportioning of FR-SCC.
3. Different test methods used for FR-SCC.
4. Fiber dispersion and orientation monitoring in FR-SCC.
5. Rheology of FR-SCC.
6. Mechanical properties of FR-SCC.

7. Shrinkage behavior of FRSCC.
8. Durability of FRSCC.
9. Structural performance of FRSCC.

2.2 Materials used for fiber-reinforced self-consolidated concrete

2.2.1 Aggregates

Aggregates used in concrete is divided generally into three categories upon the maximum size of the aggregate; coarse aggregate are those particles with maximum size more than 4.75 mm, fine aggregate are those particles with maximum size between 4.75 mm and 0.075 mm, fines are those particles with maximum size less than 0.075 mm.

2.2.1.1 Coarse aggregates

Three categories of maximum size of aggregate are specified by the Japanese Architecture Society [2]: 15, 20 and 25 mm. 20 mm is the most commonly used size. It is suggested that the content of coarse aggregates should be around 50% of the dry packed unit weight (JIS A1104, ASTM C29) [SU et al., 2001] [3]. In SCC the most commonly used size of aggregates is in range of 10 to 20 mm [SU et al., 2001] [3].

Domone [2005] [4] analyzed 68 case studies of applications of SCC, these mixes were done in the period between 1993 and 2003. Domone found that 70% of the cases used aggregates of a maximum size between 16-20mm, while 15% of the cases used aggregates of a maximum size between 10-15mm and only few cases (six cases out of 68) used aggregates larger than 20 mm with SCC. He also found that crushed rock was used more than the gravel (uncrushed) aggregates (almost three times), and the

lightweight aggregate was rarely used (only two cases out of 68). He also found that 80% of those cases had coarse aggregate content in the range of 770-925 kg/m³.

Funk and Dinger [1994] [5] proposed the following grading curve for the coarse aggregates:

$$P(d) = \frac{d^q - d_{min}^q}{d_{max}^q - d_{min}^q} \quad (1)$$

Where $P(d)$ is the cumulative passing fraction at a sieve with opening d , the maximum aggregate diameter is d_{max} and $d_{min} = 75 \mu m$, which is the minimum sieve diameter used for the particle size analysis. Brouwers and Radix [1997] [6] claimed that $q = 0.25$ is the best value to get the actual distribution of the all solids in SCC including binder materials, where $d_{min} = 0.5 \mu m$ is assumed. Fuller and Thompson [1907] [7] argued that $q = 0.5$ in Eq.1 gives the best gradation and by assuming that $d_{min} = 0$ gives back Fuller curve equation mentioned bellow.

$$P(d) = \sqrt{\frac{d}{d_{max}}} \quad (2)$$

Ferrara et al, [2007] [8] mentioned that for mix-design of fiber-reinforced self-consolidated concrete (FRSCC) the optimization of both aggregates and fibers and the optimization of binders on the other hand each is done separately so, value of $q = 0.5$ will be a reasonable choice (Ferrara 2007).

2.2.1.2 Fine aggregates

Fine aggregates help in the mobility of the mixture as well as resist the segregation of concrete. Sugár and Takács [2013] [9] investigated the effect of sand

content in SCC on its fresh and hardened properties; they used fine aggregates with four percentages: 35%, 40%, 45% and 50% of the total weight of the aggregates. They found that the sand percentage is inversely proportional to the density of fresh concrete, which means higher air content, and less compressive strength. On the other hand enhancement in the fresh properties was observed by increasing percentage of sand in terms of flow ability, passing ability as well as stability (less segregation was observed). They recommended the percentage of sand to be 50% or more. SU et al., [2001] [3] recommended that percentage to be in between 50% to 57% for SCC.

Pereira et al. [2008] [10] investigated the most appropriate proportions of three types of aggregates; fine river sand (FS), coarse river sand (CS), and crushed granite 5-12 mm (CG). Some mixtures containing different quantities of each type of aggregate were prepared each containing a constant steel fiber content of 30 kg/m³ (DRAMIX RC-80/60-BN hooked end steel fibers from Bekaert). He assumed that the most optimum mixture is the heaviest one because it corresponds to the most compact. The results showed that the best combination is 49.5% of CS, 40.5% of CG, and 10% of FS, in other words 50.5% sand and 49.5% coarse aggregates.

Domone found in the 68 analyzed cases that 80% of the mortar composition in terms of volume percentage of fine aggregates is between 41% and 52%. Okamura and Ozawa (1995) [11] recommended a value of 40% for robust and safe SCC mixes.

2.2.1.3 Fines

Kwan et al. [2014] [12] found that under wet condition, the highest packing density generally will take place when the fines content is about 15%, but on the other

hand the higher fines content the more total specific surface area of aggregates to be coated with cement paste, that's why the final effect of fines content should be positive or negative and more research is undergoing in this field.

2.2.2 Binders

Binders can be generally divided into three major groups; Cement with all its different types (Type I, II, III, IV and V), supplementary cementitious materials (fly ash, silica fumes, metakoline, lime stone filler and granulated blast furnace slag) and non-cementitious materials like expansive agents.

Domone found in the 68 analyzed cases that 80% of the powder contents (binders) were in the range 445-605 kg/m³. He found also that almost all of the cases used either binary or ternary cement blend of Portland cement with or without other additions. Limestone was the most common addition (41% of the total cases).

2.2.2.1 Cement

Yodsudjai and Wang [2013] [13] tested five different pastes made with different types of cement (Type I, I/II, II, IV and IP) for chemical shrinkage using ASTM C 1608 [14], where the water cement ratio for the five pastes was 0.4. The shrinkage for 7 hours, 24 hours, 7 days and 28 days was observed for each of the five pastes. Types I, I/II, II, and IV were tested according to ASTM C 150/C 150M [15], while one blended cement Type IP was tested according to ASTM C 595/C 595M [16]. Figure 2-1 shows that the chemical shrinkage values of pastes made with Types I, I/II, and II cements at 24 h are

only 45–50% of those at 28 days, and it is only about 30% for the paste made with Type IV cement.

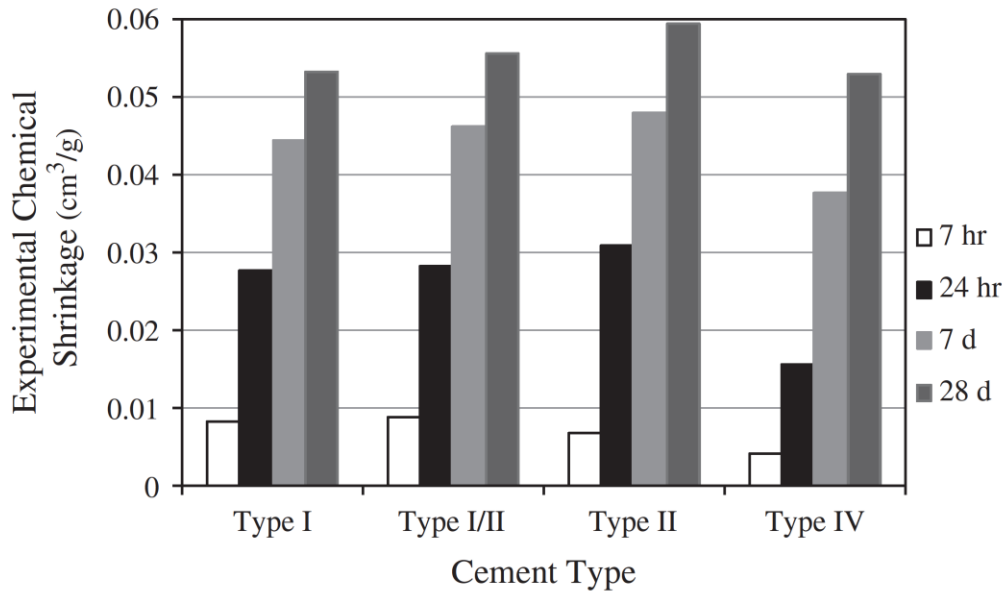


Figure 2-1: Chemical Shrinkage at different ages [13]

2.2.2.2 Supplementary cementitious materials (SCM)

El-Chabib and Syed [2013] [17] developed a total of 20 concrete mixes mixtures were made using up to 70% Portland cement replacement by supplementary cementitious materials; class C and class F fly ash, slag, and silica fume. They tested their concrete for flow ability, passing ability, stability, permeability, unrestrained shrinkage as well as compressive strength and splitting tensile strength. Their results generally showed that a high-performance self-consolidating concrete could be developed using binary, ternary, or quaternary binders with up to 70% of cement replaced by fly ash, slag, and/or silica fume. They found that: (1) Up to 70% SCM can be used SCC as partial replacement of cement and the produced concrete still workable, durable and strong. (2) Self

consolidated concrete made with 70% slag and 30% cement exhibit better fresh performance as well as higher early compressive strength compared to SCC made with only cement. (3) Using high percentages of fly ash as a replacement of cement in SCC enhances the workability and the late compressive strength (4) As shown in Figure 2-2 using up to 10% silica fume in the ternary and quaternary blends enhance the compressive strength of the SCC but reduce its workability (5) Adding high contents of SCM to SCC in general, reduces permeability as well as unrestrained shrinkage.

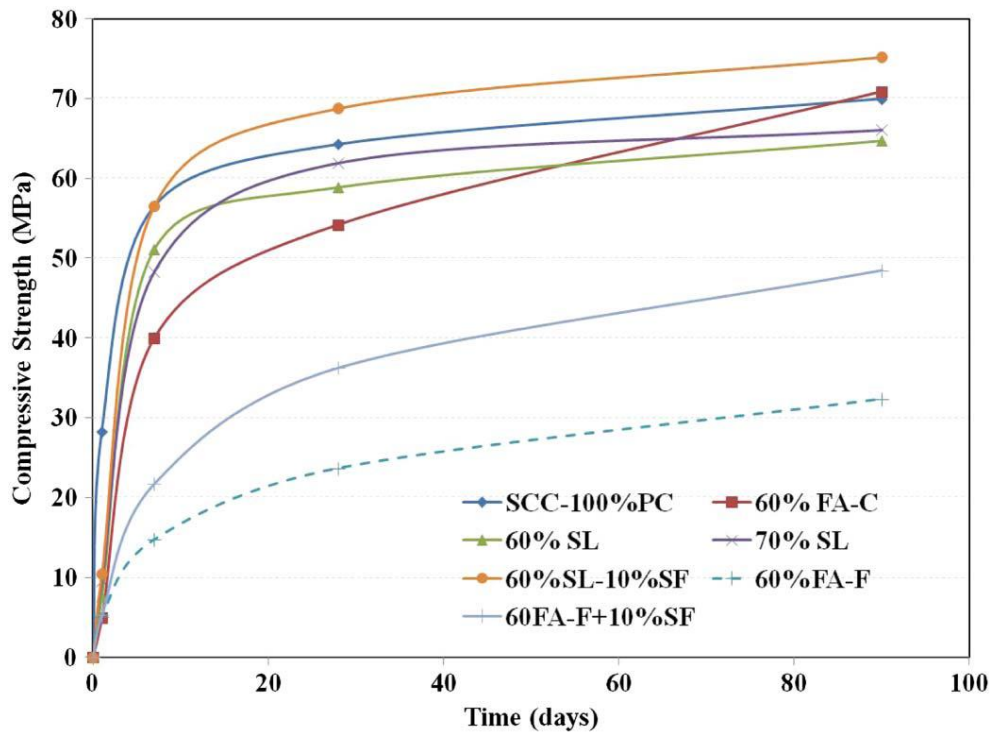


Figure 2-2: Compressive strength of SCC made with high contents of fly ash (FA) and slag (SL) [17]

Khatib [2008] investigated the influence of including fly ash (FA) on the properties of SCC. He used fly ash (EN 450) as a replacement for Portland cement by 0-80%, he also used a constant water to binder ratio of 0.36. The investigated properties included workability, compressive strength, absorption and shrinkage as well as ultrasonic pulse velocity. He found that: (1) as shown in Figure 2-3 using high percentage of FA up to 60% could produce SCC with strength as high as 40 N/mm² (2) as shown in Figure 2-4 the absorption of the SCC increase with the increase in FA content, but even with 80% FA absorption values of SCC is below 2% at 56 days of curing (3) as shown in Figure 2-4 increasing the amount of FA in SCC reduce the drying shrinkage and a linear relationship was obtained by the author between the FA content and the shrinkage of SCC, as shown in Figure 2-5 Replacing cement with 80% FA can reduce the shrinkage by two third.

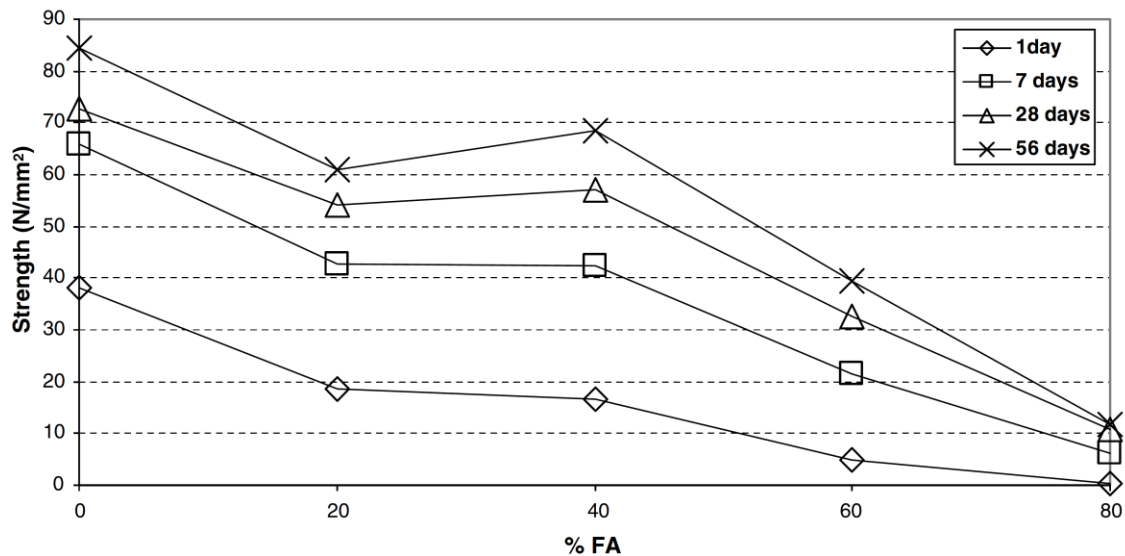


Figure 2-3: Influence of FA content on compressive strength [18]

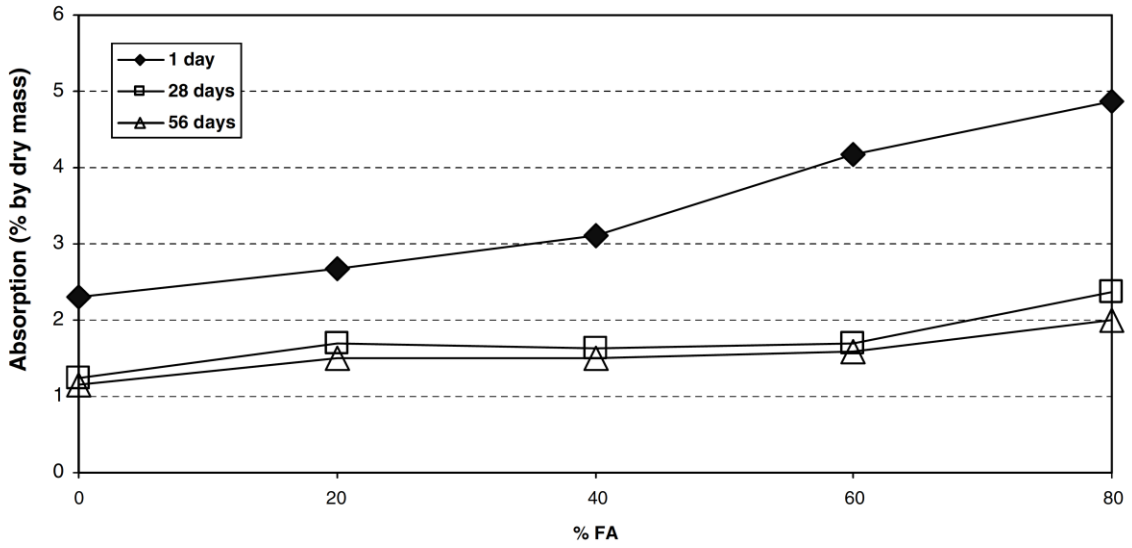


Figure 2-4: Influence of FA content on absorption [18]

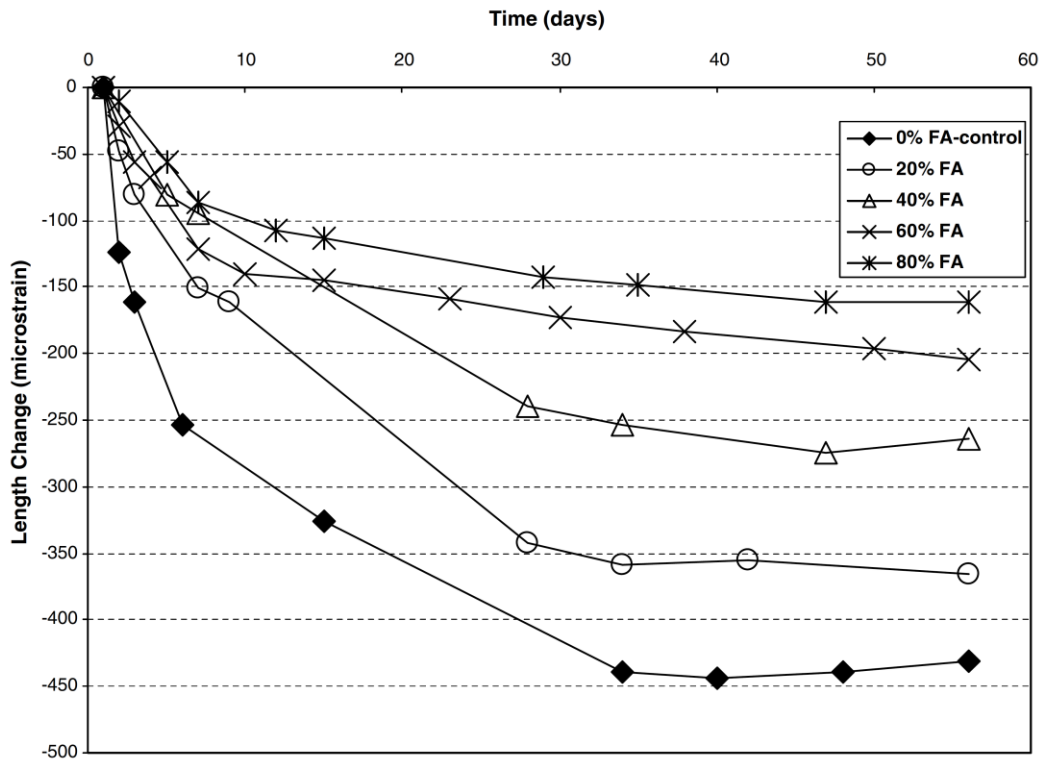


Figure 2-5: Influence of FA on shrinkage [18]

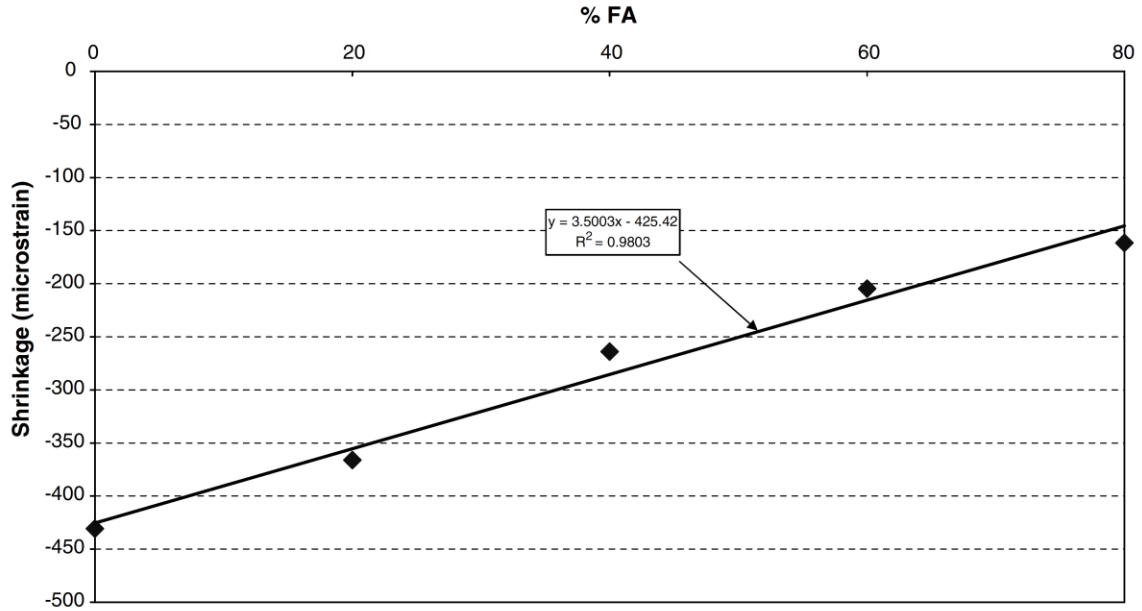


Figure 2-6: Shrinkage versus FA content at 56 days curing [18]

2.2.2.3 Expansive agents

Expansive agents can be generally divided into two major groups depending on the mechanism of the chemical reaction:

- Group one are expansive agents that produce hydroxides upon their reaction with water like the CaO-based expansive agent or the MgO-based expansive agent, which produce calcium hydroxide or magnesium hydroxide, respectively upon reacting with water. Expansion produced is about two times in volume and the expansion takes place within approximately two days (Colleparidi 1977)
- Group two are expansive agents that produce ettringite upon their reaction with water like calcium sulfoaluminate-based expansive agent. Expansion

produced is about three times in volume and the expansion takes place within approximately seven days (Collepari 1977).

2.2.3 Fibers

Many types of fibers can be used with SCC in order to enhance the shrinkage resistance, reduce cracking of concrete, and increase the tensile resistance as well as increasing concrete ductility. These types of fibers can be divided upon their material into Steel fibers, polymeric fibers, carbon fibers and natural fibers, they can also divided upon their size into macro and micro fibers. The concrete can be made using only one type of fibers or more than one type (hybrid fibers).

2.2.3.1 Steel fibers

Steel fibers can be found in different shapes either straight or crimped or hooked-end, the hook may be single (3D-fiber) or double (4D-fiber) or triple (5D-fiber). Figure 2-7 shows different types of steel fibers: crimped, 3D-hookedend, 4D-hookedend, 5D-hookedend as well as micro and macro straight steel fibers. The steel fiber length is varied from 5 to 60 mm and aspect ratios l_f/d_f , where d_f is the diameter of the fiber cross-section, from 20 to more than 100. The employed dosage of fibers varied, depending on the application, from 23-157 kg/m³ (0.25-2% by volume of concrete).



Figure 2-7: Different types of steel fibers; macro straight, crimped, 3D-hookedend, 4D-hookedend, 5D-hookedend and micro straight fibers (from left to right)

2.2.3.2 Polymeric (syntactic) fibers

Polymeric fibers can be produced from different materials: Poly vinyl alcohol fiber, nylon fibers or Polypropylene fibers. These polymeric fibers can be produced as monofilament or multifilament and these fibers can be produced as a strand or singles. These fibers can be micro or macro fibers. The lengths of macro syntactic fibers are between 25 and 54 mm. These fibers can be used either alone or in combination with steel fibers. The employed dosage of fibers varied, depending on the application, from 2.3-9 kg/m³ (0.25-1% by volume of concrete). The use of shorter polypropylene fibers to purposes other than avoiding explosive spalling under fire and high temperatures has been investigated only in very recent studies, even in combination with lightweight aggregates. [19, 20]



Figure 2-8: Different types of syntactic fibers; polypropylene micro, polypropylene macro, polypropylene macro strand, nylon micro, poly (from left to right)

2.2.4 Admixtures

Superplasticizers (SP) or high range water reducing admixtures (HRWRA) affect the interparticle forces (increase electrostatic repulsion and / or steric hindrance) and disperse the cementitious particles. This mainly leads to a decrease in yield stress. Superplasticizers can reduce water demand up to 40%, can significantly increase the slump flow of concrete as well as a necessary component in high performance concrete with very low

w/c. Domone found in the 68 analyzed cases that all the mixes included superplasticizer. The use of polycarboxylic acid-based materials were more than other materials.

Viscosity modifying agent (VMA), viscosity enhancing agent (VEA) or anti-washout admixtures increases the viscosity of the water (by adding polymers, swelling), which should be proportionally reflected in the increase in viscosity of paste, mortar and concrete. VMA increase stability of concrete and reduce cement and fines washout in case of under water concrete. Domone found in the 68 analyzed cases that in 50% of the cases a viscosity-modifying agent of some form was used. The reasons given were to provide stability and/or reduce sensitivity of the mix to variations in materials during production. Air entraining agents AEA forms air bubbles inside the paste, attract cement particles near the water-air interface forming larger concentration of cement particles around air bubbles and increase the yield stress but decrease the viscosity due to their deformability. AEA are mostly added to enhance the frost resistance of concrete. Domone found in the 68 analyzed cases that in almost 50% of the cases an air-entraining agent was used sometimes it was used to provide freeze–thaw resistance or to enhance the rheology.

2.3 Mixture proportioning of fiber-reinforced self-consolidated concrete

2.3.1 Mixture proportioning of self-consolidated concrete

SU et al., (2001) [3] proposes a mix design method for SCC in simple steps; (1) The amount of required aggregates is first determined (2) calculation of Cement content (3) calculation of mixing water content required by cement (4) calculation of SCM required

(5) calculation of mixing water content needed in SCC (6) calculation of SP dosage (7) adjustment of mixing water content needed in SCC (8) trial mixes and tests on SCC properties (9) adjustment of mix proportion.

1) Calculation of the amount of required aggregates

The content of coarse and fine aggregates can be calculated as follows:

$$W_g = PF \times W_{gL} \left(1 - \frac{S}{a}\right) \quad (3)$$

$$W_s = PF \times W_{sL} \times \frac{S}{a} \quad (4)$$

Where W_g : content of coarse aggregates in SCC (kg/m^3), W_s : content of fine aggregates in SCC (kg/m^3), W_{gL} : unit volume mass of loosely piled saturated surface-dry coarse aggregates in air (kg/m^3), W_{sL} : unit volume mass of loosely piled saturated surface-dry fine aggregates in air (kg/m^3), PF: packing factor, the ratio of mass of aggregates of tightly packed state in SCC to that of loosely packed state in air; S/a: volume ratio of fine aggregates to total aggregates, which ranges from 50% to 57%.

2) Calculation of cement content

They mentioned that HPC and SCC used in Taiwan provides a compressive strength of 20 psi (0.14 MPa)/kg cement. Therefore, the cement content to be used is:

$$W_c = \frac{f_c}{20} \quad (5)$$

Where C: cement content (kg/m^3), f_c : designed compressive strength (psi).

3) Calculation of mixing water required by cement

$$W_{wc} = \left(\frac{W}{C}\right) C \quad (5)$$

Where W_{wc} : content of mixing water content required by cement (kg/m^3), W/C: the water/cement ratio by weight, which can be determined by compressive strength.

- 4) Calculation of fly ash (FA) and ground granulated blast-furnace slag (GGBS) contents

The volume of the fly ash paste (V_{pf}) plus the volume of the GGBS paste (V_{pB}) can be calculated as:

$$V_{pf} + V_{pB} = 1 - \left(\frac{W_g}{1000 \times G_g} \right) - \left(\frac{W_s}{1000 \times G_s} \right) - \left(\frac{C}{1000 \times G_C} \right) - \left(\frac{W_{wc}}{1000 \times G_w} \right) - V_a \quad (6)$$

Where G_g : specific gravity of coarse aggregates, G_s : specific gravity of fine aggregates, G_c : specific gravity of cement, G_w : specific gravity of water, V_a : air content in SCC (%).

The total amount of Pozzolanic materials (GGBS and FA) in SCC is W_{pm} (kg/m^3), where the percentage of FA is A% and the percentage of GGBS is B% by weight. W_{pm} (kg/m^3) can be calculated from Equation (7) if $V_{pf} + V_{pB}$ is known from Equation (6).

$$V_{pf} + V_{pB} = \left(1 + \frac{W}{F} \right) \times A\% \times \frac{W_{pm}}{1000 \times G_f} + \left(1 + \frac{W}{F} \right) \times B\% \times \frac{W_{pm}}{1000 \times G_B} \quad (7)$$

W_f (FA content in SCC, Kg/m^3) and W_B (GGBS content in SCC, Kg/m^3) can be calculated using Equation (8) and (9).

$$W_f = A\% \times W_{pm} \quad (8)$$

$$W_B = B\% \times W_{pm} \quad (9)$$

Mixing water content required by FA paste can be calculated using Equation (10)

$$W_{wf} = \left(\frac{W}{F} \right) W_f \quad (10)$$

Mixing water content required by GGBS paste can be calculated using Equation (11)

$$W_{wf} = \left(\frac{W}{S}\right) W_B \quad (11)$$

5) Calculation of mixing water content needed in SCC

The mixing water content required by SCC is that the total amount of water needed for cement, FA and GGBS in mixing. It can be calculated using Equation (12)

$$W_w = W_{wc} + W_{wf} + W_{wB} \quad (12)$$

6) Calculation of SP dosage

The dosage of SP used is equal to n% of the amount of binders and its solid content of SP is m%. The SP dosage can be calculated using Equation (13)

$$W_{sp} = n\% (C + W_f + W_B) \quad (13)$$

The water content in SP can be calculated using Equation (14)

$$W_{Wsp} = (1 - m\%) W_{sp} \quad (14)$$

7) Adjustment of mixing water content needed in SCC

The mixing water is adjusted according to the moisture content of the fine and coarse aggregate as well as the water content in SP.

8) Trial mixes and tests on SCC properties

Trial mixes should be performed and SCC should be tested for all fresh properties regarding flow ability, passing ability and stability.

2.3.2 Mixture proportioning of fiber-reinforced self-consolidated concrete

Voigt et al. (2004) [21] proposed a formula for calculating the average thickness of the matrix layer (t_m) enveloping fibers and gravel particles on the basis of the multi-aspect concept.

The multi-aspect concept accounts for all factors that affect the performance of a cementitious composite. Those factors include volume, size distribution, shape, rigidity, and interaction of all constituents of the composites. In the multi-aspect concept, the composite is considered a two-phase material. The first phase creates the skeleton of the composite. The second phase fills all voids and covers all constituents of the first phase. Then an average thickness of the second phase covering all constituents of the first phase can be calculated from the volume, total surface area, and voids of the first phase. Then they expressed the average thickness of matrix covering the fibers and the gravel mathematically using Equation (15).

$$t_m = \frac{\text{Volume of Excess Matrix}}{\text{Total Surface Area of Fibers and Gravel}} \quad (15)$$

Figure 12 shows schematic explanation of multi-aspect concept. They came finally to Equation (16) to calculate the exact matrix thickness t_m .

$$t_{mortal\ after} = \frac{V_c - V_g - V_f - V_v}{A_g + A_f} \quad (16)$$

where t_m = average thickness of matrix layer cover fibers and gravel; V_c = total volume of concrete; V_g = volume of gravel; V_f = volume of fibers; V_v = volume of voids; A_g = total surface area of gravel; and A_f = total surface area of fibers. The volume of voids can be obtained using the packing density of the mixture of gravel and fibers, which can be

determined by ASTM C 29 [22]. The total surface area of fibers is the summation of the surface area of all fibers present in the composite. It can be calculated based on the fiber volume and the surface area of a single fiber. The total surface area of the gravel depends on the grading curve of the used coarse aggregates. Equation (17) and (18) (developed by the author) can be used to calculate the total surface area of the coarse aggregate.

$$A_g = KV_g \tag{17}$$

$$\text{where, } K = 6 \left\{ \frac{\%_{g1}}{d_1} + \frac{\%_{g2}}{d_2} + \frac{\%_{g3}}{d_3} + \frac{\%_{g4}}{d_4} \right\} \tag{18}$$

Where d_1 : Diameter of course of first group; $\%_{g1}$: Percentage of course aggregates having diameter d_1 and d_2 : Diameter of course of first group; $\%_{g2}$: Percentage of course aggregates having diameter d_2 and so on for $d_3, d_4, \%_{g3}$ and $\%_{g4}$

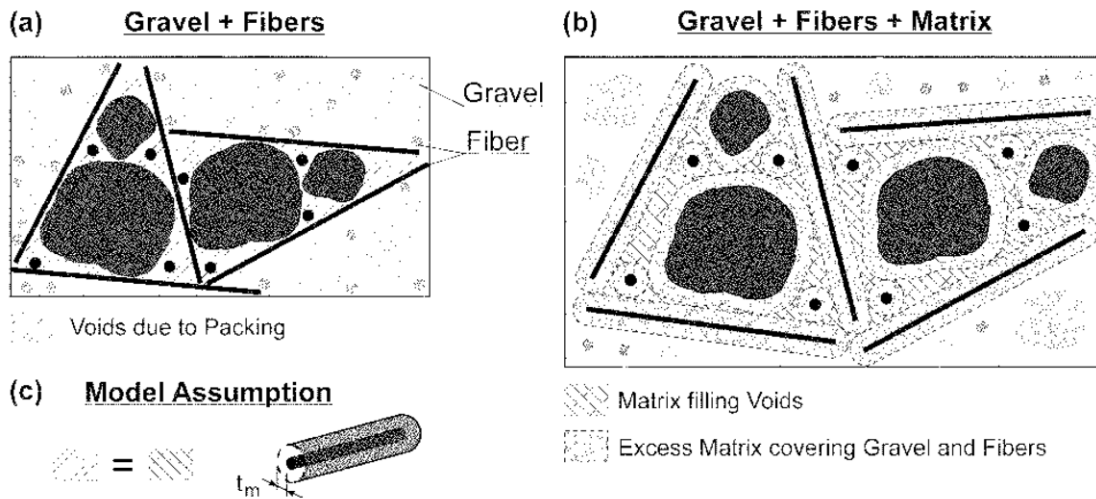


Figure 2-9: Schematic explanation of multi-aspect concept: (a) void content as result of maximum packing of gravel and fibers (without matrix); (b) distinction between matrix enveloping fibers and gravel matrix filling voids; and (c) model assumption and thickness of matrix layer covering fibers and gravel.

Khayat et al. (2014) [23] proposed a mixture-proportioning method proposed for shrinkage control in fiber-reinforced concrete (FRC) in proportioning fiber-reinforced self-consolidating concrete (FR-SCC). They considered the multi-aspect concept proposed by Voigt [21] and they used Equation (16) for calculating the thickness of mortar covering the coarse aggregates and the fibers.

$$t_{cm} = \frac{V_c - V_g - V_f - V_v}{A_g + A_f} \quad (16)$$

The mixture-proportioning method proposed by them includes reducing the volume of coarse aggregate with the addition of fibers to maintain a fixed thickness of a mortar layer t_{cm} over the fibers and coarse aggregates. They expressed the total surface area of fibers (A_f) as:

$$A_f = \frac{\% \text{ fiber} \times \text{specific gravity} \times \text{surface area of single fiber}}{\text{Volume of single fiber} \times \text{specific gravity}} \quad (19)$$

Their final proposed equation for calculating the total surface area of fibers (A_f) is:

$$A_f = \frac{4 \times V_f}{d_f} \quad (20)$$

Where V_f is an absolute volume, and not as a ratio. They performed 22 mixtures one plain SCC without fibers and 21 mixtures of FR-SCC reinforced using three polypropylene fibers, a hybrid steel-polypropylene fiber, and a steel fiber. The fiber volume ratios varied between 0.25 and 0.75%. All mixtures had a fixed water-cementitious material ratio (w/c) of 0.42. The total binder content was kept constant also at 475 kg/m³. The air content was kept between 5.5 and 7.5% using air entraining admixture (AEA). The values of t_{cm} calculated from Equation (16) are plotted against the

fiber factor ($V_f L_f / d_f$) in Figure 2-10. Figure 2-11 shows a linear relationship between the fiber factor and the reduction of coarse aggregate content to maintain a constant t_{cm} value. They concluded that for a given fiber type, as V_f increases, the value of t_{cm} is maintained by reducing the coarse aggregate content and adjusting the sand content to maintain similar fluidity of the FR-SCC as that of the reference SCC as well as other adjustments are also necessary in terms of admixture dosages, including HRWRA, VMA, and AEA.

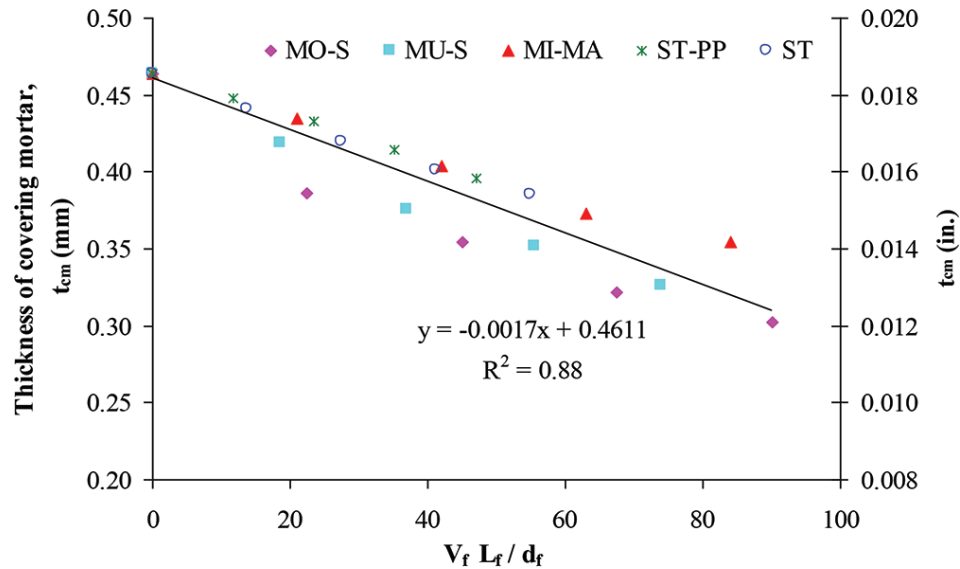


Figure 2-10: Relationship between fiber factor and thickness of covering mortar before adjustment of mixture proportions (before fixation of t_{cm}).

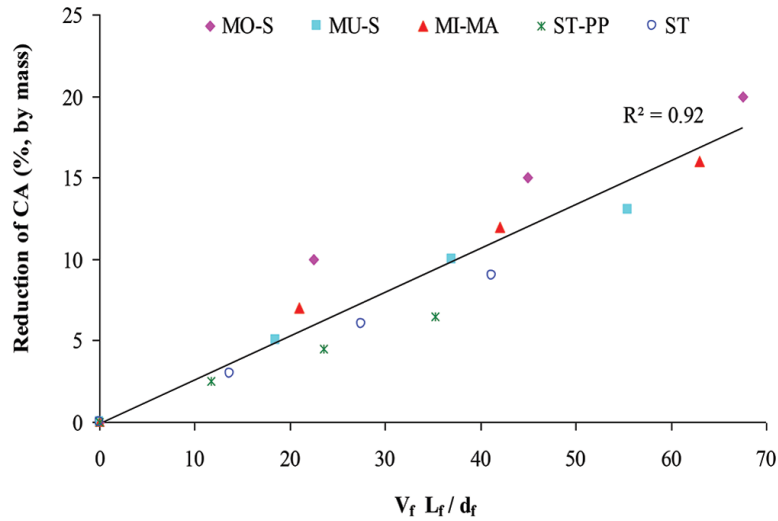


Figure 2-11: Relative reduction of coarse aggregate versus increase in fiber factor to maintain initial t_{cm} of SCC mixture

Saak et al. (2001) [24] developed the “rheology of the paste model” for proportioning SCC. They derived theoretical equations for a single spherical particle suspended in the fluid cementitious paste under the assumption that a minimum yield stress and viscosity of the cement paste, also as a function of the density difference between the particle and the paste itself, are required in order to avoid segregation under both static and dynamic conditions. They defined the average diameter (d_{av}) of the solid skeleton particles as:

$$d_{av} = \frac{\sum_i d_i m_i}{\sum_i m_i} \quad (21)$$

Where d_i is the average diameter of aggregate fraction i (defined as the average opening size of two consecutive sieves) and m_i is the mass of that fraction. A minimum volume of cementitious paste is needed to fill the voids between the aggregate particles and create a layer enveloping the particles, thick enough to ensure the required deformability and segregation resistance of concrete. The average aggregate spacing d_{ss} , defined as twice

the thickness of the excess paste layer enveloping the aggregates was expressed using Equation (22).

$$d_{ss} = d_{av} \left[\sqrt[3]{1 + \frac{V_{paste} - V_{void}}{V_{concrete} - V_{paste}}} - 1 \right] \quad (21)$$

By knowing the desired flow-viscosity ratio and by using chart in Figure 2-12 developed by Saak et al. [24] two limits of d_{ss} can be determined lower limit that below it the required workability can not be achieved and upper one that above it segregation will take place. By choosing a value between the two limits and using equation (20) to calculate the d_{av} equation (21) can be used to get the required V_{paste} . Equation (22) can be used the to calculate V_{agg} .

$$V_{concrete} = V_{paste} + V_{void} + V_{agg} \quad (22)$$

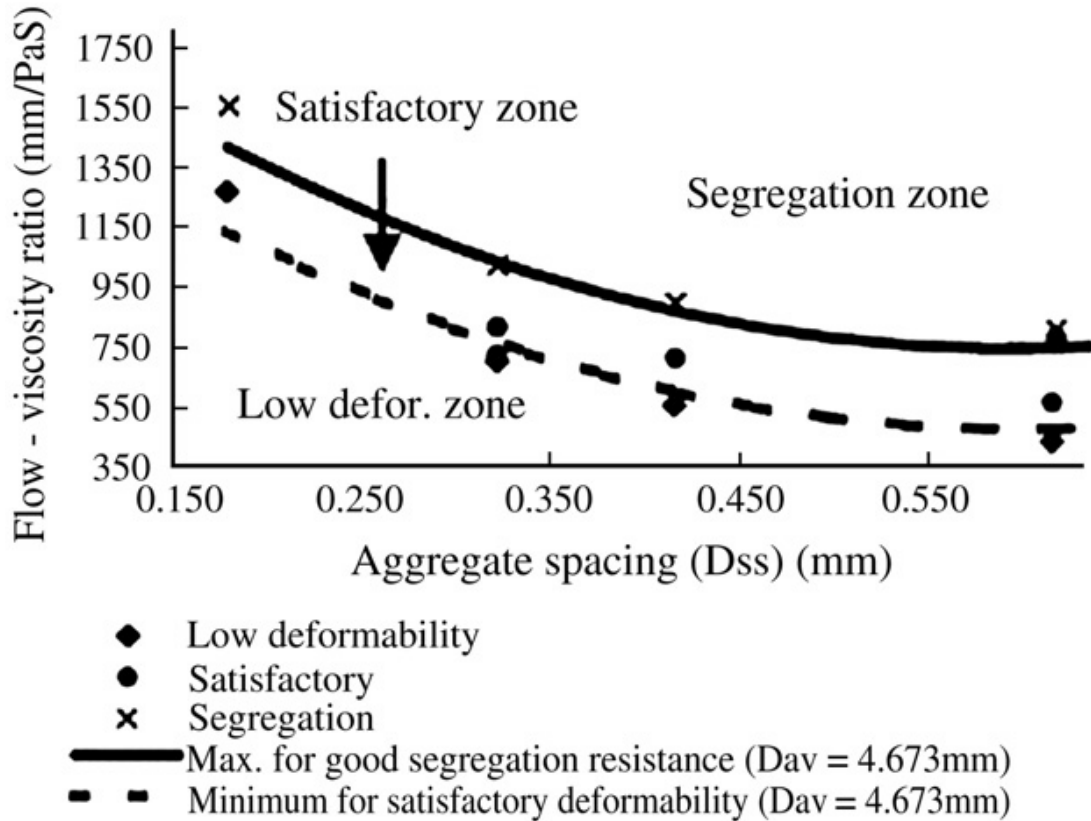


Figure 2-12: Model lines for flow viscosity ratio of experimental data and aggregate spacing d_{ss} (average diameter $d_{av}=4.673$ mm) [24]

Ferrara et al. [2007] [8] extended the rheology of the paste model developed by Saak [24] to fiber-reinforced concretes where the defined average diameter (d_{av}) of the solid skeleton particles in this type will include the coarse aggregates, the fine aggregates and the fibers. They defined the average diameter (d_{av}) as Equation (23).

$$d_{av} = \frac{\sum_i d_i m_i + d_{eq-fibers} m_{fibers}}{\sum_i m_i + m_{fibers}} \quad (23)$$

where $d_{eq-fibers}$ is defined in Eq. (24), m_{fibers} is the mass of the fibers.

$$d_{eq-fibers} = \frac{3 L_f}{1 + 2 \frac{L_f}{d_f}} \frac{\gamma_{fibers}}{\gamma_{aggregate}} \quad (24)$$

where L_f and d_f are the length and diameter of the fibers, respectively, γ_{fiber} is the specific weight of fibers and $\gamma_{\text{aggregate}}$ is the weighted average specific weight of all the aggregates. L_f was assumed equal to the developed length in the case of non-straight fibers.

2.4 Test Methods and fresh performance of fiber-reinforced self-consolidated concrete

Khayat (1999) [25] reported successful placement of SCC necessitates that the concrete exhibits excellent deformability and proper stability to flow under its own weight through closely spaced reinforcement without segregation and blockage. Insuring high stability is important to limit bleeding, segregation, and surface settlement of concrete after placement and secure uniform properties of the hardened concrete, including bond to embedded reinforcement [25]. In general, the SCC exhibits low yield value and adequate cohesiveness (moderate viscosity). In addition to the slump flow test used to evaluate deformability, the filling capacity or V-funnel flow test should be used to evaluate the ability to achieve smooth flow through restricted spacing without blockage [25].

Figure 2-13 shows a trade-off between fluidity and stability of concrete explained on a V-funnel test. A short flow out of concrete under its own weight from the funnel outlet reflects high deformability and good stability and resistance to blockage. When the concrete is proportioned with a low w/cm and a fixed dosage of HRWR, it can exhibit a relatively low slump and high viscosity, which results in a high flow time (Point A1). With the increase in w/cm, the viscosity and segregation resistance decrease and the

deformability increases, resulting in a net reduction in flow time. Further increase in deformability does not necessarily secure constant reduction in flow time, since highly flowable concrete may not possess enough cohesion between the mortar and coarse aggregate to insure uniform deformation through the tapered outlet. Therefore, because of the local coagulation of coarse aggregate that can cause blockage, the flow time can increase despite the higher non-restrained deformability. An optimum point (A2) exists where a balance between the deformability and stability can lead to the lowest flow time out for a particular mix. An increase in mortar viscosity, through the use of fine powder or a VEA, can maintain good suspension of coarse aggregate, and reduce interparticle collision and coagulation of coarse aggregate. As a result, higher stability can be assured for a given slump flow, hence securing low flow times at higher slump flow values (Point B2).

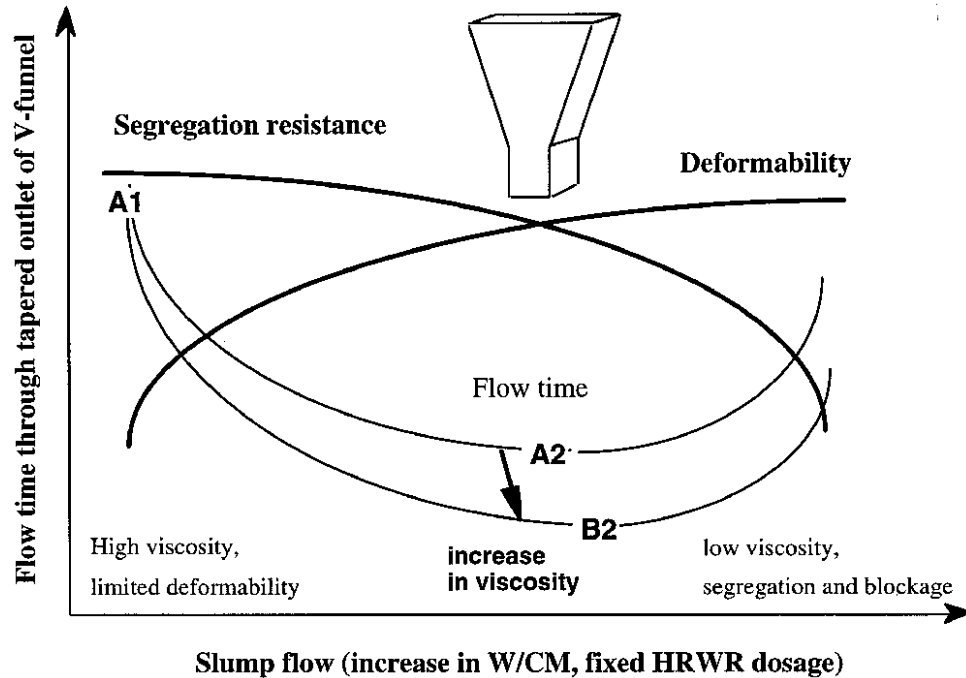


Figure 2-13: Trade-off between fluidity and stability of concrete ^[25]

Khayat et. al. (2000) [26] evaluated the suitability of using rheological parameters calculated using a concrete viscometer, filling capacity test and V-funnel flow test to assess restricted deformability of FR-SCC and discusses the effect of fiber volume, mixture proportioning, and consistency on concrete properties. The reported sixteen mixtures made with steel fibers measuring 38 mm in length used at dosages of 0, 0.5, and 1%, by volume. The mixtures were prepared with various types of binary and ternary cementitious materials and W/CM of 0.37 to 0.45. The higher W/CM mixtures incorporated a VEA to reduce the risk of segregation. Concrete mixtures with slump flow consistencies of 650 and 530 mm were prepared, with the latter representing a super workable (SWC) that would require some consolidation.

Figure 2-14 shows the V-funnel test that was employed to assess the facility of aggregate particles and mortar to change their flow paths and spread through a restricted

area without blockage. The flow of concrete is noted as the time between the removal of the outlet and seizure of flow.

Figure 2-15 shows the filling capacity test that was used to determine the facility of the concrete to deform readily among closely spaced obstacles. The center-to-center spacing between smooth copper tubes is 50 mm in two directions, resulting in a clear spacing of 34 mm. The test involves the casting of concrete in the non-reinforced section at a constant rate up to a height of 220 mm and observing the ease with which the concrete flows in the restricted region.

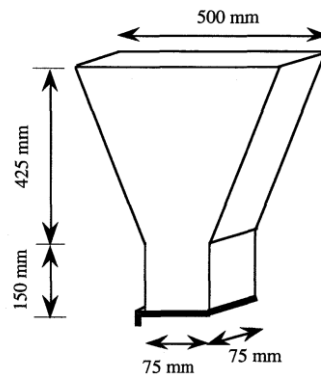


Figure 2-14: V-Funnel test used to evaluate flowability through restricted section [26]

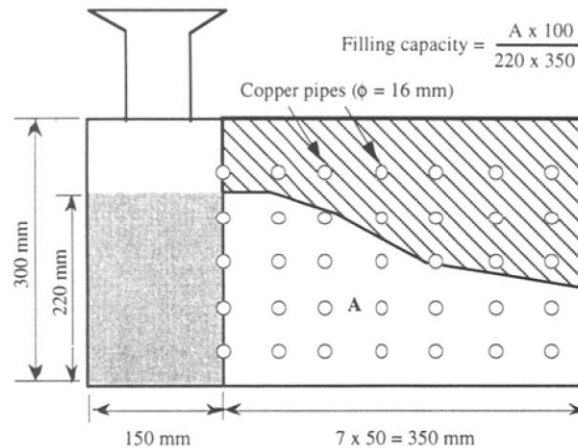


Figure 2-15: Schematic of the filling capacity apparatus [26]

The other [26] found that the slump flow test and rheological parameters are not sufficient to evaluate the restricted deformability of FR-SCC. The filling capacity or V-funnel test should be used to assess workability and blockage resistance. This is especially important when the fiber volume increases causing greater hindrance of spreading. For mixtures with a filling capacity greater than 30%, the filling capacity test becomes more suitable to assess the restricted deformability than the V-funnel test. For a given slump flow and yield stress value, the increase in fiber content reduces the filling capacity and increases plastic viscosity. The relationship between filling capacity on the one hand and yield stress and slump flow on the other hand is dependent on fiber volume. Despite the 38-mm long fibers that are similar in size to the minimum clear spacing between obstacles of the filling capacity test high deformability was obtained when the fiber volume was limited to 0.5%. At 1% fiber, the filling capacity was low but still considerably greater than that of the CONV mixture. With the decrease in fiber length to ensure compatibility with the narrowest dimension between the various obstacles, the filling capacity of the FR-SCC with 1% fibers should increase.

Khayat et. al. (2014) [23] evaluated the workability of FR-SCC. The investigated fibers included polypropylene, steel, and hybrid fibers of different properties with fiber lengths of 5 to 50 mm. Fiber volume ranged between 0.25 and 0.75%. The polypropylene fibers included a straight monofilament fiber (MO-S), a kinked multifilament fiber (MU-S), and a combined 80% macro-crimped fiber and 20% tissue-based micro-fiber (MI-MA). The aspect ratios of these fibers are 90, 74, and 84, respectively. Hybrid steel-polypropylene fibers (ST-PP) with 92 and 8% relative mass and a steel fiber (ST) were

also employed. The aspect ratios of the hybrid and steel fibers are 47 and 55, respectively. Slump flow, T50 spread time, and visual stability index (VSI) were determined. The passing ability, fiber inclusions, and mortar to change their flow paths and spread through a restricted area without blockage, was evaluated using three test methods that are typically employed to assess the passing ability of SCC: the V-funnel, L-box, and J-ring tests. The V-funnel test has an outflow opening of 65 x 75 mm (2.56 x 2.95 in.). For the L-box test, a single bar was placed in the middle of the horizontal leg, instead of three bars that are typically employed for non-fibrous SCC. The blocking ratio (H2/H1) of the L-box was determined using the H1 and H2 values corresponding to the heights of the concrete at both ends of the horizontal leg of the device. For testing the FR-SCC, the standard J-ring test (ASTM C1621) [27] was modified to increase clearance between adjacent bars to 105 or 140 mm (4.13 or 5.51 in.) from the standard value of 42.9 mm (1.69 in.) for 16 bars. The difference in concrete height between the inner and outer sections of the J-ring (Δh), as suggested in Reference [27] was used to determine the passing ability of the FR-SCC, as indicated by Equation (25).

$$\Delta h = 2(b - c) - (a - b) \quad (25)$$

where a, b, and c are the concrete heights at the center, just inside, and just outside the bars, respectively, in the J-ring device as shown in Figure 2-16.

When the standard J-ring setup was used to evaluate the passing ability of the FR-SCC, considerable blockage of the concrete was observed given the limited spacing between the reinforcing bars. No clear relationship could be established between the J-ring spread and fiber factor, particularly for mixtures with V_f greater than 0.5%. The test was then

modified to reduce the number of bars in the J-ring from 16 to six or eight bars to allow a clear spacing between adjacent bars of at least 2.5 times the length of the fibers. This led to a better comparison of the performance of different fiber types and contents. When the concrete did not present blockage or segregation, the Δh J-ring passing ability index calculated according to Equation (25) resulted in low values for the modified J-ring test. For non-fibrous SCC, this indicates excellent passing ability. This was rather misleading for FR-SCC, however, where an increase in V_f resulted in some blockage and increased the difference in concrete height between the center and inside the bars of the J-ring, thus reducing the Δh index. It was noted that in most FR-SCC mixtures, the value of $2(b - c)$ was smaller than the $(a - b)$ value because the inclusion of fibers led to the decrease of flow diameter and increase in concrete height at the center. Therefore, the method of calculation of the difference in concrete height between the inner and outer parts of the J-ring was modified to better reflect the passing ability of the FR-SCC, as illustrated in Figure 2-16. The passing ability was evaluated using to Equation (26).

$$\Delta h = 2(b - c) - (a - d) \tag{25}$$

where d is the median height between a and b as shown in Figure 2-16.

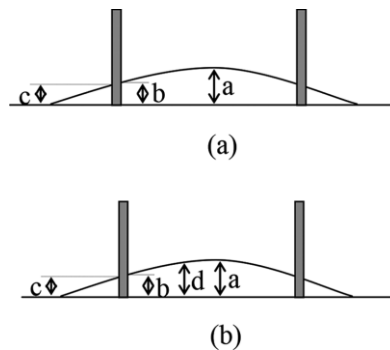


Figure 2-16: Diagram of parameters for calculation of J-ring (Δh) value proposed by: (a) Reference [27]; and (b) modified method (Equation (26)) [28]

As shown in Figure 2-17, the slump flow of FR-SCC decreases with the increase in fiber factor regardless of the fiber type. A distinction is observed between the response of FR-SCC made with synthetic fibers and that with steel fibers. For an equivalent fiber factor, FR-SCC made with steel fibers showed a greater reduction of slump flow compared with the synthetic fibers. This phenomenon may be due to the flexible fibers that can follow more easily the flow pattern than stiff steel fibers. Furthermore, the flexible synthetic fibers can fill the gap between aggregate particles rather than wedging them apart, as is the case for rigid steel fibers.

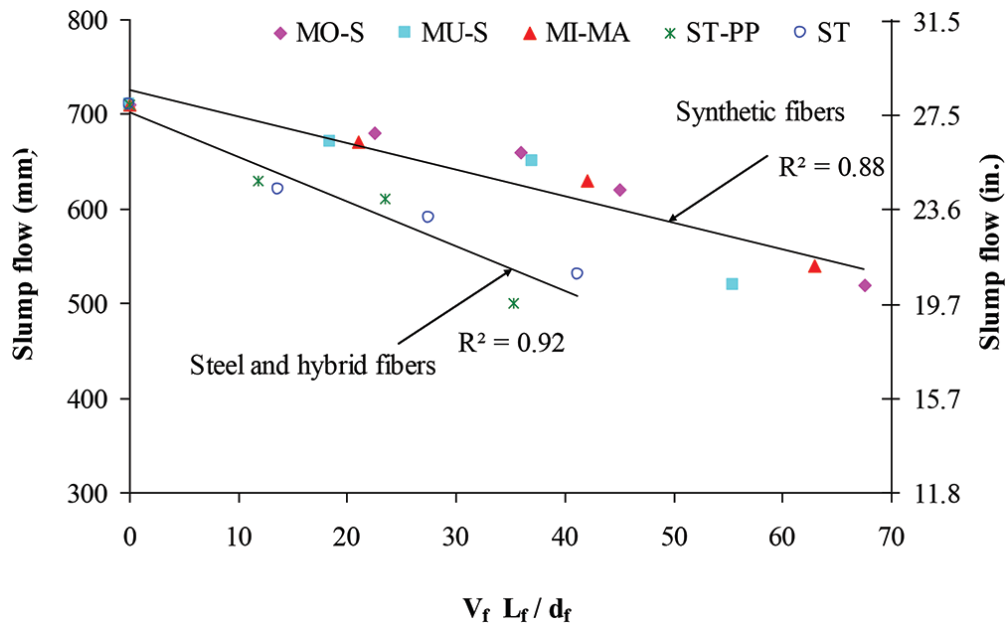


Figure 2-17: Slump flow variation versus fiber factor ^[28]

As it is the case for the filling ability, the passing ability of the concrete decreases with the increase in fiber factor. The V-funnel flow time increases with V_f regardless of fiber type, as shown in Figure 2-18. The inclusion of fibers increases internal friction and resistance to flow (viscosity). This case is more pronounced with mixtures containing

0.75% of discrete micro-synthetic fibers (MI-MA and ST-PP), which exhibited some blockage through the narrow opening of the V-funnel. A linear correlation can be established between the fiber factor and V-funnel flow time for mixtures containing 0.25 to 0.75% V_f . This relationship, however, does not consider the flow of the ST-PP, which seems to lead to some blockage given the high volume ratio of polypropylene microfibers. Both the ST-PP and MI-MA fibers incorporated at 0.5% V_f resulted in a similar V-funnel flow time of 7 seconds; an increase in V_f to 0.75% led to blockage of the flow.

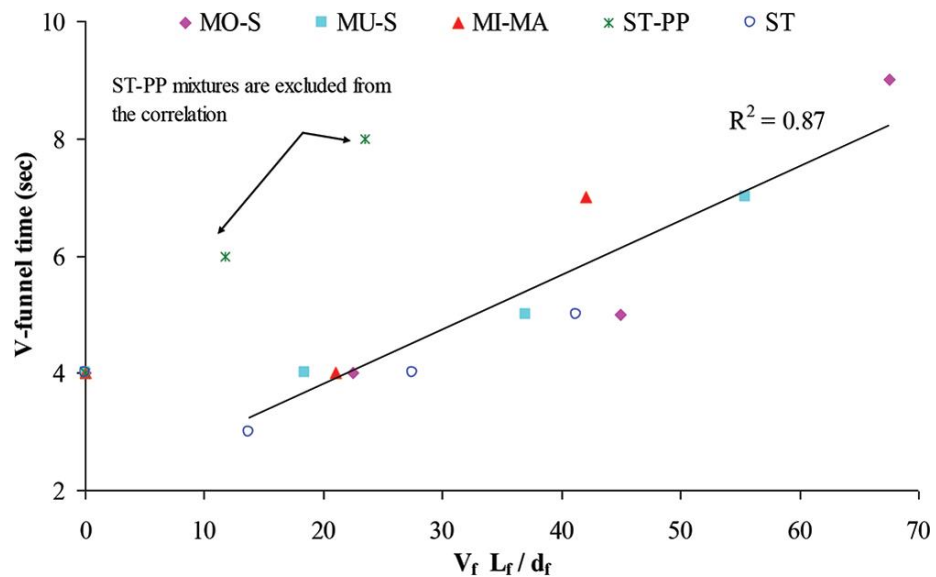


Figure 2-18: Variation in V-funnel flow time with fiber factor [28]

The H_2/H_1 values of FR-SCC were improved by 10% when a single bar was employed in the L-box test instead of three bars is typically employed for SCC. The omission of two reinforcing bars enabled better differentiation of the performance of different FR-SCC mixtures. Using a single bar in the L-box setup, the blocking ratio decreased with the increase in fiber factor Figure 2-19. As was the case for the slump flow, two linear

correlations can be established between the fiber factor and blocking ratio. The performance of the synthetic fibers was indeed different than that of the steel fibers and that of the hybrid fibers that contain 92% of metallic fibers, by mass.

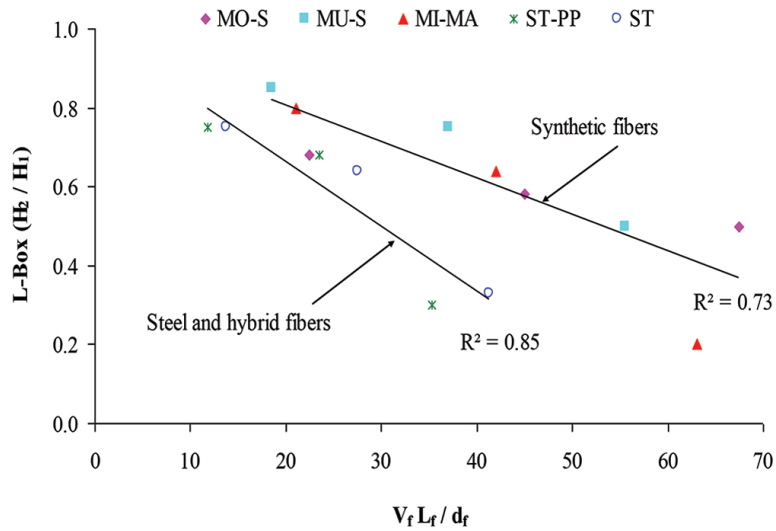


Figure 2-19: Variation of blocking ratio of modified L-box (one bar) with fiber factor [28]

The passing ability results evaluated according to Equation (25) are shown in Figure 2-20 and indicate linear correlations between the J-ring spread and fiber factor.

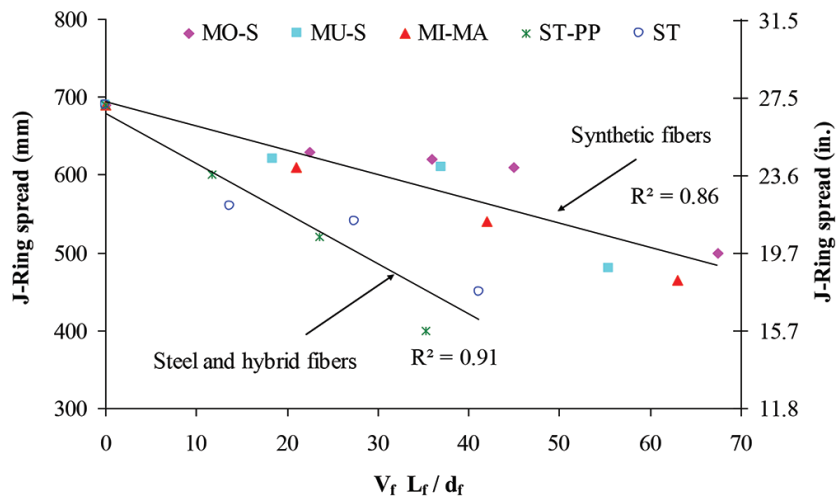


Figure 2-20: Modified J-ring flow (ring with six or eight bars) versus fiber factor [28]

An attempt was made to evaluate the passing ability of the FR-SCC regardless of the fiber type. This was done by calculating the ratio of the J-ring spread (D) to the height of concrete at the center of the J-ring (a). As shown in Fig 2-21, regardless of the fiber type, the D/a passing ability index decreases with the increase in fiber factor. This relationship includes FR-SCC mixtures with a V_f up to 0.75%. Good passing ability can be obtained when the D/a index is greater than 12, which corresponds to a V_f of 0.5% or less, regardless of the fiber type.

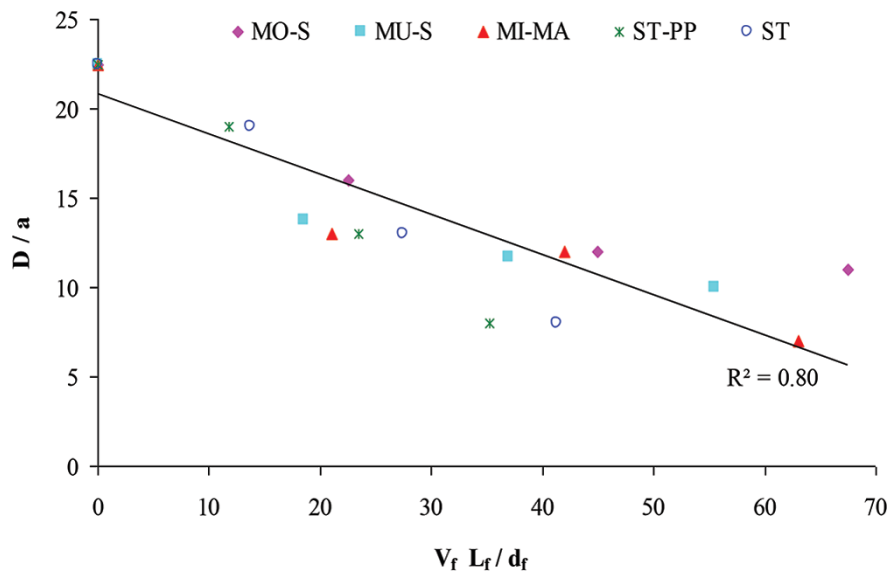


Figure 2-21: Diameter-height ratio (D/a) at center of modified J-ring test versus fiber factor ^[28]

2.5 Fiber dispersion and orientation monitoring in fiber-reinforced self-consolidated concrete

In most of the surveyed investigations, fiber dispersion and orientation were monitored by distractive way, which is manually counting the fibers on selected specimen locations. Manual counting is rather easy when low dosages of longer fibers

with average aspect ratios are used. On the other hand image analysis techniques are required for higher dosages of shorter fibers.

Different non-distractive tests were followed in order to monitor the fiber dispersion and orientation. These methods are summarized below:

1. X-ray pictures of cores or of thin slices obtained by sawing the specimens (the sample thickness is dictated by the absorption properties of the material and power of the X-ray equipment) were also taken in several investigations. Ferrara and Meda (2006) [29] investigated the fibre distribution within 40 precast pre-stressed roof elements using X-ray pictures of cores as shown in Figure 2-22.

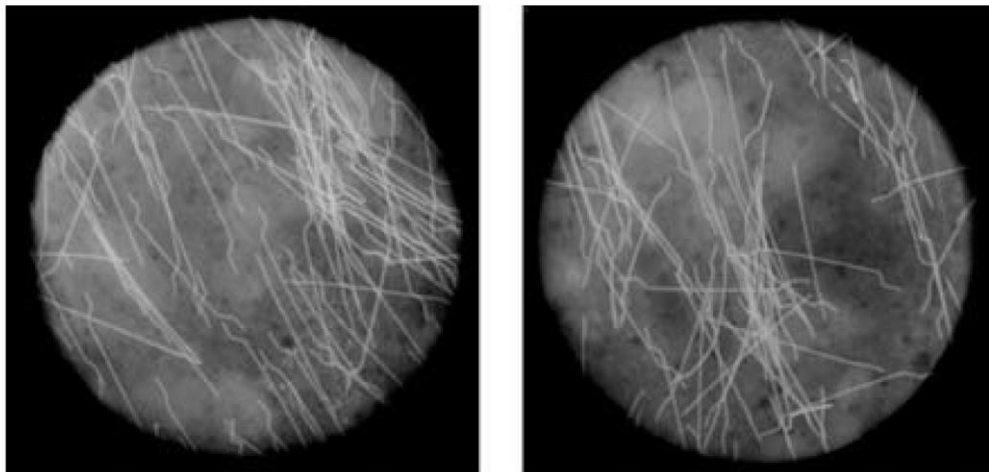


Figure 2-22: X-ray pictures of cores from precast pre-stressed roof elements [29]

2. Electrical methods, based on the effects of the fibers on the resistivity/conductivity of the composite material, has received lots of attention in the very last years. Ozyurt et. al. [30] used the Alternate Current Impedance Spectroscopy (AC-IS) for the detection of fiber dispersion and orientation. The

method is based on the frequency-dependent behavior of cementitious composites reinforced with conductive fibers, such as steel and carbon ones. These were in fact shown to be practically insulating under Direct Current (DC) and low frequencies Alternate Current (AC) while they are conductive under high frequencies AC. The method consists of applying to the specimen a voltage excitation over a range of frequencies (e.g. 10 MHz-1Hz) and measuring the amplitude and phase of the flowing current. When the real and imaginary parts of the calculated impedance Z are plotted on a Nyquist diagram, fiber reinforced cementitious composites exhibit what called dual-arc behavior (Figure 2-23). It features a low-frequency cusp (fibers act insulating), which gives the (higher) resistance of the matrix, R_m , and a high frequency cusp (fibers are conductive), which corresponds to the (lower) resistance of the fiber reinforced composite R . In order to overcome the drawback of the sensitivity of the resistivity of the concrete matrix to moisture conditions, the so-called matrix normalized conductivity is used, from which information about local fiber concentration should be easily obtained by means of a simple mixture rule approach:

$$\frac{R_m}{R} = \frac{S}{S_m} = 1 + [S_{\text{fibers}}] V_f \quad (26)$$

Where σ and σ_m are the conductivity of the fiber reinforced composite and of the matrix respectively, $[\sigma_{\text{fibers}}]$ is the intrinsic conductivity of the fibers and V_f is the fiber volume fraction.

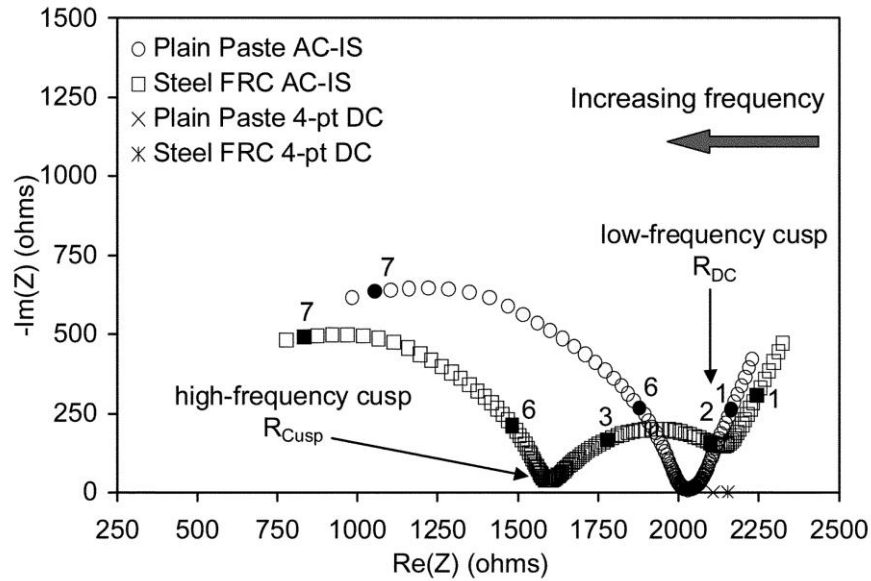


Figure 2-23: Typical Nyquist plot for plain paste and fiberreinforced composites with frequency markers (log of frequency in Hz as darkened points). [30]

- Lataste et al. [31] employed a method based on low frequency resistance measurements, with a four-electrode arrangement, aimed at reducing the effects of the poor electrical coupling. Figure 2-24 shows the recorder and switch system device as well as the four-electrode arrangement. The method has been demonstrated to be effective in detecting orientation characteristics of the discrete dispersed fiber reinforcement, because of the different resistance measured along the two directions at right angle to each other. The method is not able to provide any quantitative information about the local average concentration of the fibers. This is mainly due to the uncertainty in the assessment of the concrete matrix resistivity, because of its strong sensitivity to aging, moisture content and presence of electrolytes in the pores which also affect the measured resistivity beside the effects of fiber concentration [Ferrara [32]].

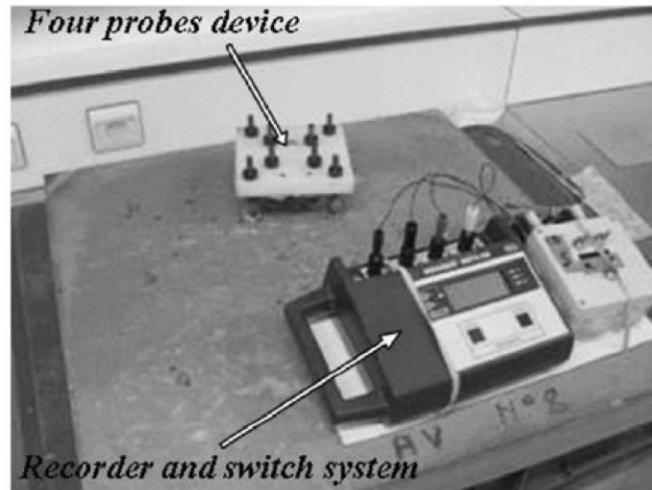


Figure 2-24: View of the measurement device and the four-electrode arrangement

4. Damme et. al. (2004) [33] presented a microwave nondestructive testing technique to measure the steel fiber content in hardened concrete slabs. The technique is based on an open-ended coaxial probe reflectometry method for measuring the effective permittivity of the steel fiber reinforced concrete and on a classical homogenization approach for determining the fiber content. Assuming a random orientation could assess the local average concentration of fibers and because of the known fiber geometry (aspect ratio) that governs their capacitive behavior: as a matter of fact the method is unsuitable for FR-SCC featuring a preferential alignment [Ferrara [32]].

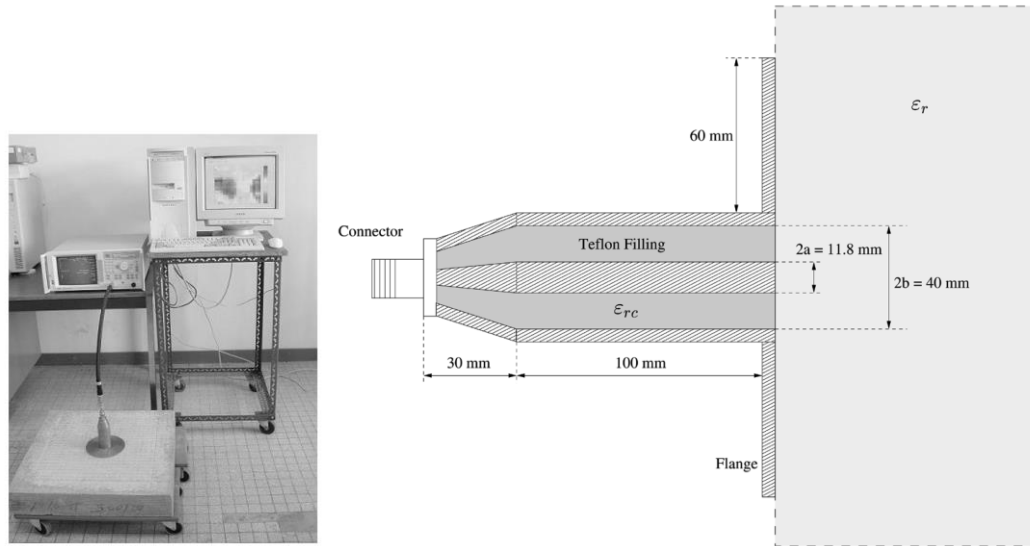


Figure 2-25: Experimental setup and a model configuration with flanged open-ended coaxial probe [33]

5. Faifer et. al. (2011) [34] proposed and validated new method which employs a probe sensitive to the magnetic properties of the steel fibers. The fundamentals of the method rely on the fact that the presence and relative position of the fibers in a fiber reinforced concrete element modify the magnetic circuit of the employed probe, when placed on the element/structure surface, thus resulting in a variation of the measured inductance. Both fiber concentration and fiber preferential orientation can be estimated using such method. Figure 2-26 shows a Layout of the magnetic probe over a fiber-reinforced concrete surface.

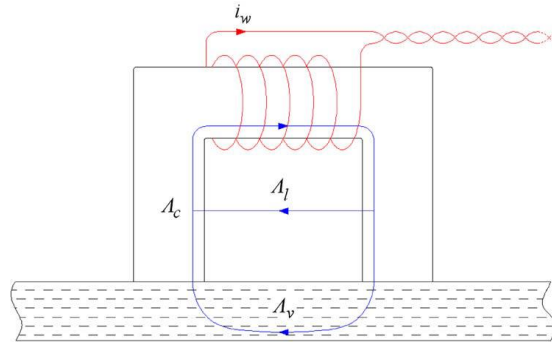


Figure 2-26: Layout of the magnetic probe.

6. Methods based on the study of heat transients and hence on the effect of fibers on the thermal properties of concrete have been also tentatively applied for the non-destructive assessment of fiber concentration. Temperature fields within a structural element can be surveyed through IR thermography. Figure 2-27 shows a nice 3D visualization of the fiber arrangement within a specimen, by means of Computed Axial Tomography (CAT) scanning [Felicetti and Ferrara (2008)] [35].

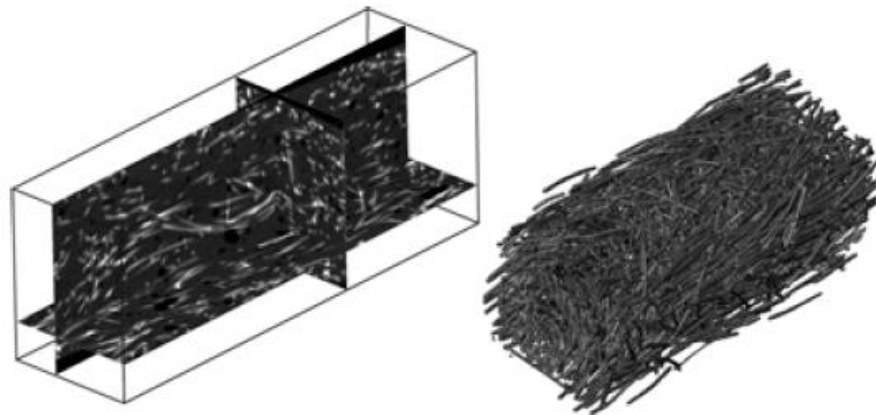


Figure 2-27: Three different orthogonal slices through a reconstructed FRC specimen from a CT-scan and 3D reconstruction of the steel fibers only [36]

2.6 Rheology of fiber-reinforced self-consolidated concrete

Martinie et. al. (2010) [37] studied the effect of rigid straight fibers on the yield stress of cementitious materials. Ten different types of fibers were used with cement paste. Figure 2-28 shows the 10 different types of fibers tested in that study. The properties of the fibers are presented in Figure 2-29. The other tested yield stress of the suspensions using a Haake viscotester VT550 and a Vane test procedure. The diameter of the Vane tool was 4 cm while the diameter of the bowl was 10 cm. The gap between the vane tool blades and the outerwall of the testing bowl was therefore 40 mm large. The height of material of the bowl was 10 cm. Both dynamic (or intrinsic) yield stress (just after mixing) and static (or apparent) yield stress (after rest) were measured to check the sensitivity of the mixture to resting time. Their results showed that there is a critical value of ϕ_f and r , where ϕ_f is the fiber volume and r is the aspect ratio of the fiber, above which fibers should tend to form clumps or balls and entrap air in the mixture. As shown in Figure 2-30 there is three consistencies of a fiber-reinforced cement paste:

- If the fiber volume fraction (ϕ_f) is far lower than $\phi_{fc}=3.2/r$, the influence of the fibers on the rheological behavior of the cementitious material should be low (Figure 2-30 (a)). As soon as ϕ_f gets close to $\phi_{fc}=3.2/r$, the influence of the fibers on the rheological behavior starts to dominate all other effects.
- For fiber volume fractions between $\phi_{fc}=3.2/r$ and $\phi_{fm}=4/r$, the behavior of the cementitious material is strongly dominated by the contact network between the fibers (Figure 2-30 (b)). The material is far stiffer than its constitutive cement paste.

- For fiber volume fractions higher than $\phi_{fm}=4/r$, the material should not be able to flow any more (Figure 2-30 (c)). Fibers should form balls and air should be entrained in the mixture.

Martinie [37] defined the total relative volume fraction as the sum of the relative volume fraction of the fibers and the relative volume fraction of the granular skeleton $\phi_f r/4+\phi_s/\phi_m$ where ϕ_s and ϕ_m are respectively the volume fraction and the dense packing fraction of the sand. Figure 2-32 shows the relative yield stress (i.e. the ratio between the yield stress of the fiber reinforced material and the yield stress of the constitutive cement paste) as a function of the total relative packing fraction of inclusions (sand and fibers). We measured the dense packing fraction of our naturally rounded sand and obtained a value equal to 68%. The amount of sand in the mixtures was kept constant, while the amount of fibers was varied. The sand contributed to the value of the relative packing fraction up to 0.65.

If the total relative packing fraction defined above is higher than 100%, fibers should tend to form clumps or balls and entrap air in the mixture. The material will not be flowable. This means that the value of $\phi_f r/4+\phi_s/\phi_m$ should stay lower than 1. The maximum amount of fibers $(\phi_f)_{max}$ in the mixture to prevent this from happening is defined by Equation (27).

$$\phi_{f_{max}} = \frac{400}{r} \left(1 - \phi_s/\phi_m \right) (in\%) \quad (25)$$

Where r is the aspect ratio of the fibers, ϕ_s is the packing fraction of sand in the mixture and ϕ_m is the dense packing fraction of the sand (of order 65% for a rounded sand). Eq. (6) captures the fact that it is possible to increase the fiber volume fraction in a given material by reducing the aspect ratio of the fiber, by reducing the packing fraction of granular skeleton or by choosing a sand displaying a higher dense packing fraction (i.e. naturally rounded sand instead of crushed sand for instance). If the total relative packing fraction $\phi_{fr}/4 + \phi_s/\phi_m$ is between 0.8 and 1, it can be considered that the mixture is optimized. If it is close to 1, it will probably be a firm mix as the contact network between fibers and aggregates will strongly diminish the ability to flow of the material. If it is close to 0.8, it will be possible to obtain a very fluid mix (even self compacting) by designing a fluid cement paste through the variation of the super-plasticizer dosage as the contribution of the direct contacts between aggregates and fibers to the consistency of the mix will be low.



Figure 2-28: Different fibers tested [37]

Length (mm)	Thickness (mm)	Aspect ratio	Shape
3	0.175	17	Straight
5	0.2	25	Straight
5	0.15	33	Straight
10	0.2	50	Straight
42	0.8	52.5	Hooked end
55	1	55	Large end
15	0.25	60	Straight
20	0.25	80	Straight
25	0.3	83	Hooked end
30	0.3	100	Hooked end

Figure 2-29: Properties of the fibers tested [37]

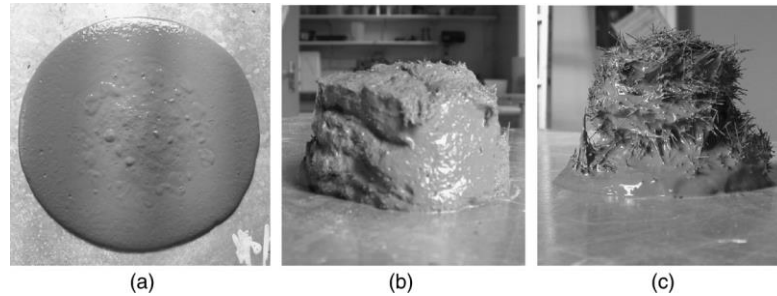


Figure 2-30: Consistency of a cement paste (water to cement ratio 0.4) mixed with fibers with various aspect ratios. (a) $\phi_f r/\alpha_m=0.18$; (b) $\phi_f r/\alpha_m=0.83$; (c) $\phi_f r/\alpha_m=1$ [37]

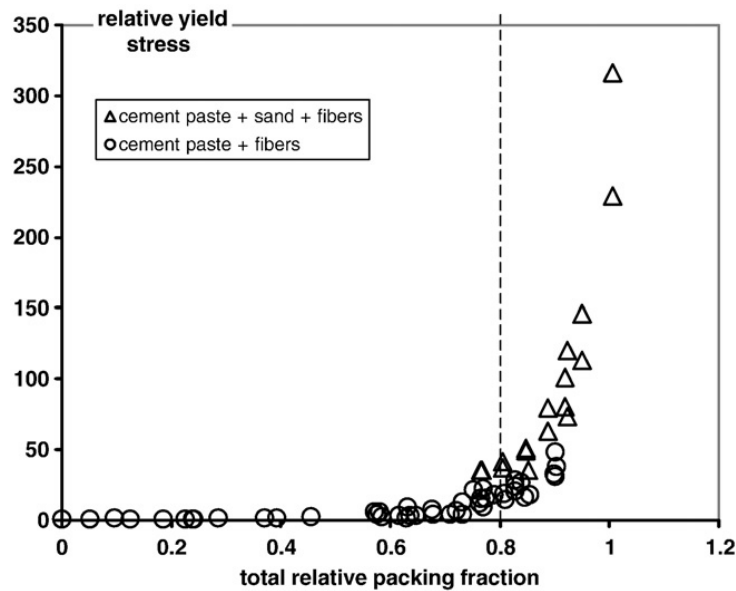


Figure 2-31: Relative yield stress as a function of the total relative packing fraction. The dashed line corresponds to the theoretical random loose packing. [37]

2.7 Mechanical properties of fiber-reinforced self-consolidated concrete

Khaloo et. al. [2014] [38] investigated the influence of steel fibers on rheological and mechanical properties of SCC with different strength classes. They used Steel fibers with hooked end with fiber length 20.6 mm, width 1.8 mm and thickness 0.5 mm (aspect ratio=20). Various fiber volume fractions of 0.5%, 1%, 1.5%, and 2% were used based on the mortar volume of SCC. Two strength classes of SCC; 40 MPa (MS) and 60 MPa (HS) were investigated. They concluded that:

(1) Addition of fibers decreases the workability as well as the passing ability of SCC as shown in Figures 2-32 and 2-33 respectively, especially with high fiber volume (2%).

(2) Addition of fibers decreases the compressive strength. In case of MS concrete addition of 2% fiber volume decreases the compressive strength by 18.5% as well as HS concrete by 7.5%.

(3) Addition of fibers increases the splitting tensile strength of the SCC specimens. Steel fibers enhance the splitting tensile strength through bridging the gap between two sides of crack opening. Addition of 2% fiber volume fraction improved splitting tensile strength by 28.5% and 17.1% with respect to the medium and high strength plain specimens, respectively.

(4) Addition of fibers increases the ultimate load capacity of the SCC beams, and it leads to an increase in the flexural strength

(5) Flexural toughness of the SCC beams increases by increasing the percentage of fibers. Steel fibers tend to increase the flexural toughness and in turn enhance the ductility of concrete elements. In low fiber volume fractions (0.5% and 1%), beams made

with medium strength SCC had more flexural toughness compared to beams made with high strength SCC class, because high strength SCC is more brittle, and fibers cannot enhance the ductility of SCC due to low amount of incorporated fiber in the matrix. However, for specimens with high fiber volume fractions (1.5% and 2%), beams with medium strength SCC class had lower flexural toughness.

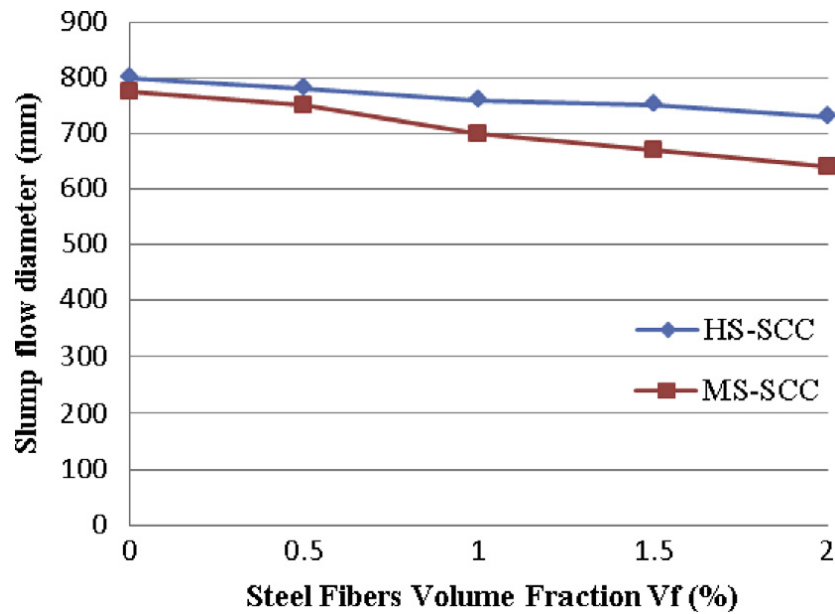


Figure 2-32: Slump flow diameter as function of fibers content ^[38]

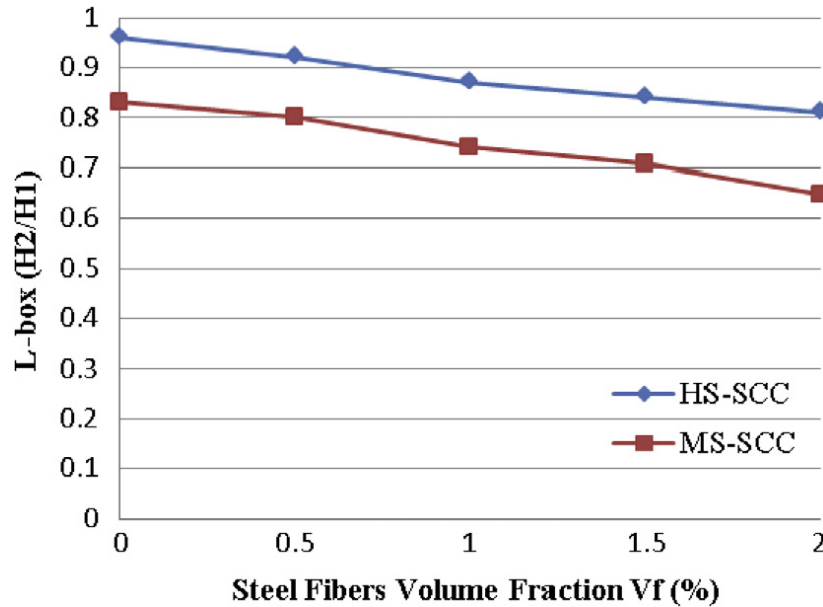


Figure 2-33: Variation of blocking ratio with increasing the percentages of steel fibers ^[38]

Khayat et al. (2014) [23] evaluated the mechanical properties of FR-SCC. The investigated fibers included polypropylene, steel, and hybrid fibers of different properties with fiber lengths of 5 to 50 mm. Fiber volume ranged between 0.25 and 0.75%. The polypropylene fibers included a straight monofilament fiber (MO-S), a kinked multifilament fiber (MU-S), and a combined 80% macro-crimped fiber and 20% tissue-based micro-fiber (MI-MA). The aspect ratios of these fibers are 90, 74, and 84, respectively. Hybrid steel-polypropylene fibers (ST-PP) with 92 and 8% relative mass and a steel fiber (ST) were also employed. The aspect ratios of the hybrid and steel fibers are 47 and 55, respectively. They tested the hardened properties included compressive, splitting tensile, and average residual strengths. They concluded that:

(1) By increasing the V_f from 0 to 0.25% and 0.5% results in an increase of 8 to 28% in compressive strength (f'_c). More increasing in V_f to 0.75% results in strength reduction of the fiber-reinforced super-workable concrete (FR-SWC) made with MO-S or ST fibers. This was not the case, however, for the MU-S, MI-MA, and ST-PP fibers that displayed similar or higher strength than SCC. Strength reduction can be due to the lack of proper consolidation as concrete cylinders were cast in one lift without any mechanical consolidation. The f'_c of FR-SCCs with V_f of 0.25 and 0.5% is higher than those of the reference SCC.

(2) The addition of fibers is also increases the splitting tensile strength (f'_{sp}) by 7 to 50%.

(3) The Average residual strength (ARS) was measured according to ASTM C1399 [39]. Figure 2-34 presents an increase in residual strength with the increase in fiber factor for different fiber types. Fibers with the highest elastic modulus and tensile strength (ST and ST-PP) yielded the best ARS, regardless of the V_f .

(4) The MU-S and ST fibers exhibit the best overall performance given their superior plastic and hardened properties, respectively. The MO-S has the lowest overall performance, mainly due to its low compressive and splitting tensile strengths.

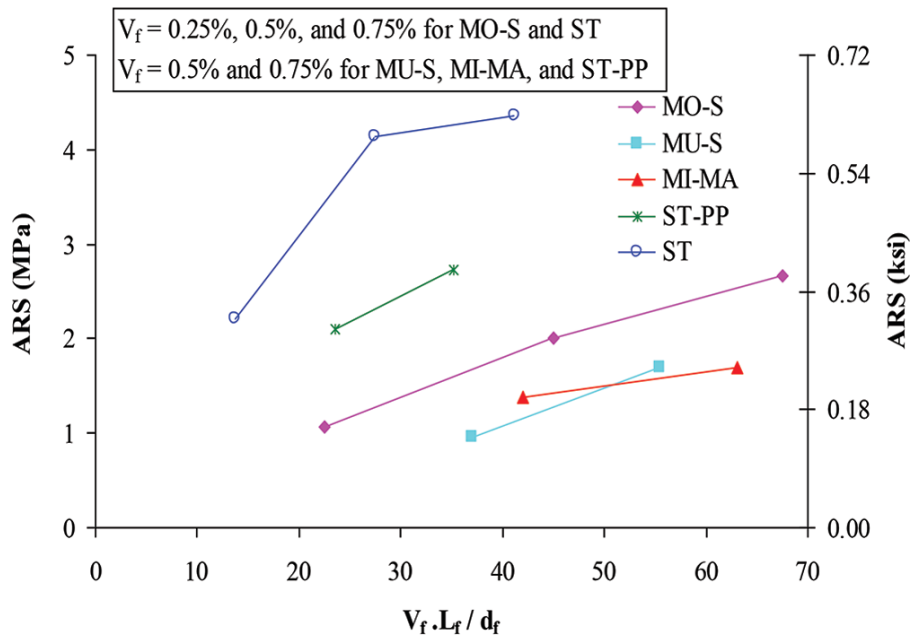


Figure 2-34: Increase in residual strength with increase in fiber factor for different fiber types^[38]

2.8 Shrinkage of fiber-reinforced self-consolidated concrete

Concrete is subjected to changes in volume either autogenous or induced. Volume change is one of the most detrimental properties of concrete, which affects the long-term strength and durability. To the practical engineer, the aspect of volume change in concrete is important from the point of view that it causes unsightly cracks in concrete. Shrinkage can be classified depending on its mechanism into:

- Plastic Shrinkage

Shrinkage of this type takes place soon after the concrete is placed in the forms while the concrete is still in the plastic state. Loss of water by evaporation from the surface of concrete or by the absorption by aggregate or subgrade is believed to be the reasons of plastic shrinkage. The loss of water results in the reduction of volume. The

aggregate particles or the reinforcement comes in the way of subsidence due to which cracks may appear at the surface or internally around the aggregate or reinforcement.

- Drying Shrinkage

Just as the hydration of cement is an ever-lasting process, the drying shrinkage is also an ever-lasting process when concrete is subjected to drying conditions. The drying shrinkage of concrete is analogous to the mechanism of drying of timber specimen. The loss of free water contained in hardened concrete, does not result in any appreciable dimension change. It is the loss of water held in gel pores that causes the change in the volume. Under drying conditions, the gel water is lost progressively over a long time, as long as the concrete is kept in drying conditions. Cement paste shrinks more than mortar and mortar shrinks more than concrete. Concrete made with smaller size aggregate shrinks more than concrete made with bigger size aggregate. The magnitude of drying shrinkage is also a function of the fineness of gel. The finer the gel the more is the shrinkage.

- Autogeneous Shrinkage

In a conservative system i.e. where no moisture movement to or from the paste is permitted, when temperature is constant some shrinkage may occur. The shrinkage of such a conservative system is known as autogeneous shrinkage. Autogeneous shrinkage is of minor importance and is not applicable in practice to many situations except that of mass of concrete in the interior of a concrete dam.

- Carbonation Shrinkage

Carbon dioxide present in the atmosphere reacts in the presence of water with hydrated cement. Calcium hydroxide $[Ca(OH)_2]$ gets converted to calcium carbonate and also some other cement compounds are decomposed. Such a complete decomposition of calcium compound in hydrated cement is chemically possible even at the low pressure of carbon dioxide in normal atmosphere. Carbonation penetrates beyond the exposed surface of concrete very slowly. The rate of penetration of carbon dioxide depends also on the moisture content of the concrete and the relative humidity of the ambient medium. Carbonation is accompanied by an increase in weight of the concrete and by shrinkage. Carbonation shrinkage is probably caused by the dissolution of crystals of calcium hydroxide and deposition of calcium carbonate in its place. As the new product is less in volume than the product replaced, shrinkage takes place.

Drying Shrinkage is the most effective shrinkage and it can be classified into unrestrained drying shrinkage and restrained shrinkage. Unrestrained drying shrinkage is accompanying by reduction in dimensions, while restrained drying shrinkage is accompanying by cracking.

2.8.1 Drying Shrinkage

2.8.1.1 Different models of drying shrinkage

The available shrinkage prediction models for concrete are mostly based on ACI 209 and CEB-FIP models. Other models (AASHTO LFRD model, GL model, B3 model and SAKATA model (1993)) are derived from these models by incorporating additional

parameters and modifications. ACI 209 and CEB-FIP models will be discussed in this section.

1. ACI 209 model [40]

$$\varepsilon_{sh}(t, t_c) = (\varepsilon_{sh})_u \frac{(t - t_c)}{T_c + (t - t_c)} \quad (26)$$

where: $(\varepsilon_{sh})_u$ is the ultimate strain of drying shrinkage (equal to 780 for standard conditions), T_c is 35 days for moist cured concrete and 7 days for steam cured concrete, t_c is 7 days for moist cured concrete (case of the present study) and 1 to 3 days for steam cured concrete.

The standard conditions of this model are:

- 7 days of moist cured concrete (or 1 to 3 days of steam cured concrete)
- Drying at 40% of RH
- 150 mm is the thickness of the member (or volume-to-surface ratio of 38 mm)
- Temperature of 21 °C

Correction factors are applied for conditions other than standard conditions [ACI 209, 1992; and GOEL et al. 2006 [41]]. In ACI 209 [1992], FANOURLAKIS et. al. [2003] [42], and SCHINDLER et al. [2007] [43] the correction factors for conditions other than standard conditions of concrete are described in detail.

2. CEB-FIP model

$$\varepsilon_{cso} = \varepsilon_s(f_{cm})(\beta_{RH}) \quad (27)$$

$$\varepsilon_s(f_{cm}) = [160 + 10\beta_{SC} (9 - 0.1f_{cm})]$$

$$\times 10^{-6} \sqrt{\frac{(t - t_c)}{\left\{ 350 \left(\frac{2A_c}{100\mu} \right)^2 + (t - t_c) \right\}}} \quad (28)$$

$$\beta_{SC} = \begin{cases} 4 & \text{for slow hardening cement SL (Type I and V)} \\ 5 & \text{for normal or rapid hardening cements N and R (Type I and III)} \\ 8 & \text{for rapid hardening high strength cements RS} \end{cases} \quad (29)$$

$$\beta_{RH} = \begin{cases} -1.55 \beta_{ARH} & \text{for } 40\% \leq RH \leq 99\%, \text{ stored in air} \\ 5 & \text{for normal or rapid hardening cements N and R (Type I and III)} \end{cases} \quad (30)$$

$$\beta_{RH} = 1 - (RH/100) \quad (31)$$

where: ε_{cso} : drying shrinkage of Portland cement concrete (mm/mm); $\varepsilon_s(f_{cm})$: Drying shrinkage obtained from RH-shrinkage chart; β_{RH} : coefficient incorporating the effect of RH on ultimate shrinkage; RH : Relative humidity; t : age of concrete at time of observation (days); t_c : age of concrete at which shrinkage initiated, i.e. end of curing (days); β_{SC} : Coefficient which depends on the type of cement; A_c : section cross area (mm); μ : perimeter of the component in contact with air (mm); f_{cm} : concrete mean compressive strength at 28 days (MPa);

The standard conditions of this model are:

- Ordinary structural concretes
- 28-day mean cylinder compressive strength varying from 12 to 80 MPa
- Mean RH of 40-100%
- Mean temperature of 5 to 30 °C

2.8.1.2 Drying shrinkage of fiber-reinforced self-consolidated concrete

Kassimi and Khayat (2010) [44] compared the measured drying shrinkage results of fiber-reinforced self-consolidating concrete (FR-SCC) to values obtained from various shrinkage prediction models. They investigated 15 FR-SCC mixtures. They used five fiber types (synthetic, steel, and hybrid fibers) of different characteristics. The fiber volume ranged between 0.25% and 0.75% for the FR-SCC. They monitored the drying shrinkage for 13 months at 50% relative humidity. Prismatic specimens measuring 75×75×285 mm were prepared to evaluate drying shrinkage in accordance to ASTM C 157 [44]. Then they compared the drying shrinkage results to values that can be predicted from various shrinkage models, including the AASHTO LFRD (2007) [45], ACI 209 (1992), CEB- FIP (1990) [46], Gardner-Lockman (2000) [47], Bažant B3 (1995b) [48], and Sakata (1993) [49] models that are proposed for conventional, non-fiber-reinforced concrete. The AASHTO 2004 model, modified by Khayat and Long (2010) (KL2010 model) [50] proposed for self-consolidating concrete (SCC) is also considered. They modified the shrinkage models to fit the test results of the fibrous mixtures. This was carried out by introducing correction factors that take into consideration the use of SCC and fibers. Table 2-1 shows the original shrinkage models used to compare with the monitored values.

Table 2-1: Original shrinkage models ^[44]

Model	Equation
ACI 209	$\varepsilon_{sh}(t, t_c) = (\varepsilon_{sh})_u \frac{(t - t_c)}{T_c + (t - t_c)}$; T_c and t_c : time (day) related to curing method.
AASHTO 2007	$\varepsilon_{sh} = -k_{vs}k_{hs}k_fk_{td}0.48 \times 10^{-3}$; k_{vs} : factor for the effect of the volume-to-surface ratio of the component; k_{hs} : humidity factor; k_f : factor for the effect of concrete strength; k_{td} : time development factor.
CEB-FIP 90	$\varepsilon_{cso} = \varepsilon_s(f_{cm})(\beta_{RH})$; $\varepsilon_s(f_{cm})$: drying shrinkage obtained from (RH) shrinkage chart; β_{RH} : coefficient incorporating the effect of RH on ultimate shrinkage.
B3	$\varepsilon_{sh}(t, t_c) = -\varepsilon_{shu}k_hS(t)$; ε_{shu} : ultimate shrinkage; k_h : factor depends on RH; $S(t)$: time function for shrinkage.
GL2000	$\varepsilon_{sh}(t - t_c) = \varepsilon_{shu}\beta(h)\beta(t)$; ε_{shu} : notional ultimate shrinkage strain; $\beta(h)$: correction term for effect of humidity on shrinkage; $\beta(t)$: correction term for the effect of time on shrinkage.
Sakata 1993	$\varepsilon_{sh}(t, t_0) = \varepsilon_{sh\infty} [1 - \exp\{-0.108(t - t_0)^{0.56}\}]$; $\varepsilon_{sh\infty}$: ultimate shrinkage strain; t_0 : time drying started (day).
Khayat and Long (2010)	$\varepsilon_{sh} = -k_c k_s k_h \left(\frac{t}{35 + t} \right) \times 0.51 \times 10^{-3}$ (moist-cured); k_c : cement factor proposed for AASHTO 2004 model; k_s : size factor; k_h : humidity factor. In this paper, the AASHTO 2004 is used with a proposed cement factor of 0.918, which corresponds to the characteristics of normal-set cement.

For each set of shrinkage data and for each model, statistical software that was employed (LAB Fit) considers a factor, which would give the closest theoretical fitting to the experimental data. For each model, the individual A_i factors for each mixture are then used to determine a mean correction value (A). An example of this approach is given in Figure 2-35 for one FR-SCC mixture where the modified AASHTO 2007 model given a correction factor A_i is used to ensure better fitting of the data. The mean correction factors for a given model (A) are given in Figure 2-37. Linear correlations between measured and predicted shrinkage values in terms of slope of the correction and the

correlation factor (R) for the investigated FR-SCC and FR-SCM mixtures are also indicated in Figure 2-36.

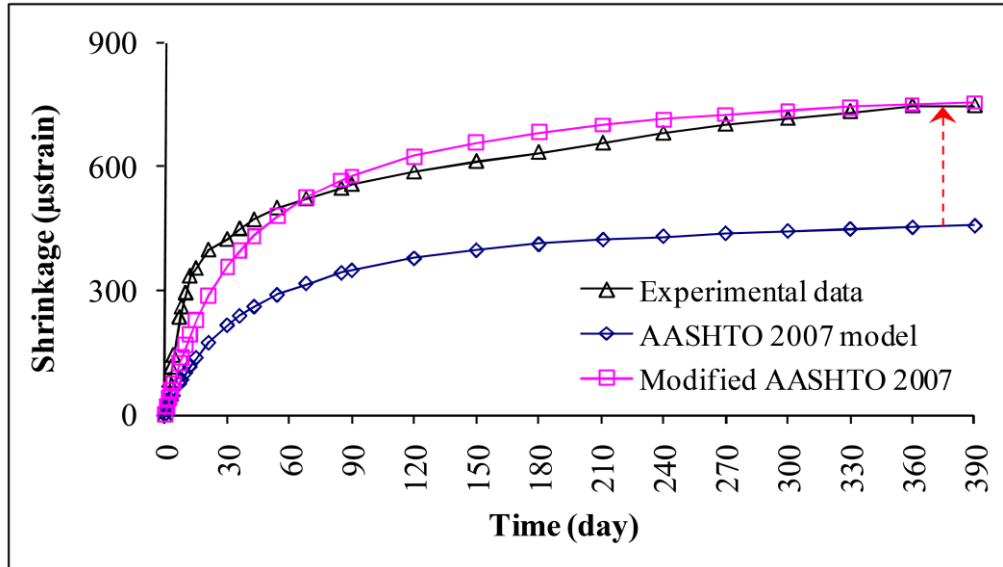


Figure 2-35: Divergence between predicted and modified shrinkage (MO-S 0.3% mixture) ^[44]

	N*	Prediction model		Modified model		
		Slope	R	Slope	R	A**
FR-SCC						
AASHTO 2007	15	0.76	0.93	1.33	0.98	1.71
ACI 209		1.11	0.91	1.28	0.97	1.02
B3		0.75	0.86	0.79	0.92	0.97
CEB-FIP		0.62	0.92	0.94	0.98	1.45
GL2000		0.87	0.92	0.89	0.97	0.96
KL2010		0.97	0.89	1.17	0.97	1.13
Sakata		1.38	0.91	1.12	0.99	0.77

Figure 2-36: Predicted vs. measured shrinkage values determined using various models before and after modifications of the drying shrinkage models ^[44]

As shown in Figure 2-37 with the use of the proposed correction factors (A) for each of the seven investigated shrinkage models, a much better predicting of the shrinkage data of FR-SCC is established.

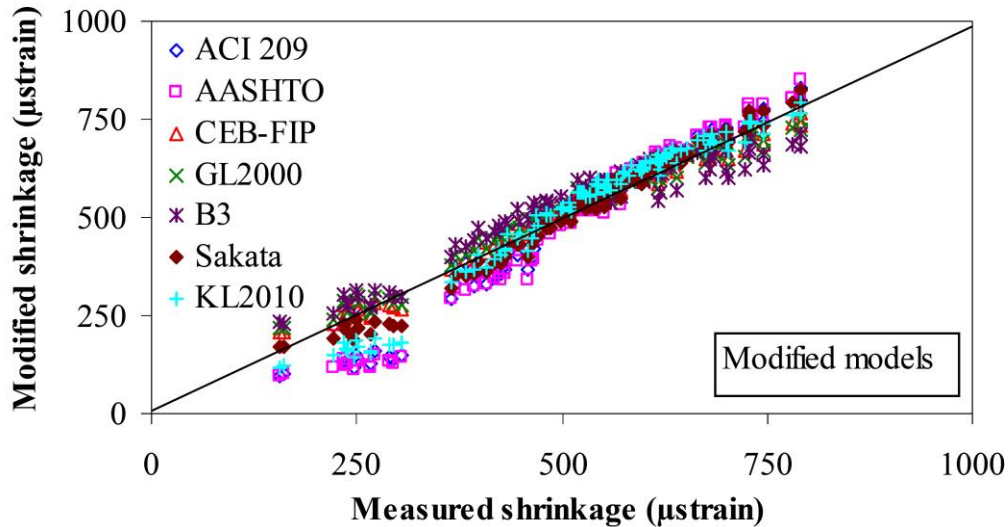


Figure 2-37: Shrinkage prediction of FR-SCC mixtures using the seven modified models^[44]

Kassimi and Khayat [51] mentioned also that the modified Sakata model followed by the modified CEB-FIP model provided the best overall prediction of the shrinkage results of the FR-SCC.

2.8.1.3 Restrained shrinkage of fiber-reinforced self-consolidated concrete

Kassimi and Khayat (2010) [51] compared the potential of reducing cracking of various SCC and FR-SCC mixtures with 0.42 w/c. Shrinkage mitigation measures included the use of fibers and/or a shrinkage-reducer admixture (SRA) or an expansive agent (EA). In total, 13 mixtures were investigated using the ring test method (ASTM C 1581) [52]. Four reference mixtures were prepared, including a non-fibrous SCC mixture,

two SCC mixtures with polypropylene and steel fibers incorporated at 0.5% by volume. The four mixtures were also prepared with the addition of SRA or EA. The SRA and EA contents were 2% and 6% of the cementitious materials, by mass, respectively. Fibers used in this investigation included kinked multifilament synthetic fibers (MU-S) and hooked-end steel fibers (ST) with lengths of 50 and 30 mm and aspect ratios of 74 and 55, respectively. Figure 2-38 shows the development of ring strains for some mixtures during drying. The t_{cr} values are also indicated. Figure 2-39 shows time for cracking of the investigated mixtures as well as the drying shrinkage micro strain. They mentioned that the incorporation of fibers provided similar or less drying shrinkage (ϵ_u) (reduction of up to 8%) than the reference SCC made without any fibers. The incorporation of MU-S fiber did not affect t_{cr} . While, the incorporation of ST fiber delayed t_{cr} by 150% compared to the reference SCC. This is due to the lower ϵ_u and due to the effect of anchorage of the hooked ends resisting to fiber slipping from the cementitious matrix. Generally, fibers reduced w_{cr} by 40% and 50% for MU-S and ST types, respectively compared to the reference SCC. The introduction of EA in SCC mixtures containing MU-S and ST fibers permitted a reduction in ϵ_u by 17-37%, an enhancement in t_{cr} by 330% and 627% and a reduction in w_{cr} by 37% and 70%, respectively, compared to SCC mixture containing EA without any fibers. The combination of ST fibers and EA provided the lowest cracking potential (t_{cr} of 35.6 days and the smallest w_{cr} of 83 μm) amongst all of the investigated mixtures. For the SCC with ST fibers and EA, cracks did not lengthen along the ring height. There is a synergetic effect of the following ingredients on cracking potential: fibers-SRA, fibers-EA, and fibers-SRA-EA. The longer

t_{cr} is, the narrower is the w_{cr} for the investigated mixtures (R^2 of 0.58). The relationship is better when only the fibrous mixtures are considered (R^2 of 0.82), as indicated in Fig 2-40.

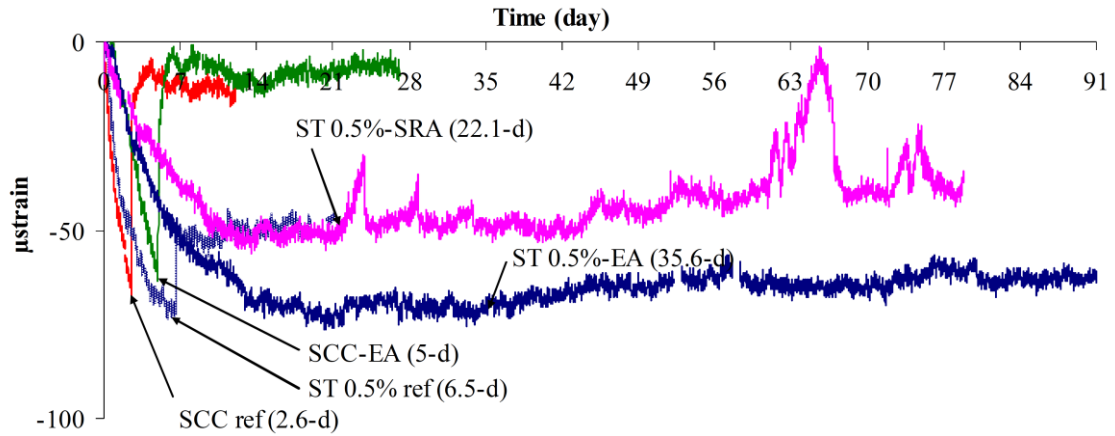


Figure 2-38: Development of strains in the inner ring due to concrete contraction [51]

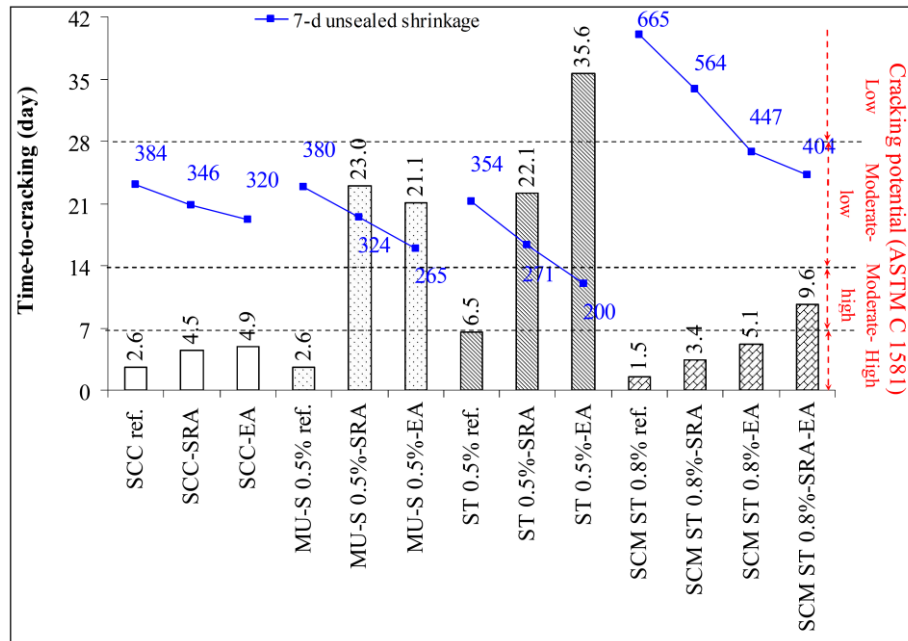


Figure 2-39: Time for cracking of the investigated mixtures [51]

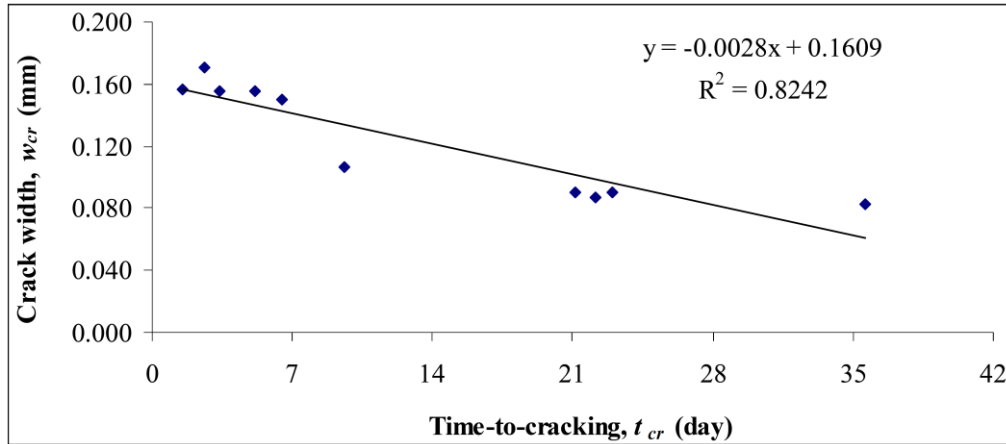


Figure 2-40: Crack width as function of time-to-cracking for fiber-reinforced mixtures ^[51]

Voigt et. al., (2004) [21] compared the performance of different fiber types, fiber blends, and welded-wire fabric (WWF) in their ability to prevent and control drying-shrinkage cracking. Restrained shrinkage ring tests were conducted on fiber-reinforced concrete mixtures to determine the age of the first visible crack and maximum crack width. Table 2-2 shows the different fibers investigated as well as their properties.

Figure 2-41 shows age of first crack for all tested materials as difference with respect to plain concrete. They mentioned that age increases with increasing fiber volume in all cases. Furthermore, it can clearly be seen that the best-performing fiber for all three-fiber volumes is the Flat End 30 mm fiber. The advantage of this fiber type is especially obvious for the lower fiber volumes of 0.125% and 0.25%. In the case of the fiber volume of 0.25%, no difference in cracking age can be found among the remaining fiber types.

Table 2-2: Dimensions of tested fibers and WWF

Shape/material	Length	Equivalent diameter	Aspect ratio	View
Flat End (steel)	30 mm	0.60 mm	50	
	50 mm	1.00 mm	50	
Hooked End (steel)	50 mm	1.00 mm	50	
Crimped (steel)	38 mm	1.14 mm	33	
	50 mm		44	
Profiled (steel)	20 mm	0.78 mm	26	
Crimped (polypropylene)	50 mm	0.90 mm	56	
Fibrillated (polypropylene)	20 mm	< 0.05 mm	~ 400	
Multifilament (polypropylene)	5 to 15 mm	< 0.05 mm	~ 100 to 300	
WWF* (steel)	Spacing: 152 mm	3.4 mm	—	

*WRI designation: metric = 152 x 152 mm—WM9 x MW9; inch-pound = 6 x 6 in.—W1.4 x W1.4.

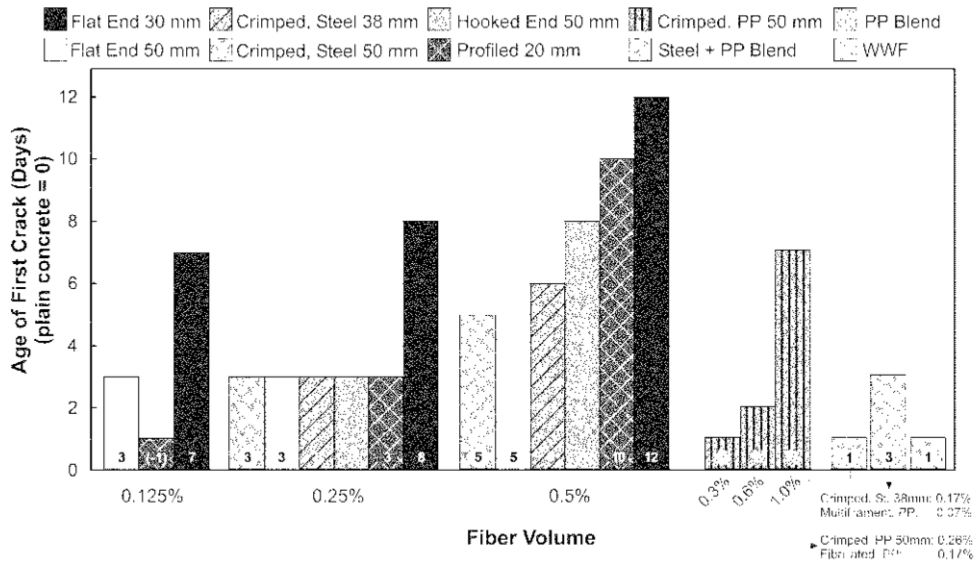


Figure 2-41: Age of first crack for all tested materials as difference with respect to plain concrete (cracking age for plain concrete = 15 days) [21]

Figure 2-42 shows the maximum crack width for all tested mixtures relative to plain concrete [21]. Voigt measured maximum crack width 42 days after the casting of the specimens. They found similar behavior for the age of cracking, the maximum crack width decreases with increasing fiber volume for an individual fiber type. The best performing reinforcement is again the fiber Flat End 30 mm. The mixtures containing this fiber have the smallest crack width for all three-fiber volumes.

They finally concluded that the fiber Flat End 30 mm is the best-performing reinforcement, concerning age of first crack and maximum crack width. This is valid for all investigated fiber volumes. The polypropylene fiber Crimped, PP 50 mm is efficient in reducing the maximum crack width in all fiber volumes. Compared with plain concrete, the crack width could be reduced by more than 50%, even when the fibers are used in low volumes. The tested fiber blend of Crimped, Steel 38 mm and Multifilament, PP (Steel + PP Blend) performs well with a minor drawback in the maximum crack width. This hybrid fiber blend most likely has an improved resistance against plastic shrinkage cracking (caused by the multifilament fibers), which would improve the overall performance. The polypropylene fiber blend (PP Blend) containing Crimped, PP 50 mm and Fibrillated PP fibers performs on the level of the corresponding single fiber mixture (Crimped, PP 50 mm for $V_f = 0.3\%$). Under the assumption of an improvement in the plastic shrinkage cracking resistance caused by the Fibrillated PP fibers, this fiber blend provides a better shrinkage reinforcement than the single fiber mixture (Crimped, PP 50 mm for $V_f = 0.3\%$)

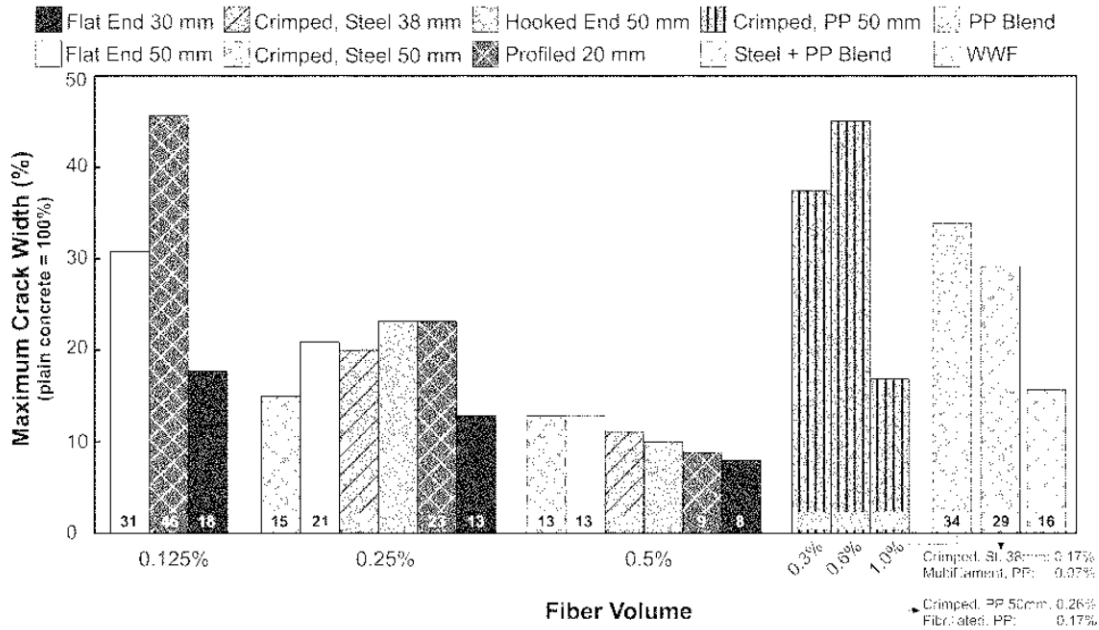


Figure 2-42: Maximum crack width for all tested materials relative to plain concrete (crack width for plain concrete = 100%) [21]

2.9 Freeze-thaw durability of fiber-reinforced self-consolidated concrete

Richardson et al. (2012) [52] examined the effects of freeze/thaw cycles starting at 5 days of curing where the concrete has reached about half of the design strength. The test methods used to evaluate durability were weight loss and relative pulse velocity. They carried a freeze/thaw test to ASTM 666 B [53] for 300 cycles and then they observed the enhanced freeze/thaw protection by the use of polypropylene fibres in concrete when compared to plain and air entrained concrete. The fibre adopted was 12×6.5 denier; Type 1 extruded polypropylene fibre (Type1), quality assured to ISO 9001-2 and used at two doses, first dose of 0.9 kg/m^3 and the second dose of 1.8 kg/m^3 . The air entrainment was to produce a design mix with an air content of $5\% \pm 1.5\%$ in accordance with

commercial batching procedures and acceptance limits. The dosage rate of the Cemex air entrainment agent was 50 ml/ 50 kg CEM1. They prepared six samples as shown in Figure 2-43. The freeze/thaw test cubes were subjected to air freezing and water thawing to establish the degree of durability. Following a pilot study to determine the optimum frequency of freeze/thaw cycles, it was found that two freeze/thaw cycles were possible in a 24-h cycle. Measurements were taking to determine weight loss, relative pulse velocity, density, compressive strength, and strain, to determine the modulus of elasticity after the freeze/thaw test. To obtain the relative dynamic modulus as required by the ASTM test, a pulse velocity test to BS 1881:Part 203 was performed using transverse readings. Figure 2-44 shows the pulse velocity for all concrete types vs the number of completed freeze/thaw cycles. They calculated the durability factors using the equation illustrated in ASTM 666B. The values were as follows: A – Plain concrete – 1.323, B – Air entrained concrete – 100.47, E – 0.9 kg/m³ fibre – 116.55, F – 1.8 kg/m³ fibre – 113.08. Cubes B, E and F showed an improvement in the final pulse velocity readings, compared to their original values. The plain concrete cube A, showed little resistance to the effects of freeze/thaw damage. They finally mentioned that the effect of Type 1 polypropylene fibres is to reduce water absorption and increase resistance to freeze/thaw damage when use in medium/low strength concrete, resulting in increased durability.the inclusion of fibres can increase the air void system when compared to plain concrete, thus providing an alternative to air entrainment as a method of freeze/thaw protection.

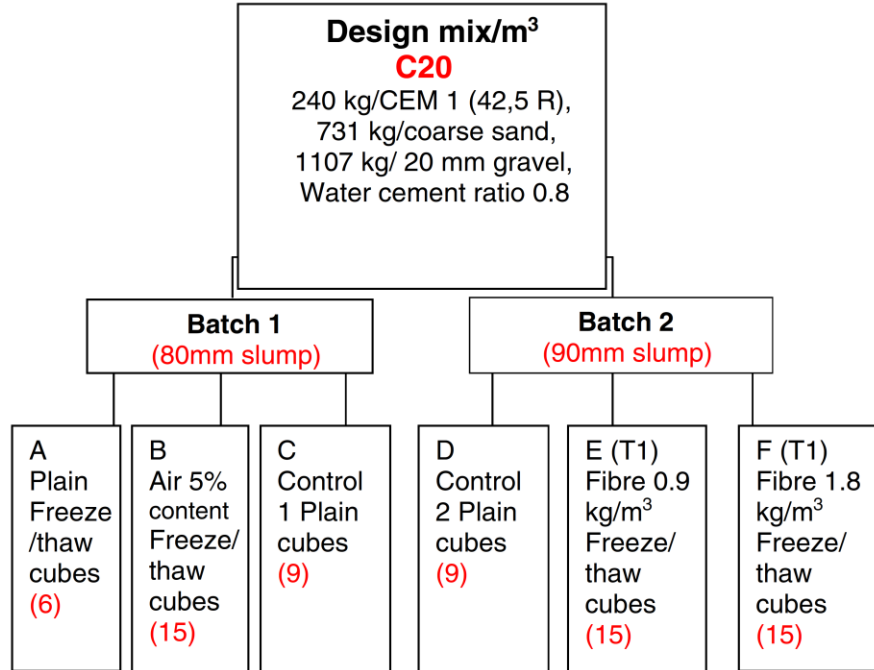


Figure 2-43: Design mix and batching procedure

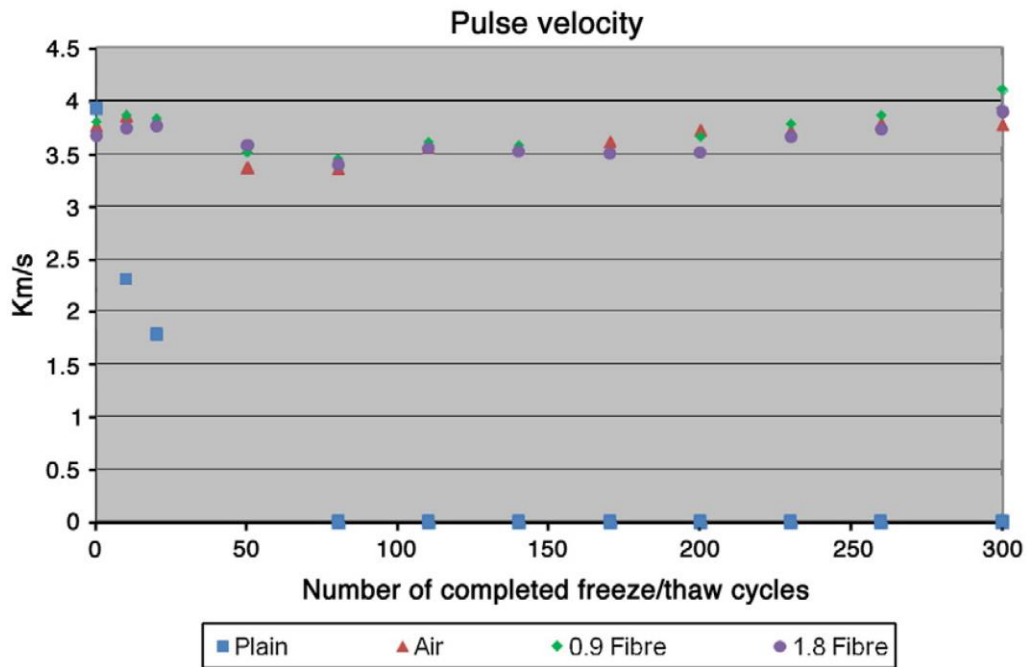


Figure 2-44: Pulse velocity for all concrete types

Yildirim and Ekinici (2012) [54] studied the effect of different fibers on the freeze-thaw durability of concrete. They used micro-structured polypropylene and glass fibers separately and in combination with macro-structured steel fibers in the concrete. They conducted their experiments in order to determine weight-loss and durability factor based on ultrasound pulse velocity of 12 different concrete series produced according to ASTM C-666 [53]. They investigated the separate and combined effects of the fibers used in the concrete in terms of the rapid freeze-thaw period. Figure 2-45 shows the technical properties of steel, polypropylene and glass fibers.

Properties	SF	PF	GF
Size (mm)	60	20	12
Dimension (mm)	0.75	0.05	0.014
Brittleness	80	400	857
Density (kg/mm ³)	7480	910	2680
Modulus of elasticity (MPa)	200000	3500-3900	72000
Tensile strength (MPa)	1100	320-400	1700
The number of fibers per kilogram	4600	82 Million	200 Million

Figure 2-45: Technical properties of steel, polypropylene and glass fibers

They produced concrete including fibers with different percentages within the same main compounds. K represents the control concrete specimen, while S, P and G represent the concrete specimens including steel, polypropylene and glass fibers, respectively. They produced three series of concrete, including 0.5 (S 0.5), 0.75 (S 0.75) and 1 (S 1) % as volumetric of hooked steel fibers respectively. Another six series of concrete were produced with the use of polypropylene and glass fibers of 0.1 % (P and G). They defined the symbols of the fiber material used in the mixture fiber specimens as SP and SG. They were both used separately and in combination with macro-structured steel fibers of 0.5

(SP 0.5 and SG 0.5), 0.75 (SP 0.75 and SG 0.75) and 1 (SP 1 and SG 1)%. Figure 2-46 shows Durability factors determined after freeze-thaw cycles for all the 12 mixtures. They concluded that using polypropylene fiber in all the concrete specimens to be reinforced by fibers in consideration of the effects of freeze-thaw cycles will be advantageous. Steel fibers did not cause any difference in terms of freeze-thaw cycles but did cause some negative effects for mixture concrete. It is important that glass fibers should not be used in the places exposed to freeze-thaw cycles, or that concrete should be protected against this effect.

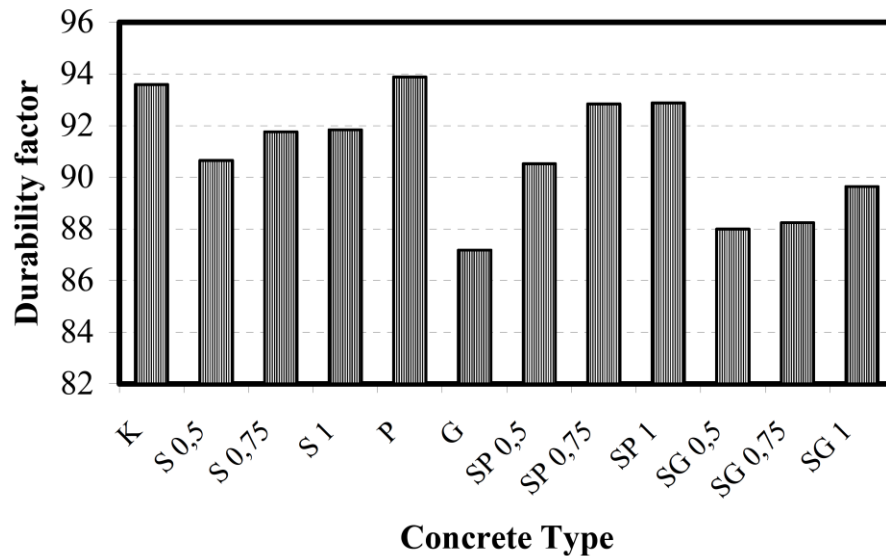


Figure 2-46: Durability factors determined after freeze-thaw cycles

2.10 Structural performance of fiber-reinforced self-consolidated concrete structural elements

This section consists of six sections; first section summarizes the literature related to the flexural performance of fiber-reinforced concrete beams, second section summarizes the literature related to the flexural crack resistance of fiber-reinforced concrete beams, third

section summarizes the literature related to the repair of reinforced concrete beams using fiber-reinforced self-consolidated concrete, fourth section summarizes the literature related to the shear performance of fiber-reinforced concrete beams, fifth section summarizes the literature related to the structural performance fiber-reinforced concrete columns, section number six summarizes the literature related to the bond strength between the steel rebar and fiber-reinforced concrete.

2.10.1 Flexural performance of fiber-reinforced concrete beams

Fritih et. al. (2013) [55] studied the effect of steel fiber reinforcement on the behavior of Self-Compacting Concrete (SCC) beams. They carried out bending tests in order to examine the effect of low fiber content (0.25% by volume) on the flexural behavior of beams with different amounts of steel rebar reinforcement. They compared the behavior of reinforced concrete beams cast either with control SCC and the one of Fiber-Reinforced Self-Compacting Concrete (FRSCC). FIBRAFLEX, shown in Figure 2-47 was used. As shown in Figure 2-47 also the ribbon-shaped fibers are 30 mm long, 1.6 mm wide and 0.03 mm thick, and belong to the family of metallic glass materials



Fiber type	Amorphous metal
Length (mm)	30
Cross section (mm ²)	Rectangular 1.6 × 0.03
Density	7.20
Tensile strength (MPa)	2000
Elastic modulus (GPa)	140
Specific properties	Stainless

Figure 2-47: Amorphous metallic fibers used and the main characteristics [55]

They concluded that global mechanical behavior is not affected by the fiber content used. Just a slight enhancement of stiffness after crack initiation is observed in the case of

beams with a low longitudinal reinforcement ratio. This can be explained by the relatively greater tension stiffening effect induced by a better tensile stress transfer by fibers to the concrete through the crack opening. Yielding, ductility and load bearing capacity are not improved with the addition of fibers. The fibers do not modify the failure mode.

Guan et al., (2013) [56] investigated the effect of longitudinal reinforcement ratio, volume dosage of steel fiber and the beam height on flexural behavior of steel fiber reinforced high-strength concrete beams by conducting a parametric experimental study. Four longitudinal reinforcement ratios, four steel fiber volume dosages and four different beam heights were used. As shown in Figure 2-48, 10 beams of steel fiber reinforced high-strength concrete and 1 beam of reinforced concrete were designed to investigate the flexural behavior of steel fiber reinforced concrete beams. The length and diameter of the steel fiber were 32.14 and 0.9 mm, respectively. At the end of the curing period of 28 days, the beams were taken out from the curing room and were prepared for the test of flexural behavior. Three-point bending beam method was employed in their study. They found that compared with the reinforced concrete beam, the bearing capacity and the measured deflection of the steel fiber reinforced high-strength beam are much larger and the breaking of the compression zone is not too serious, which reflects the improvement of reinforcing and toughening of steel fibers. As shown in Figure 2-49 considerable increase for the ultimate flexural capacity of the steel fiber reinforced high-strength concrete beams was observed by increasing the steel fiber volume dosage.

Specimen no.	Longitudinal reinforcement ratio (%)	Steel fiber volume dosage (%)	Beam height (mm)
1	0.77	1.5	300
2	1.39	1.5	300
3	2.10	1.5	300
4	2.70	1.5	300
5	1.39	0	300
6	1.39	0.5	300
7	1.39	1.0	300
8	1.39	2.0	300
9	1.39	1.5	250
10	1.39	1.5	300
11	1.39	1.5	350

Figure 2-48: Design parameters of the specimen beams [56]

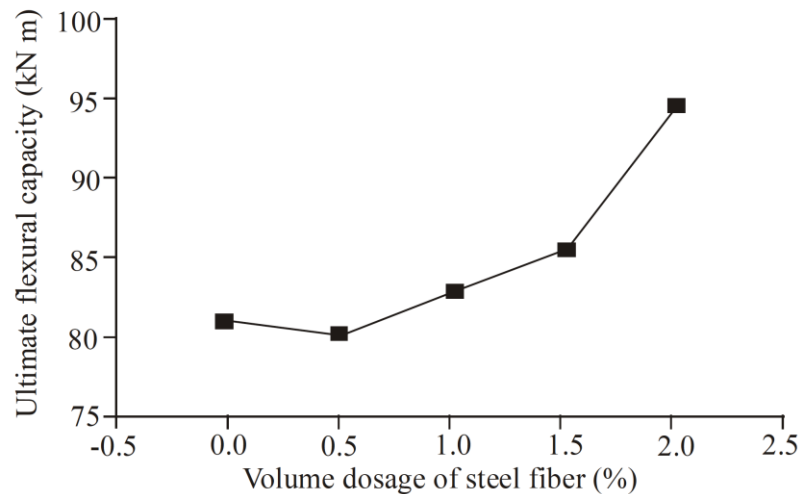


Figure 2-49: Ultimate flexural capacity versus steel fiber volume dosage [56]

2.10.2 Flexural crack resistance of fiber-reinforced concrete beams

Pons et. al. (2007) [57] compared the crack resistance of self-compacting concrete with various proportions of metal fibres as well as ordinary vibrated concrete. They used macrofibres, 30-mm amorphous metal, 50-mm long polypropylene and a hybrid of them.

Fibre-reinforced ordinary concrete placed with the help of vibration (VC) and self-compacting concrete (SCC) were designed to achieve a 28-day average compressive strength of about 35 MPa. The fibre contents investigated were 20 kg/m³ (0.27% by volume) for the amorphous metal fibres and 9 kg/m³ (0.98% by volume) for the polypropylene fibres. The hybrid mix was the combination of 50% of the previous contents for the respective fibre types. As shown in Figure 2-50, they performed four-point bending tests on 100 × 100 × 500mm prisms. They plot the crack width Vs the load for different beams as shown in Figure 2-50 according to RILEM TC162 [58] and also they plot the load Vs deflection for different be. The results showed that the high modulus and high bond amorphous metal fibres at the dosage of 20 kg/m³ in concrete (SCCMF) provided a strain hardening behaviour phase that developed in the range 0–0.2mm of crack mouth openings and increased the maximum flexural load of the material by about 50% in comparison with fibre-free concrete (SCC) (Figure 2-51). Afterwards, the fibres began to break and the residual load bearing capacity decreased until it was almost zero (Figure 2-50). Polypropylene fibres at the dosage of 9 kg/m³ in concrete (SCCSF) provided no increase in peak strength in comparison with SCC. The hybrid mix SCCMSF added the qualities of its two constitutive reinforcements. The resultant effects seem to be weighted according to the relative content of each fibre component. Figure 2-53 shows the comparison between the flexural behaviour of vibrated and self-compacting concretes. Because the maximum bending loads of both types of concretes were not exactly the same, they did normalize the load-deflection curves. For that purpose reference to the peak load of the synthetic fibre reinforced materials was considered as

representative of the peak load of the concrete matrix alone. Even though slight differences were observed between the two types of concrete, they indicated that a better fibre-matrix bond was achieved for self-compacting specimens than for vibrated ones. Indeed, with regard to polypropylene slipping fibres, the post crack strength plateau of SCCSF was higher than that of VCSF. When only high modulus and high bond amorphous metal fibres were incorporated, the peak strength of SCCMF was higher than the one of VCMF and the following decrease caused by the breaking of the fibres prevented from slipping was steeper for SCCMF than for VCMF. When the properties of each kind of fibre were combined, the same observations could be made as above, which pointed out a better fibre-matrix bond in self-compacting concrete.

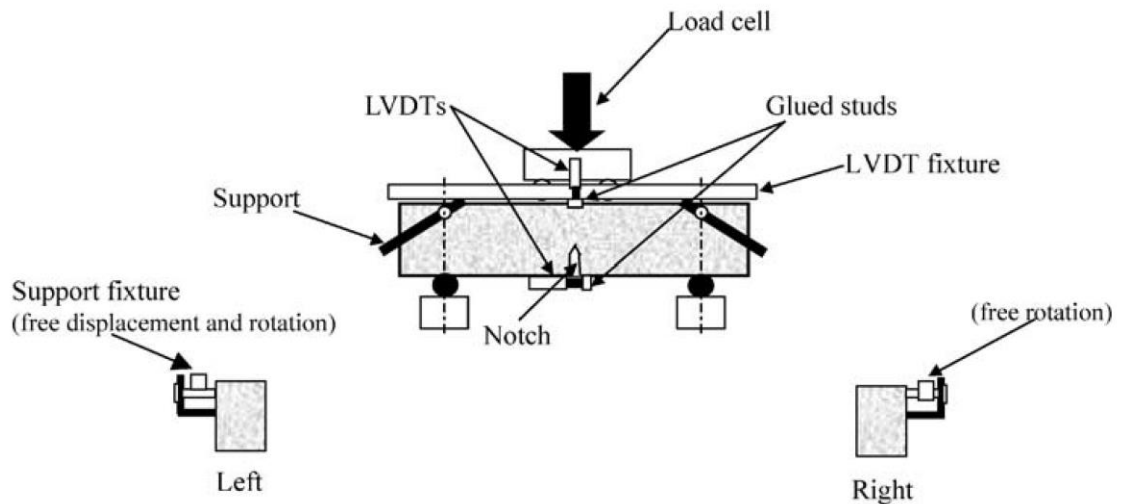


Figure 2-50: Four-point bending test

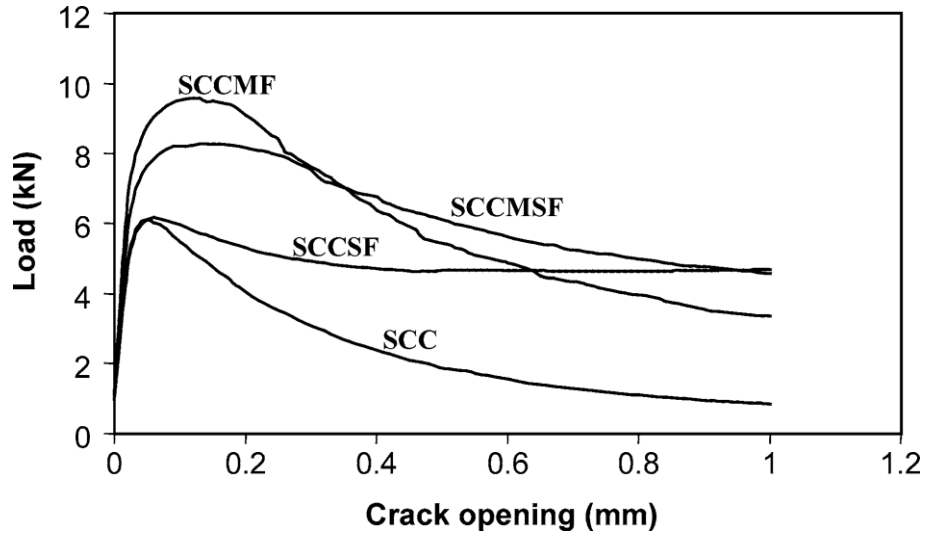


Figure 2-51: Average load-crack opening curves of the self-compacting concretes

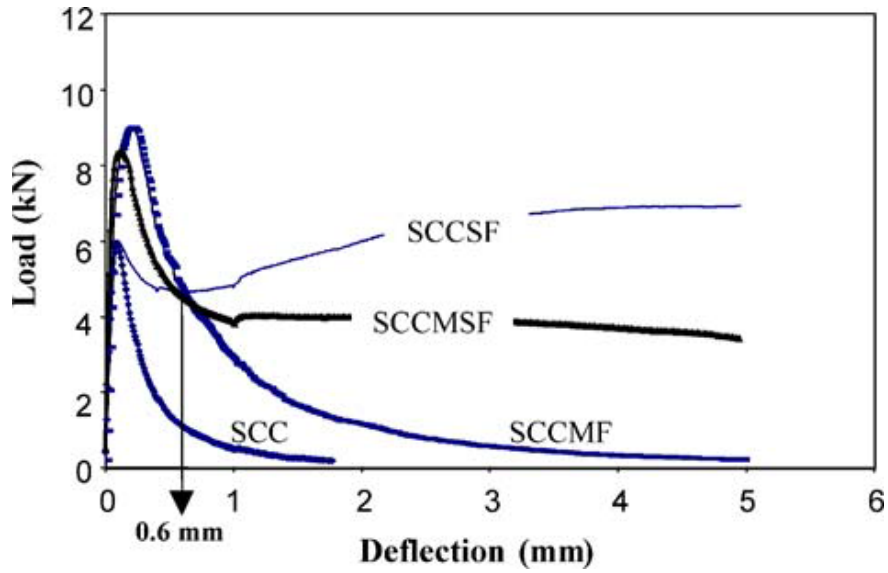


Figure 2-52: Average load-deflection curves of self-compacting concretes

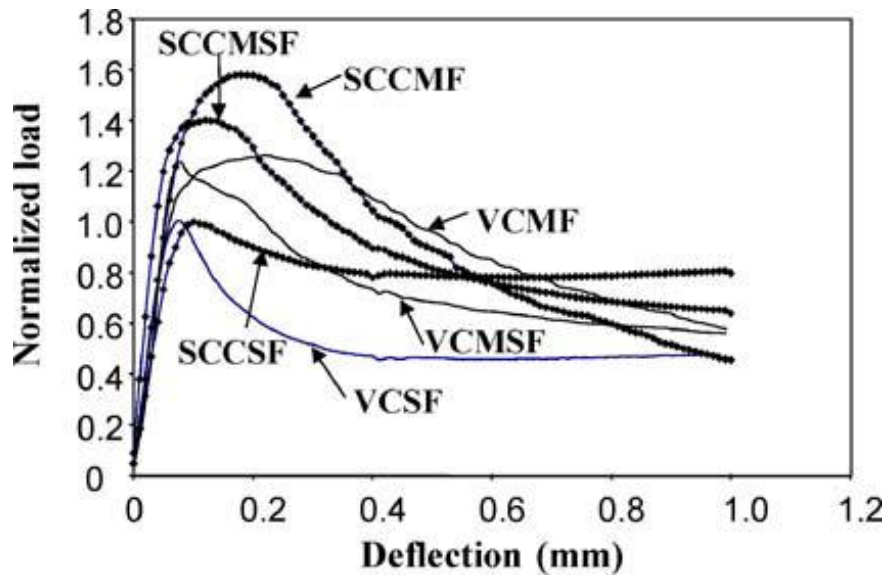


Figure 2-53: Average load-deflection curves – comparison between vibrated and self-compacting concretes

2.10.3 Repairing of concrete beams using fiber-reinforced self-consolidated concrete

Kassimi et. al. (2014) [59] investigated fiber-reinforced self-consolidating concrete (FR-SCC) to assess its potential value as a repair material of reinforced concrete beams. They optimized a total of 10 repair mixtures to repair 10 full-scale beams. The mixtures included eight FR-SCC mixtures, one fiber-reinforced self-consolidating mortar, and a reference self-consolidating concrete (SCC) made without fibers. They employed four types of fiber reinforcement: steel, two kinds of polypropylene, and hybrid fibers. Each fiber type was used at two volume contents of 0.3 and 0.5% for the FR-SCC mixtures and at 1.4% for the steel fibers in the mortar mixture. The beams were 3100 mm (122.05 in.) long, 250 mm (9.84 in.) wide, and 400 mm (15.75 in.) deep. They cast the beams using conventional vibrated concrete except for the lower 125 mm (4.92 in.) zone

of the beam, representing a damaged area in the tension zone. After curing, they repaired the bottom layer using the self-consolidating mixtures. Then they tested the beams under four-point bending over a simply supported clear span of 2600 mm (102.36 in.). The casting of the concrete beams representing existing concrete elements was performed with the steel cage placed inverted in the formwork with the tension reinforcement at the top. The tension reinforcement and exposed stirrups were temporarily covered with duct tape to prevent any contact with substrate concrete and assure good bond between the reinforcement and repair material. After curing, they removed the duct tape, and the beams were placed with the tension reinforcement at the bottom. Then they cast the repair layer using the optimized self-consolidating mixtures. The repair material was placed through a funnel into a 140 mm (5.51 in.) diameter hole located at the edge of the beam. The hole was made by fixing a plastic cylinder mold along the depth of the beam during the casting of the conventional vibrated concrete (CVC) beam. They made three additional holes equidistant along the length of the beam, as shown in Figure 2-54, to expel air and to monitor flow of the concrete.

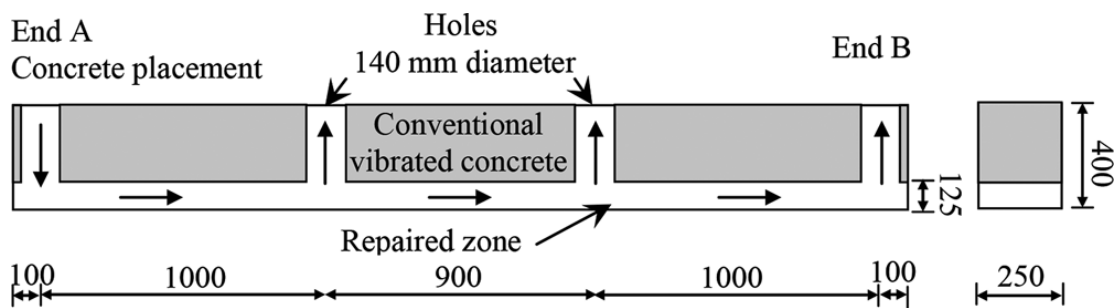


Figure 2-54: 1—Schematic of composite beam specimen. (Note: Dimensions in mm; 1 mm = 0.039 in.)

Then they removed the plastic molds before the repair casting. The external sides of the formwork were fabricated using plexiglass to enable visual observation of the flow of the self-consolidating repair material during casting. To enhance bond between the existing and new concrete, they sprayed the surface of the existing concrete with a surface-retardant liquid soon after casting the CVC. After 24 hours, they cleaned the exposed concrete by removing the retarded surface mortar using water-spraying to expose coarse aggregate and enhance bond to the repair material, as shown in Figure 2-55.



Figure 2-55: Roughened surface of base concrete before casting repair materials

All beams were reinforced with two 20M bars as the main tensile reinforcement and two 10M bars as the top reinforcement. The shear reinforcement was double-legged stirrups of 8 mm (0.31 in.) in diameter spaced at 150 mm (5.91 in.). They prepared the beams with the CVC that was cast monolithically to serve as a reference beam, while the other beams were composite beams consisting of CVC and a repair section along the bottom of

the beams (Figure 2-55). They tested the beams approximately at 180 days under four-point bending over a simply supported span of 2600 mm (102.36 in.), as shown in Figure 2-56.

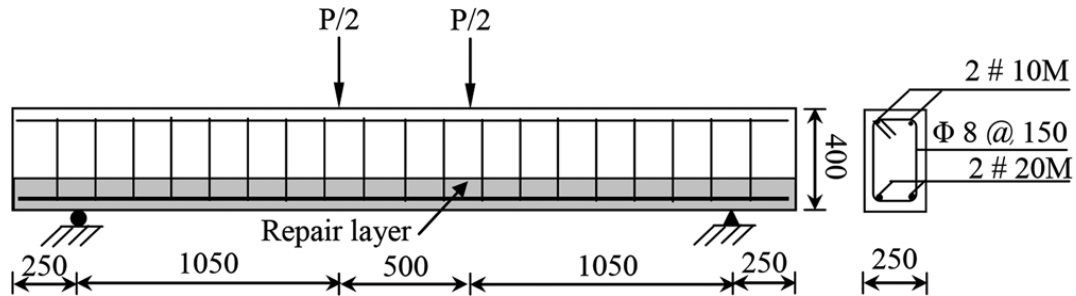


Figure 2-56: Beam dimensions (in mm).

The load was monotonically applied at a stroke-controlled rate of 1.2 mm/min (0.047 in./min) using a 500 kN (112.4 kip) closed-loop MTS actuator. All beams were instrumented with electrical resistance strain gauges bonded on reinforcing bars and the top concrete surface at midspan. They measured the midspan deflections using two LVDTs fastened at each side of the beam. They installed two high-accuracy LVDTs (± 0.001 mm [$\pm 3.93 \times 10^{-5}$ in.]) at positions of first cracks to measure crack width as shown in Figure 2-57.

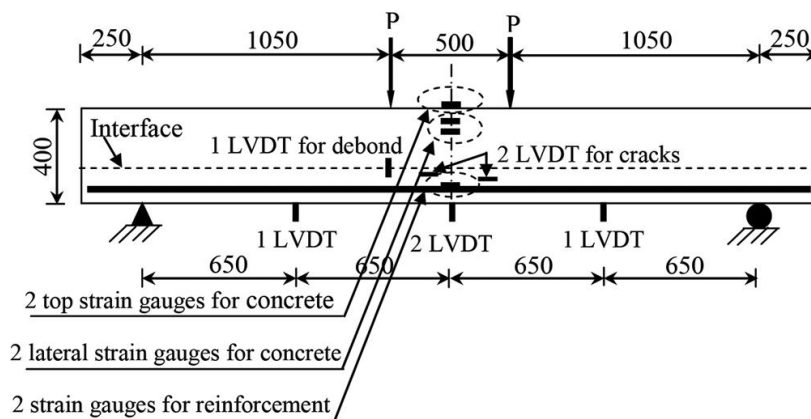
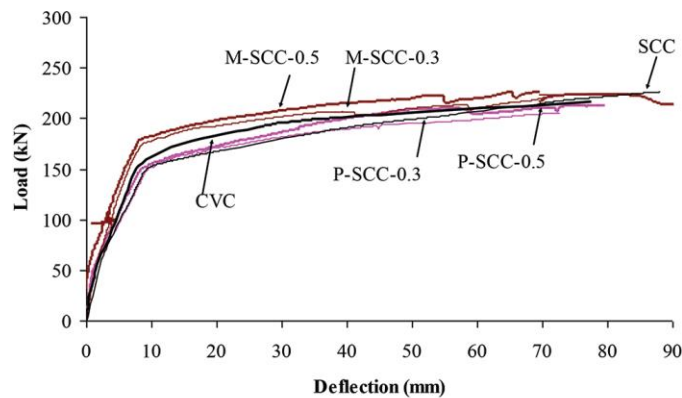
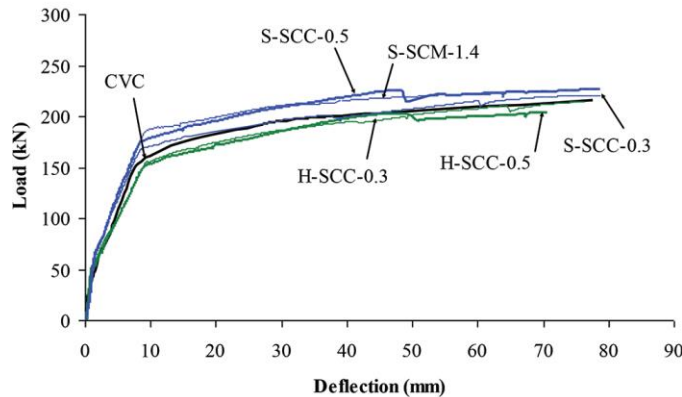


Figure 2-57: Loading and strain-control systems (dimensions in mm)

The ultimate load capacity of the control monolithic beam was 216 kN (48.6 kip) and those of the repaired beams ranged between 204 and 230 kN (45.9 and 51.7 kip) showing a spread of $\pm 6\%$ of the strength of the monolithic beam. Therefore, 94% of the initial load capacity can be restored using thier repair materials. The maximum load-carrying capacity was attained with the SCC and S-SCC-0.3 beams, while the H-SCC-0.5 beam had the lowest load-carrying capacity. Figure 2-58 shows the load-deflection relationships of the control monolithic beam and beams repaired beams.



(a)



(b)

Figure 2-58: Load-deflection response of control beam with: (a) beams repaired with SCC and mono- and multifilament polypropylene FR-SCC; and (b) beams repaired with hybrid and steel FR-SCC, and steel FR-SCM.

They calculated the theoretical flexural strength of the repaired beams ($P_{u\text{ calc}}$) assuming composite behavior and linear strain distribution in the beam between two cracks, which is similar to ACI 318 [60] ultimate strength design method considering the extra tensile strength of the fibrous concrete and adding the strength provided by the reinforcing steel to obtain flexural strength. The ultimate flexural capacity of the beam can be calculated using Equation (32) proposed by them.

$$M_u = A_s f_y \left(d - \frac{a}{2} \right) + A_s' f_y' \left(\frac{a}{2} - d' \right) + \sigma_t b (h - e) \left(\frac{h}{2} + \frac{e}{2} - \frac{a}{2} \right) \quad (32)$$

Where A_s and A_s' are the areas of tensile and compressive steel reinforcement, respectively; f_y and f_y' are the yield stresses of tensile and compressive steel reinforcement, respectively; d and d' are the distances from the extreme compression fiber to the centroids of tensile and compressive steel reinforcement, respectively; a is the depth of rectangular stress block; b is the width of the beam; h is the overall thickness of the beam; e is the distance from extreme compression fiber to the top of fibrous concrete; and σ_t is the tensile stress of fibrous concrete, which can be calculated according to the Equation (33) for concrete with steel fibers proposed by ACI Committee 544 [61].

$$\sigma_t = 0.00772 \frac{L_f}{d_f} V_f F_{be} \quad (MPa) \quad (32)$$

Where L_f is the fiber length; d_f is the fiber diameter; V_f is the percent by volume of fibers; and F_{be} is the bond efficiency of the fiber, which varies from 1.0 to 1.2 depending on fiber characteristics. The mean $P_{u\text{ exp}}/P_{u\text{ calc}}$ was 1.40 with a coefficient of variation of 5%.

3 Experimental Program

3.1 Materials

3.1.1 Binders

Type I/II ordinary portland cement (OPC) was used in this study. Class C FA was employed in the binary cementitious systems. Two Types of EA were used; G-Type EA and K-Type EA. G-Type EA is CaO-based system in which the formation of calcium hydroxide (Ca(OH)_2) crystals causes expansion. K-Type EA which is calcium sulfoaluminate-based system in which the formation of ettringite upon reaction with water causes expansion. Table 3-1 presents the physical and chemical characteristics of the cementitious materials used in this study.

Table 3-1: Physical and chemical characteristics of cementitious materials and expansive agents

	OPC	Class C FA	K-Type EA	G-Type EA
SiO ₂ %	19.8	36.5	7.7	12.6
Al ₂ O ₃ %	4.5	24.8	7	5.7
Fe ₂ O ₃ %	3.2	5.2	1.2	1.9
CaO %	64.2	28.1	50.1	82.6
MgO %	2.7	5	0.1	0.1
SO ₃ %	3.4	2.5	26	-
Na ₂ O eq. %	-	-	0.6	0.9
CaCO ₃ %	3.3	-	-	-
Blaine surface area, m ² /kg	390	498	-	-
Denisty	3.14	2.71	2.9	3.1
LOI %	1.5	0.5	2.1	-

3.1.2 Chemical admixtures

The chemical admixtures used in this study were polycarboxylate-based high-range water-reducer (HRWR) to increase flowability of FR-SCC and FR-SWC, synthetic resin-type air-entraining admixture (AEA) to enhance the air void system, and polysaccharide viscosity-modifying admixture (VMA) to increase viscosity of concrete and to increase stability. Table 3-2 shows the characteristics of the chemical admixtures.

Table 3-2: Characteristics of chemical admixtures

	Solid content (%)	Specific gravity
HRWRA	23	1.05
VMA	1.5	1
AEA	12.5	1.01

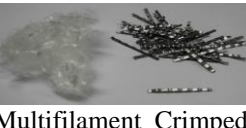
3.1.3 Aggregates

Continuously graded natural sand with a fineness modulus of 2.6 and crushed limestone aggregate with a nominal maximum aggregate size of 12 mm (0.5 in.) were used with FR-SWC, while the same type of natural sand was used with pea gravel aggregate with a nominal maximum aggregate size of 10 mm (3/8 in.). The lime stone coarse aggregate, the pea gravel coarse aggregate and sand had specific gravities of 2.54, and 2.63, respectively, and water absorption values of 3.81% and 0.62%, respectively.

3.1.4 Fibers

Eight fiber types were incorporated to FR-SCC and FR-SWC, including propylene synthetic fiber (PLP), four types of hooked steel fiber (ST1), (3D), (4D) and (5D), carbon fiber, hybrid of crimped steel fiber and polypropylene multifilament fiber (STPL), and micro-macro steel fibers (STST) were incorporated at a fiber volume of 0.5% to FR-SCC and at 0.5% and 0.75% to FR-SWC. Table 3-3 presents the characteristics of the fibers.

Table 3-3: Characteristics of fibers

	ST1	STST		PLP	STPL		3D	4D	5D	CA
Material	Macro Steel	80% Macro Steel	20% Micro Steel	Pro-pylene	8% Poly-propylene	Steel	Steel	Steel	Steel	Carbon
Shape ⁽¹⁾	Hook 	Hook 	Straight 	Mono-flament 	 Multifilament Crimped					
Color	Golden	Golden	Golden	Transp.	Transp.	Grey	Grey	Grey	Grey	Black
Cross section	Cir.	Cir.	Cir.	Rec.	Cir.	Rec.	Cir.	Cir.	Cir.	Cir.
Specific gravity	7.85	7.85	7.85	0.92	0.91	7.85	7.85	7.85	7.85	7.85
Length (mm)	30	30	13	40	5-15 ⁽²⁾	50	60	60	60	102
Equiv. diameter (mm)	0.55	0.55	0.2	0.44	0.05	0.9	0.92	0.92	0.92	3.18
Aspect Ratio	55	55	65	91	100-300	56	65	65	65	32
Modulus of elasticity (Gpa)	200	200	200	9.5	N.A.	7.16	210	210	210	242
Tensile strength (Mpa)	1100-1300	1100-1300	1100-1300	620	Neglected	413	1160	1160	1160	4137

3.2 Mixture proportioning

Voigt et al., (2004) [21] proposed a formula for calculating the average thickness of the matrix layer (t_m) enveloping fibers and gravel particles on the basis of the multi-aspect concept. Then they expressed the average thickness of matrix covering the fibers and the gravel mathematically using Equation (1).

$$t_m = \frac{\text{Volume of Excess Matrix}}{\text{Total Surface Area of Fibers and Gravel}} \quad (1)$$

They came finally to Equation (2) to calculate the exact matrix thickness t_m .

$$t_{mortal\ after} = \frac{V_c - V_g - V_f - V_v}{A_g + A_f} \quad (2)$$

Where t_m = average thickness of matrix layer cover fibers and gravel; V_c = total volume of concrete; V_g = volume of gravel; V_f = volume of fibers; V_v = volume of voids; A_g = total surface area of gravel; and A_f = total surface area of fibers. The volume of voids can be obtained using the packing density of the mixture of gravel and fibers, which can be determined by ASTM C 29 [2]. The total surface area of fibers is the summation of the surface area of all fibers present in the composite. It can be calculated based on the fiber volume and the surface area of a single fiber. The total surface area of the gravel depends on the grading curve of the used coarse aggregates. Equation (3) and (4) (developed by the author) can be used to calculate the total surface area of the coarse aggregate.

$$A_g = KV_g \quad (3)$$

$$\text{Where, } K = 6 \left\{ \frac{\%g_1}{d_1} + \frac{\%g_2}{d_2} + \frac{\%g_3}{d_3} + \frac{\%g_4}{d_4} \right\} \quad (4)$$

Where d_1 : Diameter of course of first group; $\%_{g1}$: Percentage of course aggregates having diameter d_1 and d_2 : Diameter of course of first group; $\%_{g2}$: Percentage of course aggregates having diameter d_2 and so on for d_3 , d_4 , $\%_{g3}$ and $\%_{g4}$

Khayat et al., (2014) [23] proposed a mixture-proportioning method for FR-SCC. They considered the multi-aspect concept proposed by Voigt [1] and they used Equation (2) for calculating the thickness of mortar covering the coarse aggregates and the fibers.

The mixture-proportioning method proposed by Khayat et al. (2014) includes reducing the volume of coarse aggregate with the addition of fibers to maintain a fixed thickness of a mortar layer t_{cm} over the fibers and coarse aggregates. They expressed the total surface area of fibers (A_f) as:

$$A_f = \frac{\% \text{ fiber} \times \text{specific gravity} \times \text{surface area of single fiber}}{\text{Volume of single fiber} \times \text{specific gravity}} \quad (5)$$

Their final proposed equation for calculating the total surface area of fibers (A_f) is:

$$A_f = \frac{4 \times V_f}{d_f} \quad (6)$$

where V_f is an absolute volume, and not as a ratio.

3.2.1 Procedure for mixture proportioning design of FR-SCC

The mix design procedure was used to adjust the mixture proportioning of SCC when adding the fibers to SCC. The reference SCC mixture proportioning is given in Table 2 and is referred as R1. This mixture proportioning was followed by Khayat et al., (2014)

[2]. Eight steps were followed to get the mixture proportioning of FR-SCC, these steps is mentioned below:

First: calculate mixture volumes before adding fibers by multiplying the mixture proportioning mass by the specific gravity of each component in the mixture.

Second: calculate K using equation (4) where K is a constant depending on the grain size distribution of the coarse aggregate.

$$K = 6 \left\{ \frac{\%_{g1}}{d_1} + \frac{\%_{g2}}{d_2} + \frac{\%_{g3}}{d_3} + \frac{\%_{g4}}{d_4} \right\} \quad (4)$$

Third: calculate specific area of coarse aggregates using equation (2)

$$A_g = KV_g \quad (2)$$

Fourth: calculate specific area of fibers using equation (6)

$$A_f = \frac{4 \times V_f}{d_f} \quad (6)$$

Fifth: determine mortar thickness using equation (7)

$$t_{mortar\ before} = \frac{V_c - V_{gb} - V_v}{A_{gb}} = t \quad (7)$$

Sixth: calculate volume of coarse aggregates after adding fibers using equation (8)

$$V_g = \frac{V_c - V_v - tA_f}{tK + 1} \quad (8)$$

Seventh: calculation of volume of sand after adding fibers (V_s) using equation (9)

$$V_{sb} + V_{gb} = V_s + V_g + V_f \quad (9)$$

Eighth: calculate the mixture proportioning after adding fibers, by knowing the volume fractions of the fibers, sand, and aggregate while the other components are left constants before and after the addition of fibers. The AEA was added to all mixtures to secure air volume of a value $7.5\% \pm 1.5\%$. w/c was kept constant for all mixtures at 0.42.

The above mix design procedure was followed first to calculate the mixture proportionating for 12 different FR-SCC mixtures and 12 FR-SWC mixtures prepared to optimize the binder proportioning in Task 2A. After optimizing the binder proportioning, the same procedure was followed to calculate the mixture proportionating for the optimized FR-SCC mixtures (R1, R2, R3, 1, 2, ...7) and the optimized FR-SWC mixtures (R1, 1, 2, 3, ...10) in Task 2A and Task 2B as shown in Tables 3-4 and 3-5, respectively.

Table 3-4: Mixture proportions for the optimized SCC and FR-SCC

	Fiber type	V _f (%)	Water kg/m ³	Cement Type I/II kg/m ³	Fly Ash kg/m ³	Expansive Agent		Sand kg/m ³	Coarse Agg. kg/m ³	VMA ml/m ³	HRWR ml/m ³	AEA ml/m ³
						Type	kg/m ³					
R1	-	0	193	475	0	-	-	746	747	4167	1083	104
R2	ST1	0.5	193	319	137	-	-	780	681	4286	1429	104
R3	-	0	193	332	142	-	-	746	747	4182	1545	104
1	ST1	0.5	193	306	131	K-Type	38	728	734	4167	2083	104
2	ST1	0.5	193	319	137	G-Type	19	728	734	4167	1458	104
3	PLP	0.5	193	319	137	G-Type	19	731	731	4167	1875	104
4	3D	0.5	193	319	137	G-Type	19	723	739	4167	1500	104
5	STPL	0.5	193	319	137	G-Type	19	721	740	4167	1803	104
6	STST	0.5	193	319	137	G-Type	19	733	732	4167	1875	104
7	CA	0.5	193	319	137	G-Type	19	717	745	4167	1500	104

Addition of fibers to SCC results in decreasing of the flowability of FR-SCC, so addition of HRWRA is required, which may result in concrete segregation. VMA increases the viscosity of concrete that’s why VMA was added to enhance stability of FR-SCC.

Table 3-5: Mixture proportions for the optimized SWC and FR-SWC

	Fiber type	V _f (%)	Water kg/m ³	Cement Type I/II kg/m ³	Fly Ash kg/m ³	Expansive Agent		Sand kg/m ³	Coarse Agg. kg/m ³	VMA ml/m ³	HRWR ml/m ³	AEA ml/m ³
						Type	kg/m ³					
R1	-	0	157	380	0	-	-	851	850	2500	1730	45
1	ST1	0.5	157	255	110	G-Type	19	942	727	2500	1730	50
2	3D	0.5	157	255	110	G-Type	19	872	800	2500	1410	55
3	4D	0.5	157	255	110	G-Type	19	872	800	2500	1545	50
4	5D	0.5	157	255	110	G-Type	19	872	800	2500	1820	50
5	STPL	0.5	157	255	110	G-Type	19	864	809	2500	2045	48
6	STST	0.5	157	255	110	G-Type	19	921	752	2500	1820	41
7	PLP	0.5	157	255	110	G-Type	19	924	746	2500	2500	36
8	ST1	0.75	157	255	110	G-Type	19	972	690	3727	2430	41
9	STST	0.75	157	255	110	G-Type	19	945	721	3727	2275	43
10	5D	0.75	157	255	110	G-Type	19	872	800	3727	2320	43

The filling ability requirements for FR-SWC are less than those of FR-SCC, so less amount of binders can be optimized in case of FR-SWC. The minimum amount of binders optimized for stable FR-SWC was 380 kg/m³ vs. 475 kg/m³ in case of FR-SCC. Lower amount of VMA was required in case of FR-SWC compared to FR-SCC. Following the concept of constant thickness of mortar for designing FR-SWC resulted in lowering the amount of coarse aggregates and increasing the amount of sand and the variation was increased in case of increasing the fiber volume from 0.5% to 0.75%.

3.2.2 Mixing Procedure for FR-SCC and FR-SWC

The mixing procedure followed consisted of the following steps, which was proposed by HWANG (2006) with few modifications: The sand was homogenized for 30 seconds. Two samples were taken; one from the homogenized sand and the other one from the coarse aggregate to determine the water contents. The water, sand, and coarse aggregate contents were then adjusted. The coarse aggregate, the fibers (in case of FR-SCC), half of water content and the AEA were then added and mixed for one minute. The binder (and EA if used) were then added then mixed for 30 seconds. Approximately 1/4 amount of the mixing water plus 3/4 of the HRWRA volume were then added and mixed for one minute. The remaining 1/4 amount of water with the VMA was then added, and the concrete mixed for three minutes. The mixer was then switched off and the mixed materials were left for one minute. The volume needed of HRWRA was corrected with the remaining 1/4 HRWRA volume. The material was mixed again for two minutes. Concrete temperature during mixing and testing was approximately 20°C (68°F).

3.3 Experimental program

Task 2: Mix design of SCC and SWC

Task 2A: Binder optimization for SCC, FR-SCC, SWC and FR- SWC

The aim of this task was to develop and optimize the binders proportioning of FR-SCC and FR-SWC that exhibit superior workability and stability (both static and dynamic stability) and resulting in the highest mechanical properties. A steel fiber (ST1-hooked end) was systematically introduced to the mixtures at a fiber volume of 0.5%. As

described in Table 3-6, different series of tests will be carried out in the optimization. The tested parameters were as follows:

- Concrete type (SCC and SWC)
- Fly ash replacement (0, 30% and 50%)
- Type of expansive agent (EA) (CaO and k-component)
- Expansive agent dosage (0, 4% and 8%)
- MSA (3/8 and 0.5 in.)

The testing program that was followed in this Task is elaborated in Table 3-9.

Table 3-6. Test parameters used to optimize FR-SCC and FR-SWC mixtures for Task 2A

SCC					SWC				
No.	MSA (in.)	Fly Ash Replacement (%)	EA Type	EA Dosage (%)	No.	MSA (in.)	Fly Ash Replacement (%)	EA Type	EA Dosage (%)
1	3/8	0	-	-	12	0.5	0	-	-
2	3/8	30	-	-	13	0.5	30	-	-
3	3/8	50	-	-	14	0.5	50	-	-
4	3/8	0	CaO	4	15	0.5	0	CaO	4
5	3/8	30	CaO	4	16	0.5	30	CaO	4
6	3/8	0	CaO	8	17	0.5	0	CaO	8
7	3/8	30	CaO	8	18	0.5	30	CaO	8
8	3/8	0	k-component	4	19	0.5	0	k-component	4
9	3/8	30	k-component	4	20	0.5	30	k-component	4
10	3/8	0	k-component	8	21	0.5	0	k-component	8
11	3/8	30	k-component	8	22	0.5	30	k-component	8

A steel fiber (3D-hooked end) will be used for all the mixtures at a volume replacement of 0.5%

Task 2B: Selection of fiber type for FR-SCC and FR-SWC

Eight fiber types were tested, as follows: Steel fibers – hooked end (3D), Steel fibers – hooked end (4D), Steel fibers – hooked end (5D), Steel fibers – hooked end (ST1),

Carbon fiber (CA) , Propylene Straight monofilament syntactic fibers (PLP), A hybrid of Steel and polypropylene Multifilament (STPL), Micro-Macro steel fiber (STST).

Table 3-7 summarized the testing matrix that was used in Task 2B to optimize fiber type for FR-SCC and FR-SWC. In total, 16 mixtures were tested according to the program in Table 3-8.

Table 3-7: Mixture matrix for Task 2B

SCC and FR-SCC					
No.	MSA (in.)	Fly Ash Replacement (%)	EA Type & Dosage	Fiber Type	Fiber Volume (%)
1	3/8	30% was determined from Task 2A	4% G-Type and 8% K-Type were determined from Task 2A	No fibers	0.5
2				ST1	
3				3D	
4				STST	
5				PLP	
6				STPL	
7				CA	
SWC and FR-SWC					
No.	MSA (in.)	Fly Ash Dosage (%)	EA Type & Dosage	Fiber Type	Fiber Volume (%)
8	0.5	30% determined from Task 2A	4% G-Type and 8% K-Type were determined from Task 2A	No fibers	0.5
9				ST1	
10				3D	
11				4D	
12				5D	
13				STST	
14				PLP	
15				STPL	
16				CA	

Task 2C: Optimizing fiber volume for FR-SWC

Four types of fibers (ST1, STST, 5D, and STPL) were incorporated to FR-SWC at a fiber volume of 0.75%, only three types of fibers (ST1, STST, and 5D) showed acceptable

workability. FR-SWC made with the acceptable three fibers at a fiber volume of 0.75% were evaluated for fresh properties and Mechanical properties.

The passing ability, stability and the HRWRA dosage to secure the required flowability were included in an overall performance evaluation of fresh properties. The mechanical properties of the optimized FR-SCC and FR-SWC mixtures were included in the overall evaluation as well. Three FR-SCC mixtures were optimized in addition to the SCC reference and four FR-SWC mixtures were optimized besides the SWC reference. The selected FR-SCC mixtures and FR-SWC mixtures was evaluated in next tasks which included measurement of drying shrinkage, resistance to shrinkage cracking, frost durability, and structural performance.

Task 2D: Shrinkage and durability evaluation of FR-SCC and FR-SWC

Four FR-SCC mixtures and four FR-SWC mixtures beside SCC and SWC references were optimized from the last three subtasks and were evaluated for drying shrinkage, restrained shrinkage and freeze/thaw durability.

The Experimental program followed including testing for:

1. Fresh properties and rheology
2. Mechanical properties and flexural crack resistance
3. Shrinkage
4. Freeze/thaw durability
5. Structural performance (will be elaborated in Chapter 5)

- a) Structural performance of FR-SWC and FR-SCC monolithic beams
- b) Structural performance of CVC beams repaired using FR-SCC

Table 3-8: Proposed concrete test methods

Property		Test Method	Test Title/Description	Task	
Fresh Properties					
Physical	Unit Weight	ASTM C 138	Standard test method for density (unit weight)	2A	2B,C
	Air Content (10-70 min)	ASTM C 231	Standard test for air content of freshly mixed concrete by the pressure method		
Filling Ability	Slump/Slump Flow & T50 (10-70 min)	ASTM C 143 ASTM C 1611	Standard test for slump flow of SCC/hydraulic-cement concrete	2A	2B,C
Passing Ability (SCC)	J-Ring (10-70 min)	ASTM C 1621	Standard test for passing ability of SCC by J-ring	2A	2B,C
Passing Ability	Modified J-Ring (10-70 min)	Reference 5		2A	2B,C
Stability	Surface Settlement			-	2B,C
	Visual Stability Index	ASTM C 1611		2A	2B,C
	Sieve Test			2A	2B,C
	Bleeding	ASTM C 232		2A	2B,C
Rheology	Yield Stress & Plastic Viscosity (10-70 min)	Contec 5 Rheometer		-	2B,C
Hardened Properties					
Compressive Strength (28 and 56 d)		ASTM C 39	Standard test for compressive strength of cylindrical concrete specimens	2A	2B,C
Splitting Tensile Strength (28 and 56 d)		ASTM C 496	Standard test for splitting tensile strength of cylindrical concrete specimens	2A	2B,C
Flexural Strength (28 and 56 d)		ASTM C 78	Standard test for flexural strength of concrete	-	2B,C
Fracture Energy (28 and 56 d)		ASTM C 1609			2B,C
Flexural toughness (28 and 56 d)		RILEM			2B,C
Modulus of Elasticity (28 and 56 d)		ASTM C 469	Standard test for static modulus of elasticity	-	2B,C
Drying Shrinkage (7d moist curing)		ASTM C 157		-	2D
Restrained Shrinkage		ASTM C 1581 AASHTO PP34	Two standard tests in ASTM and AASHTO	-	2D
Freeze-Thaw Resistance		ASTM C 666			2D

3.3.1 Fresh properties and rheology

All of the investigated mixtures were tested for slump flow and visual stability index (VSI). Fresh property testing included slump flow, J-Ring, modified J-Ring [2], bleeding, air content, specific gravity, and surface settlement. The modified J-Ring was carried out for the FR-SCC and consists of a ring with eight bars compared to 16 bars in the standard test (ASTMC1621). The J-Ring, the modified J-Ring, bleeding, air content, specific gravity and surface settlement tests were performed for mixtures that showed acceptable workability. Table 3-9 shows the desired workability requirements. Slump flow was measured after 10 and 70 min.

Figure 3-1 shows different fresh properties testing, and Figure 3-2 shows measuring rheological properties using two different rheometers; ICAR rheometer and Contec 5 rheometer.



Figure 3-1: Testing fresh properties



Figure 3-2: Rheological properties measurement

Table 3-9: Workability requirements for FR-SCC and FR-SWC

Property	Filling ability	Passing ability	Stability		
			Visual Stability Index	Bleeding	Surface Settlement
Test	Slump flow	Modified J -Ring			
Requirements for FR-SCC	650-700 mm	$R_{slump} - R_{ring} = 50 \text{ mm}$	0-1	< 1%	< 0.5%
Requirements for FR-SWC	500-550 mm	$R_{slump} - R_{ring} = 50 \text{ mm}$	0-1	< 1%	< 0.5%

3.3.2 Mechanical properties and flexural crack resistance

Sampling of 4 x 8 in. cylinders to determine compressive strength, splitting tensile strength and modules of elasticity, four beams 3 x 3 x 16 in. for flexural strength (ASTM C78) and flexural toughness (ASTM C1609) and four notched beams (6 x 16 x 22 in.) for crack resistance (RILEM TC-162) was done for the mixtures that showed acceptable workability. Figure 3-3 shows the mechanical properties testing including compressive strength, splitting tensile strength, modules of elasticity, flexural strength, flexural

toughness and flexural crack resistance. All of the hardened properties were tested after 28 days and 56 days moist curing.



Figure 3-3: Mechanical properties testing

3.3.2.1 Flexural performance testing

Figure 3-4 shows the test setup used to evaluate flexural performance of FR-SCC and FR-SWC beam specimens. Molded beam specimens having a square cross-section 3 x 3 in. and length of 16 in. of fiber-reinforced concrete were tested in flexure using a four-point loading arrangement. A closed-loop, servo-controlled testing system and roller supports that are free to rotate on their axes were incorporated. Load and net deflection were monitored and recorded to an end-point deflection of 0.8 in. Data were recorded and plotted by means of an X-Y plotter, or they are recorded digitally and subsequently used to plot a load-deflection curve. Points termed first-peak was used to calculate flexural strength (Modulus of rapture). Area under load-deflection curve up to 0.8 in. deflection expressed the toughness of each specimen.

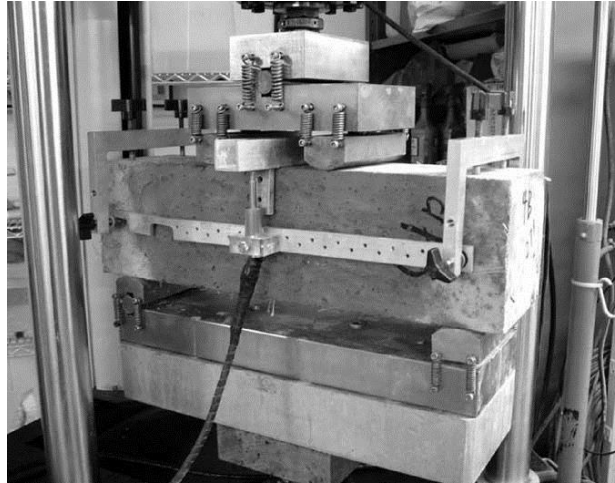


Figure 3-4: Test setup for flexural performance of FR-SCC and FR-SWC beams

3.3.2.2 Crack resistance testing

Test setup mentioned in RILEM TC 162-TDF was followed as shown in Figure 3-5. Concrete beams of 6 x 6 in. cross section with a length of 22 in. having a notch of 0.2 in. width and a one in. depth in the mid-span were used. MTS closed loop testing machine which was capable of producing a constant rate of increase of deflection (0.008 in./min) was used. The span length of the three-point loading test was 20 in. a Crack mouth opening displacement (CMOD) sensor was applied at the notch and connected to a data accusation system to measure the crack width with time. The MTS machine stored the load applied with time. The data accusation system and MTS machine started monitoring the data at the same exact time. The specimen was loaded continuously up to 3.5 mm (1.378 in.) crack width. The data from MTS machine and the data accusation system were combined to plot the load vs. (CMOD) up to 1.378 in. The peak load and the residual load at 1.378 in. was monitored for all of the tested specimens.

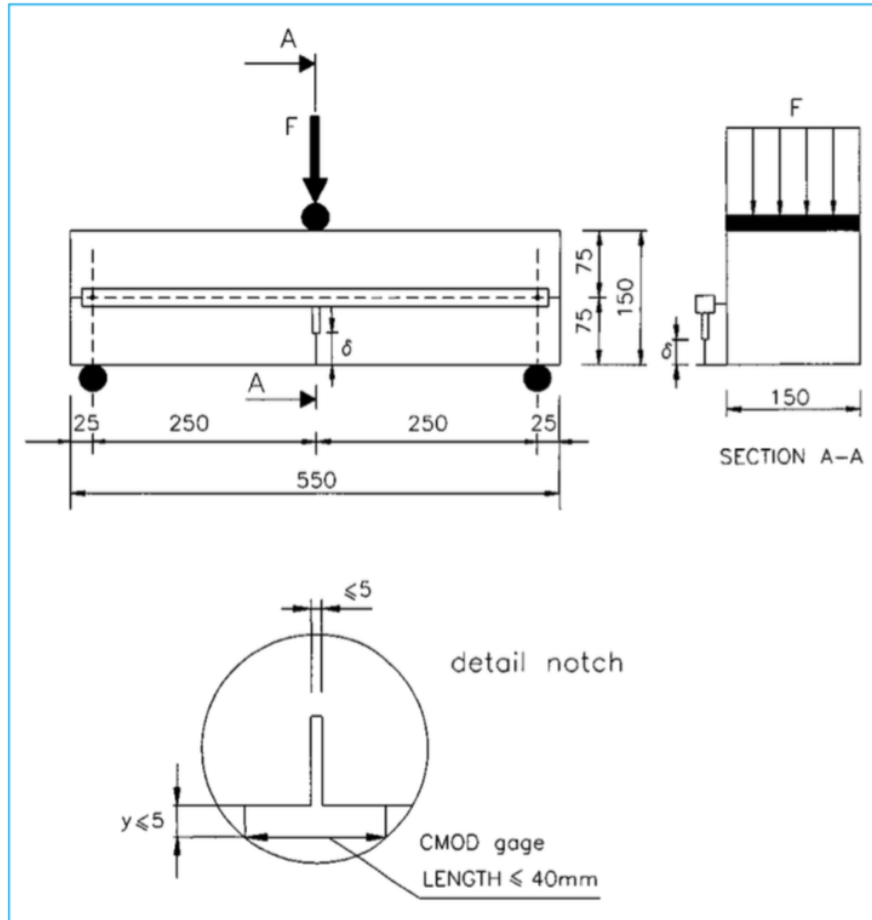


Figure 3-5: RILEM TC 162-TDF Test setup for testing Crack resistance for FR-SCC and FR-SWC (dimensions in mm)

3.3.3 Shrinkage

3.3.3.1 Drying shrinkage

Three $3 \times 3 \times 11.25$ in. prismatic specimens were taken for each mixture to be tested for drying shrinkage in accordance to ASTM C 157. Digital type extensometer was used to measure the initial and the shrink lengths of the prisms. The samples were cured for seven days then transferred and stored in a temperature and humidity controlled room of

temperature 23 °C and relative humidity of 50% RH. Shrinkage was measured up to 365 days.

3.3.3.2 Restrained shrinkage

Restrained shrinkage was evaluated in accordance to ASTM C1581. A ring-type test was performed which consists of two 6 in. height concentric rings; inner steel ring of thickness 0.5 in. and diameter 13 in. and outer cardboard ring of diameter 16 in. The two rings were fixed using bolts with eccentric washers. Concrete was cast in between the two rings. Upon transfer of the test specimens to the testing environment (a temperature and humidity controlled room of temperature 23°C and relative humidity of 50% RH), immediately the bolts with eccentric washers were loosen, and the washers were rotated so they are not in contact with the steel ring and outer ring. The rings were left to cure for 24 hours by covering then using wet burlaps.

Three strain gages were attached to the inner surface of the steel ring. The gauges were used to monitor stress development induced by restrained shrinkage in the concrete. The steel strain was monitored immediately after casting with subsequent readings taken every 20 min until concrete cracking. A sudden decrease in steel strain was taken as a sign of shrinkage cracking in the concrete. Two concrete rings were sampled for each concrete mixture.

3.3.4 Freeze-thaw durability

Three 3 × 3 × 16 in. prismatic specimens were taken for each mixture to be tested for freeze-thaw resistance in accordance to ASTM C666 procedure A. The concrete prisms

were cured first for 28 days before moving to the freeze-thaw chamber for testing. Specimens were subjected to 300 freeze-thaw cycles. After every 30 cycles, the mass loss and transverse frequency of concrete specimens were determined. The ultrasonic pulse velocity test was used to calculate the dynamic modulus of elasticity of the specimens.

4 Test Results and Discussion

4.1 Test results of Task 2A

In Task 2A, concrete mixtures were tested to evaluate workability, air content, passing ability and stability. This included a reference of SCC and SWC with no fibers and other mixtures with different binder proportionating as shown in Table 4-1. The concrete was tested for air content, slump flow, modified J-ring, and bleeding. The mixtures were sampled to prepare 12 cylinders to evaluate compressive strength and splitting tensile strength at 28 and 56 days.

Table 4-1: Test parameters used to optimize FR-SCC and FR-SWC mixtures for Task 2A

SCC					SWC				
No.	MSA (in.)	Fly Ash Replacement (%)	EA Type	EA Dosage (%)	No.	MSA (in.)	Fly Ash Replacement (%)	EA Type	EA Dosage (%)
1	3/8	0	-	-	12	0.5	0	-	-
2	3/8	30	-	-	13	0.5	30	-	-
3	3/8	50	-	-	14	0.5	50	-	-
4	3/8	0	CaO	4	15	0.5	0	CaO	4
5	3/8	30	CaO	4	16	0.5	30	CaO	4
6	3/8	0	CaO	8	17	0.5	0	CaO	8
7	3/8	30	CaO	8	18	0.5	30	CaO	8
8	3/8	0	k-component	4	19	0.5	0	k-component	4
9	3/8	30	k-component	4	20	0.5	30	k-component	4
10	3/8	0	k-component	8	21	0.5	0	k-component	8
11	3/8	30	k-component	8	22	0.5	30	k-component	8

A steel fiber (ST1-hooked end) will be used for all the mixtures at a volume replacement of 0.5%

4.1.1 Fresh properties

Tables 4-2 and 4-3 show the fresh properties of FR-SCC and FR-SWC, respectively. Total amount of binders was first optimized for FR-SWC at 380 kg/m^3 which results in a stable mixture with the desired workability properties. The mixtures with 30% fly ash replacement (Mixture 2 and Mixture 15) showed better performance in fresh state and also in hardened state compared to mixtures having 0% or 50% fly ash, so 30% fly ash replacement is selected. AEA was used with both FR-SCC and FR-SWC to secure air volume between 6% to 9%. Slump flow was adjusted using HRWRA between 650 to 700 mm in case FR-SCC and between 500 to 550 in case FR-SWC. All mixtures were very stable having VSI of 0. Different proportioning of binders did not have a significant effect on passing ability of FR-SCC and FR-SWC. The use of the K-Type EA lead to high degree in loss of workability with time compared to the reference mixture made without any expansive agent or with G-Type EA as shown in figure 4-1. FR-SCC with no EA lost 22% of the slump flow in 60 mins. FR-SCC with 4% Type-G EA lost 8% of the slump flow in 60 mins compared to 50% in case of 8% Type-K EA.

Table 4-2: Fresh properties for SCC and FR-SCC

No	FA	EA	Fibers	Unitweight (kg/m^3)	Air (%)	Slump flow (mm)	Modified J-Ring (mm)	VSI	Bleeding (%)
1	0	0	0	2198	6.6	680	660	0	0.426
2	0	0	0.5% ST1	2158	7.6	660	630	0	0
3	30%	0	0.5% ST1	2218	6.6	670	660	0	0.742
4	50%	0	0.5% ST1	2185	5.7	670	630	0	1.14
5	0	4% G-Type	0.5% ST1	2210	6.8	665	630	0	0.68
6	0	8% G-Type	0.5% ST1	2189	7.5	665	640	0	0.07
7	0	4% K-Type	0.5% ST1	2166	6.5	670	600	0	0
8	0	8% K-Type	0.5% ST1	2243	6.2	670	560	0	0.258
9	30%	4% G-Type	0.5% ST1	2216	6.5	660	620	0	0.651
10	30%	8% G-Type	0.5% ST1	2195	7	680	660	0	0.304
11	30%	4% K-Type	0.5% ST1	2221	6.2	660	630	0	0.178
12	30%	8% K-Type	0.5% ST1	2229	6.2	670	620	0	0.196

Table 4-3: Fresh properties for SWC and FR-SWC

No	FA	EA	Fibers	Unit weight (kg/m ³)	Air (%)	Slump flow (mm) 10 min	Modified J-Ring (mm)	VSI	Bleeding (%)
13	0	0	0	2188	10.5	500	490	0	0
14	0	0	0.5% ST1	2206	6.2	500	430	0	0
15	30%	0	0.5% ST1	2234	5.8	500	480	0	0.34
16	50%	0	0.5% ST1	2250	7.2	540	450	0	0.26
17	0	4% G-Type	0.5% ST1	2271	6.2	530	500	0	0.1
18	0	8% G-Type	0.5% ST1	2233	7.9	560	530	0	0.62
19	0	4% K-Type	0.5% ST1	2289	6.8	550	450	0	1.1
20	0	8% K-Type	0.5% ST1	2210	6.3	495	480	0	0
21	30%	4% G-Type	0.5% ST1	2310	5.8	550	510	0	0.5
22	30%	8% G-Type	0.5% ST1	2245	7.4	550	500	0	0.8
23	30%	4% K-Type	0.5% ST1	2291	6.5	560	490	0	1
24	30%	8% K-Type	0.5% ST1	2245	6.1	510	490	0	0

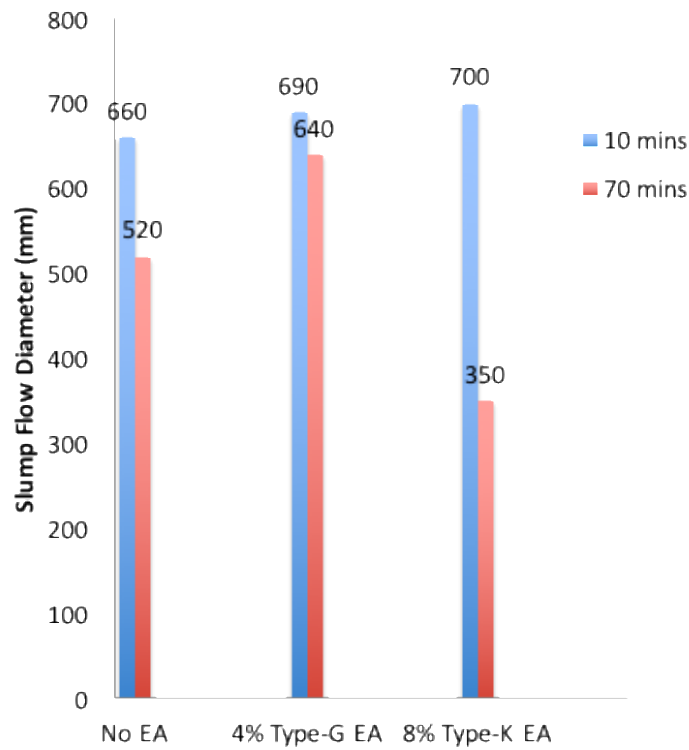


Figure 4-1: Flow diameters for FR-SWC after 10 and 70 mins

4.1.2 Mechanical properties

Tables 4-4 and 4-5 show the compressive strength and the splitting tensile strength for FR-SCC and FR-SWC, respectively. The 56-day compressive strength and splitting tensile strength for 30% FA replacement are higher than those of 50% FA replacement in FR-SCC by 61% and 41%, respectively. In case of FR-SWC, the 56-day compressive strength and splitting tensile strength for 30% FA replacement are higher than those of 50% FA replacement by 140% and 100%, respectively. The Conex (G-Type EA) and the K-component (K-Type EA) expansive agents were employed at dosage rates of 0, 4% and 8%. The 30% and 0% FA replacements were selected to be employed with G-Type EA with different percentages (0%, 4% and 8%) and K-Type EA also with different percentages (0%, 4% and 8%).

Table 4-4: Mechanical properties for SCC and FR-SCC

No	FA	EA	Fibers	Compressive strength (psi)		Splitting tensile strength (psi)	
				28 d	56 d	28 d	56 d
1	0	0	0	3723	5375	303	426
2	0	0	0.5% ST1	3882	5680	520	527
3	30%	0	0.5% ST1	3782	5690	608	643
4	50%	0	0.5% ST1	2759	3527	445	456
5	0	4% G-Type	0.5% ST1	3723	5442	658	685
6	0	8% G-Type	0.5% ST1	4134	4765	426	452
7	0	4% K-Type	0.5% ST1	4254	4780	425	457
8	0	8% K-Type	0.5% ST1	5793	6000	554	606
9	30%	4% G-Type	0.5% ST1	5336	5753	303	426
10	30%	8% G-Type	0.5% ST1	5060	5276	546	595
11	30%	4% K-Type	0.5% ST1	5441	5751	457	474
12	30%	8% K-Type	0.5% ST1	5336	5753	630	653

Table 4-5: Mechanical properties for SWC and FR-SWC

No	FA	EA	Fibers	Compressive strength (psi)		Splitting tensile strength (psi)	
				28 d	56 d	28 d	56 d
13	0	0	0	3279	3656	340	352
14	0	0	0.5% ST1	5355	5789	533	537
15	30%	0	0.5% ST1	5065	5755	526	530
16	50%	0	0.5% ST1	2142	2366	255	256
17	0	4% G-Type	0.5% ST1	7458	7849	591	635
18	0	8% G-Type	0.5% ST1	4714	5388	492	508
19	0	4% K-Type	0.5% ST1	6240	7072	913	652
20	0	8% K-Type	0.5% ST1	4594	4931	445	324
21	30%	4% G-Type	0.5% ST1	5709	5932	558	567
22	30%	8% G-Type	0.5% ST1	5351	5616	472	557
23	30%	4% K-Type	0.5% ST1	5679	5850	528	553
24	30%	8% K-Type	0.5% ST1	5910	6130	582	599

Figure 4-2 shows that the compressive strength and splitting tensile strength for the FR-SCC mixtures having 30% fly ash with different expansive agent types and dosage rates. Figure 4-3 shows the compressive strength and splitting tensile strength for the SWC mixtures having 30% fly ash with different expansive agent types and dosages. For both the FR-SWC and FR-SCC mixtures, the same results were observed: the use of 4% Type-G replacement resulted in better performance than concrete with 8%. However, in the case of the K-Type EA, concrete with 8% K-component replacement yield better results than those with 4% dosage rate.

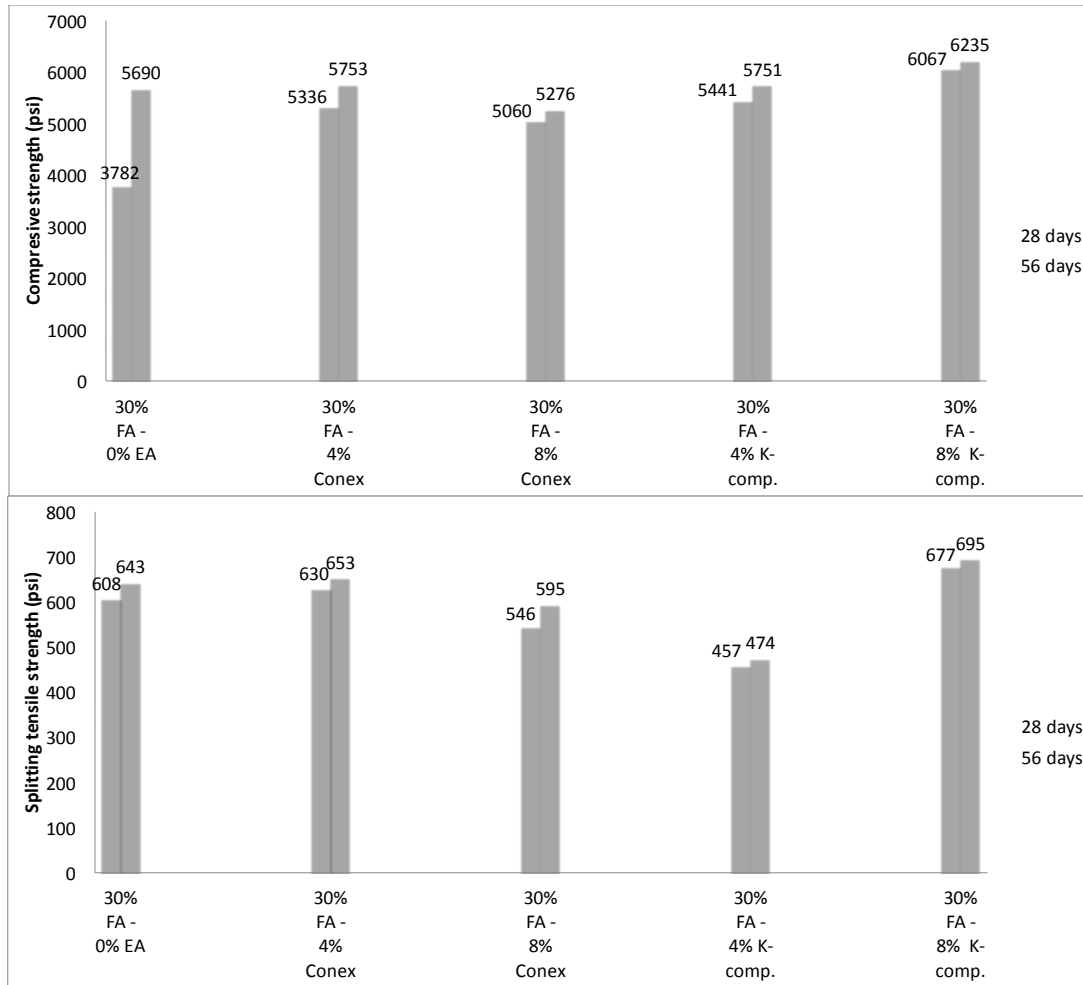


Figure 4-2: Compressive strength and splitting tensile strengths of FR-SCC mixtures having 30% fly ash and different types and dosage rates of expansive agents

In case of FR-SCC made with 4% Type-G EA had a higher compressive strength compared to 0% EA and 8% EA by 5% and 7%, respectively, while the splitting tensile strength was higher in case of 4% Type-G EA compared to 0% EA and 8% EA by 5% and 10%, respectively. FR-SCC made with 8% Type-K EA had a higher compressive strength compared to 0% EA and 4% EA by 10% and 9%, respectively, while the splitting tensile strength was higher in case of 8% Type-K EA compared to 0% EA and 4% EA by 9% and 45%, respectively.

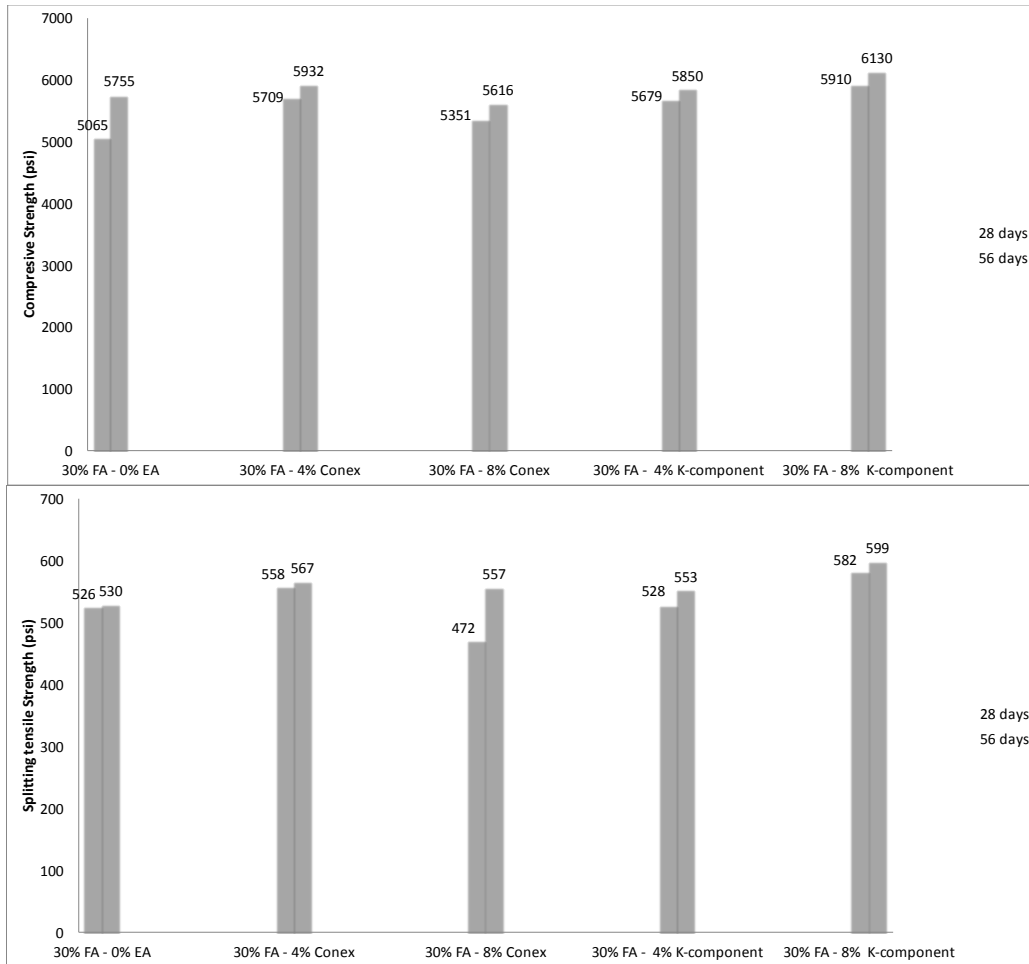


Figure 4-3: Compressive strength and splitting tensile strengths of FR-SCC mixtures having 30% fly ash and different types and dosage rates of expansive agents

In case of FR-SWC made with 4% Type-G EA had a higher compressive strength compared to 0% EA and 8% EA by 3% and 5%, respectively, while the splitting tensile strength was higher in case of 4% Type-G EA compared to 0% EA and 8% EA by 7% and 4%, respectively. FR-SWC made with 8% Type-K EA had a higher compressive strength compared to 0% EA and 4% EA by 6% and 5%, respectively, while the splitting tensile strength was higher in case of 8% Type-K EA compared to 0% EA and 4% EA by 13% and 9%, respectively.

4.2 Test results of Task 2B and Task 2C

In Task 2B eight fiber types were tested, as follows: Steel fibers – hooked end (3D), Steel fibers – hooked end (4D), Steel fibers – hooked end (5D), Steel fibers – hooked end (ST1), Carbon fiber (CA), Propylene Straight monofilament syntactic fibers (PLP), A hybrid of Steel and polypropylene Multifilament (STPL), Micro-Macro steel fiber (STST). The different fibers were incorporated to FR-SCC and FR-SWC at 0.5% fiber volume. Fibers that showed acceptable workability were sampled and tested for mechanical properties.

In Task 2C four types of fibers (ST1, STST, 5D, and STPL) were incorporated to FR-SWC at a fiber volume of 0.75%, only three types of fibers (ST1, STST, and 5D) showed acceptable workability. FR-SWC made with the acceptable three fibers at a fiber volume of 0.75% were evaluated for fresh properties and Mechanical properties.

Overall performance was performed for all FR-SCC and FR-SWC. The passing ability, stability and the HRWRA dosage to secure the required flowability were included in an overall performance evaluation of fresh properties. The mechanical properties of the optimized FR-SCC and FR-SWC mixtures were included in the overall evaluation as well. Three FR-SCC mixtures were optimized in addition to the SCC reference and four FR-SWC mixtures were optimized besides the SWC reference. The selected FR-SCC mixtures and FR-SWC mixtures was evaluated in next tasks which included measurement of drying shrinkage, resistance to shrinkage cracking, frost durability, and structural performance.

4.2.1 Fresh properties

Table 4-6 summarize the workability requirements for FR-SCC and FR-SWC. All the mixtures first were tested for slump flow and the dosage of HRWRA was adjusted for each mixture to have a slump flow of 650 to 700 mm in case a FR-SCC mixtures and 500-550 mm in case of FR-SWC mixtures. The VSI was observed for all of the mixtures, the mixtures with VSI of 2 or more were rejected. Other fresh properties tests were only performed for mixtures with VSI of 0 or 1.

Table 4-6: Workability requirements for FR-SCC and FR-SWC

Property	Filling ability	Passing ability	Stability		
			Test	Slump flow	Modified J -Ring
Requirements for FR-SCC	650-700 mm	$R_{slump} - R_{ring} = 50$ mm	0-1	< 1%	< 0.5%
Requirements for FR-SWC	500-550 mm	$R_{slump} - R_{ring} = 50$ mm	0-1	< 1%	< 0.5%

Table 4-7 and Table 4-8 summarize the fresh properties of FR-SCC and FR-SWC mixtures, respectively. The AEA demand for propylene fibers (PLP) fibers and hybrid fibers of polypropylene and steel (STPL) was lower than that of ST1 and STST.

Table 4-7: Fresh properties of SCC and FR-SCC mixtures

No	Fiber type	V_f (%)	EA Type	Unit weight (kg/m^3)	Air (%)	Slump flow (mm) 10 min/60 min	Modified J-Ring D/a (mm/mm)	VSI	Bleeding (%)	Surface Settlement (%)
R1	-	0	-	2152	6.5	680/640	650/29	0	0.61	0.57
R2	ST1	0.5	-	2149	8	660/520	580/43	0	0.3	0.35
R3	-	0	-	2155	8	670/530	660/30	0	0.33	0.20
1	ST1	0.5	K-Type	2205	7	700/350	630/47	0	0	0.31
2	ST1	0.5	G-Type	2184	6.8	690/640	605/45	0	0	0.64
3	PLP	0.5	G-Type	2090	8.5	670/500	550/44	1	0.47	0.53
4	3D	0.5	G-Type	-	-	660/-	-	3	-	-
5	STPL	0.5	G-Type	2102	9	690/520	620/43	0	0.38	0.65
6	STST	0.5	G-Type	2144	8	700/535	600/40	0	0.41	0.34
7	CA	0.5	G-Type	-	-	660/-	-	3	-	-

Table 4-8: Fresh properties of SWC and FR-SWC mixtures

No	Fiber type	V_f (%)	Unit weight (kg/m^3)	Air (%)	Slump flow (mm) 10 min/60 min	Modified J-Ring D/a (mm/mm)	VSI	Bleeding (%)	Surface Settlement (%)
R1	-	-	2130	7.8	570/255*	565/26	0	0	0.16
1	ST1	0.5	2254	8.8	505/205*	470/32	0	0	0.28
2	3D	0.5	2206	9	580/180*	450/30	0	0	0.14
3	4D	0.5	2280	8	540/175*	430/29	0	0	0.22
4	5D	0.5	2238	8.7	510/165*	400/27	0	0	0.13
5	STPL	0.5	2206	9	525/205*	430/31	0	0	0.20
6	STST	0.5	2268	7.5	540/230*	440/29	0	0	0.39
7	PLP	0.5	-	-	490	-	2	-	-
8	ST1	0.75	2314	6.9	550/255*	540/45	0	0	0.36
9	STST	0.75	2280	7.5	540/115*	430/37	0	0	0.32
10	5D	0.75	2278	8	560/125*	500/45	0	0	0.19

Generally, fibers decreased the workability of FR-SCC, especially the passing ability. The increase in fiber factor ($V_f L_f/ d_f$) decreased the passing ability of FR-SCC. Figure 4-4, for FR-SCC mixtures, and Figure 4-5, for FR-SWC mixtures, show the relationship between the fiber factor and the modified J-Ring ratio, the ratio between the diameter of spread to the average height (D/a) is referred to as passing ability index and is shown to decrease with the increase in fiber factor regardless of the fiber type. Similar relationship was reported in [23]. Type K EA had significant effect in reducing slump flow of FR-SCC with time, especially with the moderate w/c of 0.42 in use. The decrease in fluidity resulted in enhancement of stability compared to others with Type G EA or without any EA. Type G EA is shown to increase the passing ability of FR-SCC, but it can decrease slightly stability.

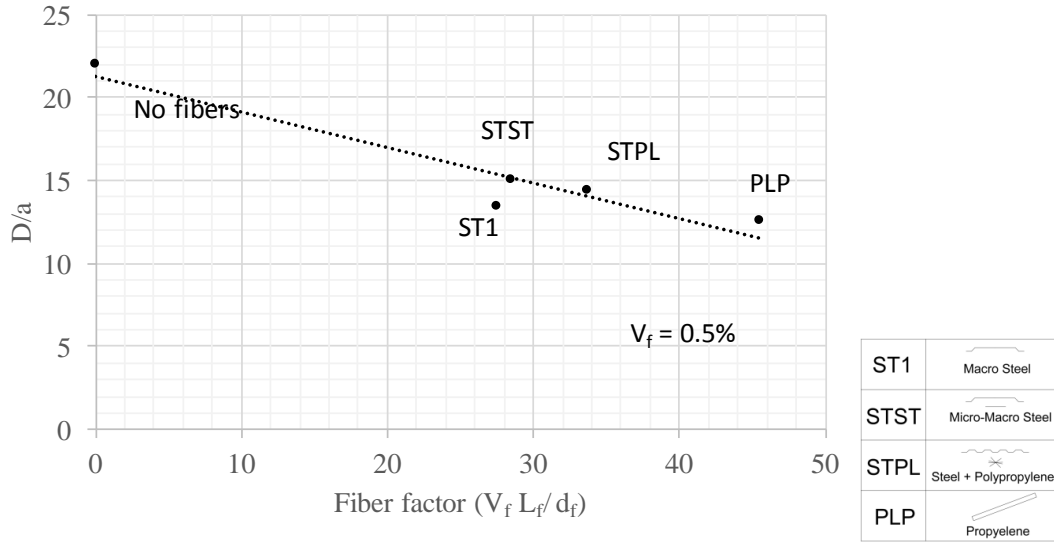


Figure 4-4: Effect of the fiber factor on the passing ability of FR-SCC

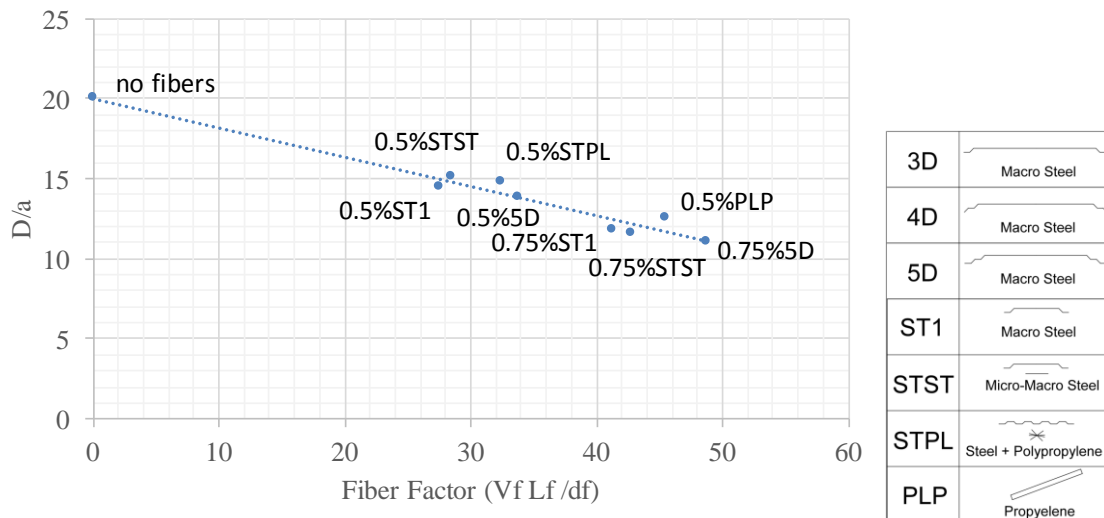


Figure 4-5: Effect of the fiber factor on the passing ability of FR-SWC

Figure 4-5 combines the modified J-Ring passing ability results of FR-SWC from Task 2B ($V_f = 0.5\%$) and Task 2C ($V_f = 0.75\%$), which generalize the results from Task 2B to different fiber factors 0.5% and 0.75% compared to 0.5% only in Task 2B. Increasing fiber factor resulted in decreasing of the Passing ability for all of the fibers employed.

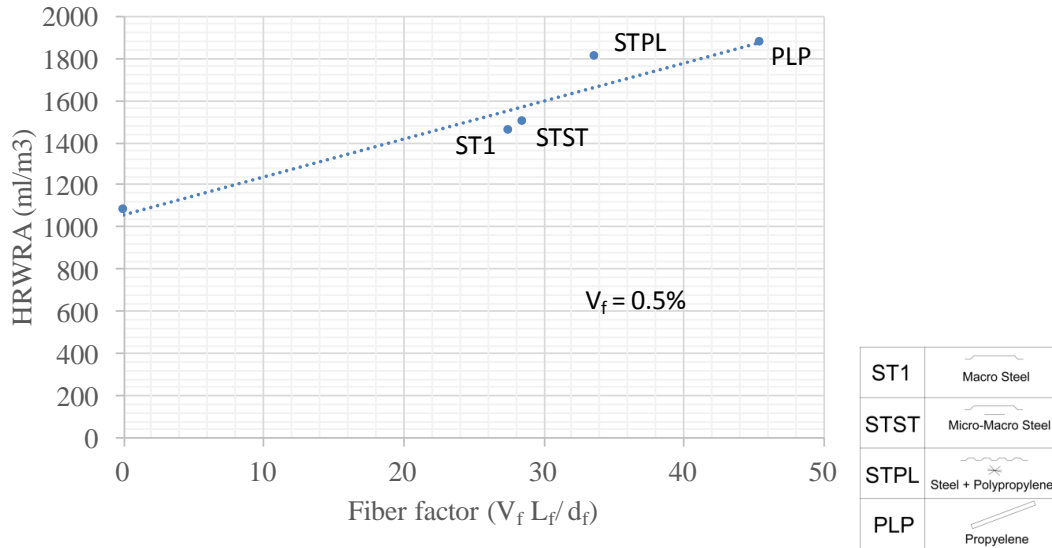


Figure 4-6: Effect of the fiber factor on the HRWRA demand of FR-SCC

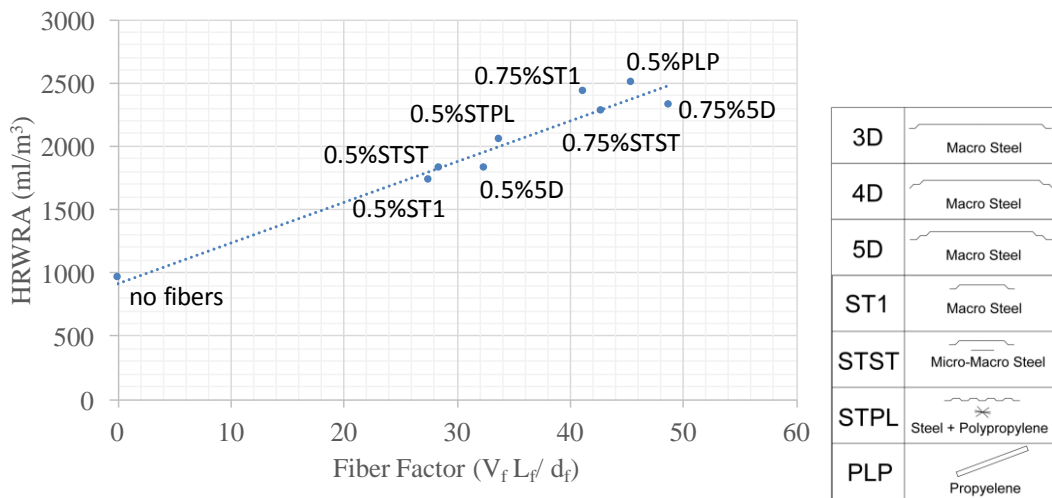


Figure 4-7: Effect of the fiber factor on the HRWRA demand of FR-SWC

Figure 4-6 shows the directly proportional relationship between fiber factor and the HRWRA demand of FR-SCC. Figure 4-7 combines the HRWRA demand of FR-SWC from Task 2B ($V_f = 0.5\%$) and Task 2C ($V_f = 0.75\%$), which generalize the results from Task 2B to different fiber factors 0.5% and 0.75% compared to 0.5% only in Task 2B.

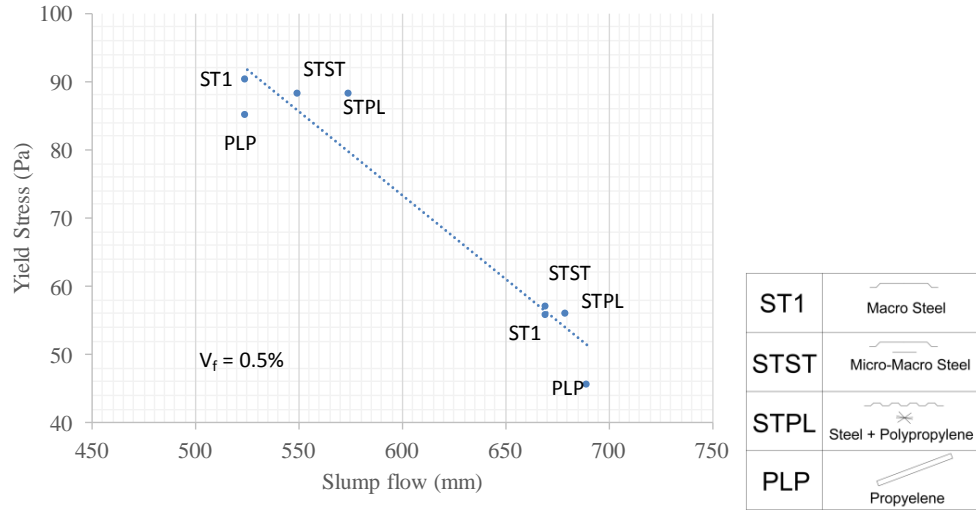


Figure 4-8: Effect of the fiber factor on the yield stress of FR-SCC

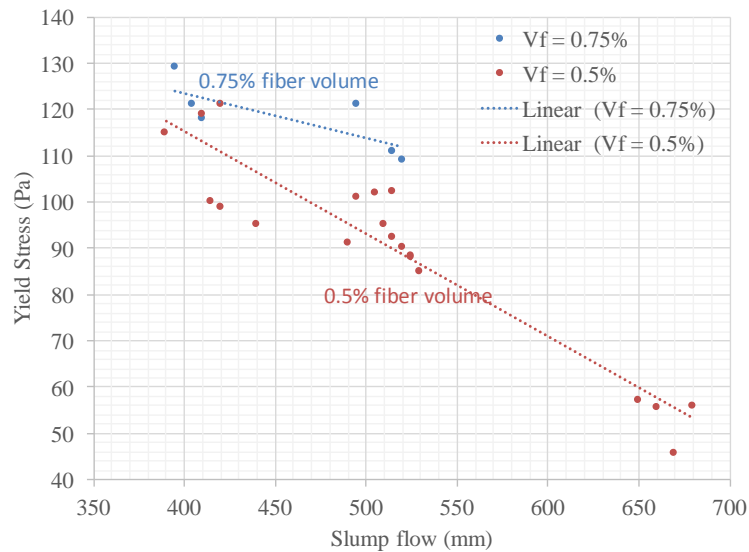


Figure 4-9: Effect of the fiber factor on the yield stress of FR-SWC

Figure 4-8 show the inversely proportional relationship between fiber factor and the yield stress of FR-SCC, where all fibers were incorporated at 0.5% fiber volume. Figure 4-8 show two inversely proportional relationships (for 0.5% and 0.75% fiber volumes) between fiber factor and the yield stress of FR-SWC. Increasing fiber factor resulted in increasing of the yield stress for all of the fibers employed.

4.3 Mechanical properties

Table 4-9 summarizes the compressive strength, splitting tensile strength, flexural strength, toughness, crack resistance, and elastic modulus of SCC and FR-SCC. The incorporation of Hooked end steel fibers (ST1) increased the 56-day compressive strength of SCC by 8% and 17% in mixtures containing 4% and 8% G-type and K-type, respectively. On the other hand, the combination between 30 mm hooked end steel fibers and micro steel fibers (STST) increased compressive strength by 30%. The use of 0.5% ST1 increased the 56-day splitting tensile strength by 43% and 56% in mixtures containing 4% and 8% G-type and K-type, respectively. The use of the combined macro-micro steel fibers (STST) increased the splitting tensile strength by 68%. A hybrid of 50 mm crimped steel fibers and micro polypropylene fibers (STPL) increased the 56-day splitting tensile strength by 12%. Propylene fibers (PLP) increased the 56-day splitting tensile strength of SCC by 11% in the case of the 40 mm Propylene fibers (PLP) with 4% G-type EA. The 56-days flexural strength with the use of 0.5% ST1 increased by 17% and 5% in mixtures containing 4% and 8% G-type and K-type, respectively. The combination between 30 mm hooked end steel fibers and micro steel fibers (STST) increased the 56-day flexural strength by 32%.

Table 4-9: Hardened properties of FR-SCC

No	Fiber type	V _f (%)	EA Type	Compressive strength (psi)		Splitting tensile strength (psi)		Flexural strength (psi)		Toughness (lb.in)		First Crack stress (psi)		Residual stress (psi)		Elastic Modulus (Ksi)	
				28 d	56 d	28 d	56 d	28 d	56 d	28 d	56 d	28 d	56 d	28 d	56 d	28 d	56 d
R1	-	0	-	4540	4780	325	360	381	410	4.75	5.13	425	459	0	0	4350	4340
R2	ST1	0.5	-	4560	4780	420	465	676	729	106	114	456	493	323	349	3860	4070
R3	-	0	-	4350	4470	315	340	465	500	4.42	4.78	-	-	-	-	4240	3870
1	ST1	0.5	K-Type	5100	5110	500	530	490	526	72	78	495	535	459	488	3910	4020
2	ST1	0.5	G-Type	4700	5080	440	485	540	585	88	95	545	590	236	246	3810	4030
3	PLP	0.5	G-Type	4020	4230	365	380	360	388	30	33	369	399	151	166	3450	3740
4	STPL	0.5	G-Type	3840	5000	365	380	453	482	30	34	485	523	234	260	3340	3730
5	STST	0.5	G-Type	5090	5900	490	570	612	668	95	110	535	562	354	385	3810	4130

Table 4-10 summarizes the compressive strength, splitting tensile strength, flexural strength, toughness, crack resistance, and elastic modulus of SWC and FR-SWC. Incorporation of fibers to SWC generally enhance the mechanical strength specially the toughness and the crack resistance. Hooked end steel fibers increased the 56-days compressive strength of SWC about 8% in case of the 30 mm hooked end steel fibers (ST1) at fiber volume (V_f) 0.5% and by 18% at 0.75% V_f, while combination between 30 mm hooked end steel fibers and micro steel fibers (STST) can increase the compressive strength about 12% at 0.5% V_f and by 20% at 0.75% V_f. 5D fibers at 0.5% V_f increase the compressive strength by 13% and by 18% at V_f of 0.75%. Hooked end steel fibers can increase the 56-day splitting tensile strength of SWC about 58% in case of the 30 mm hooked end steel fibers (ST1) at fiber volume (V_f) 0.5% and by 113% at 0.75% V_f, while combination between 30 mm hooked end steel fibers and micro steel fibers (STST) can increase the splitting tensile strength about 66% at 0.5% V_f and by 92% at 0.75% V_f. 5D fibers at 0.5% V_f increase the splitting tensile strength by 87% and by 108% at V_f of

0.75%. In case of the hybrid of 50 mm crimped steel fibers and polypropylene fibers (STPL) at V_f of 0.5% increase the splitting tensile strength of SWC by 20%. Hooked end steel fibers can increase the 56 days' flexural strength of SWC about 6% in case of the 30 mm hooked end steel fibers (ST1) at fiber volume (V_f) 0.5% and by 15% at 0.75% V_f , while combination between 30 mm hooked end steel fibers and micro steel fibers (STST) can increase the flexural strength about 24% at 0.5% V_f and by 35% at 0.75% V_f . 5D fibers at 0.5% V_f increase the flexural strength by 11% and by 114% at V_f of 0.75%. In case of the 4D steel fibers at V_f of 0.5% can increase the flexural strength of SWC by 10%.

Table 4-10: Hardened properties of FR-SWC

No	Fiber type	V_f (%)	EA Type	Compressive strength (psi)		Splitting tensile strength (psi)		Flexural strength (psi)		Toughness (lb.in)		First Crack stress (psi)		Residual stress (psi)		Elastic Modulus (Ksi)	
				28 d	56 d	28 d	56 d	28 d	56 d	28 d	56 d	28 d	56 d	28 d	56 d	28 d	56 d
R1	-	-		5500	6425	400	415	629	680	6.1	6.7	397	430	0	0	3750	4050
1	ST1	0.5	G-Type	5350	6940	520	655	670	720	108	117	546	590	505	545	3930	4150
2	3D	0.5	G-Type	4515	5150	405	575	613	660	95	105	697	750	557	599	3310	3050
3	4D	0.5	G-Type	5585	6895	605	710	703	750	100	109	835	900	600	645	4060	3050
4	5D	0.5	G-Type	6060	7250	740	775	703	755	107	115	1392	1501	931	999	3770	4140
5	STPL	0.5	G-Type	4910	6295	470	495	616	660	24	26	468	505	66	72	3690	3930
6	STST	0.5	G-Type	6050	7170	620	690	785	840	131	142	909	980	682	735	4150	4200
7	ST1	0.75	G-Type	6660	7585	860	885	729	780	114	120	857	925	461	496	3830	4150
8	STST	0.75	G-Type	7460	7680	790	795	849	920	134	146	900	970	496	535	4400	4680
9	5D	0.75	G-Type	6595	7250	845	865	1339	1455	189	202	938	1010	674	725	3770	4140

4.3.1 Toughness

The incorporation of fibers had a considerable impact on ductility of SCC as shown in Figure 4-10 the load deflection curves of beams made with different FR-SCCs. The incorporation of Hooked end steel fibers (ST1) increased the 56-day toughness of SCC

by 20 and 16 times in mixtures containing 4% and 8% G-type and K-type, respectively. The combination of 30 mm hooked end steel fibers and micro steel fibers (STST) increased the toughness by 23 times. The 0.5% fiber volume of propylene fibers (PLP) increased the toughness of the FR-SCC by six times, while the use of STPL fibers increased the 56-day toughness by seven times.

Some of the FR-SCC was shown to exhibit strain softening after concrete cracking such as the case for the STPL and PLP, which results in lower toughness compared to other FR-SCC mixtures made with ST1 and STST that had strain hardening. The incorporation of EA did not have a significant effect on ductility of FR-SCC.

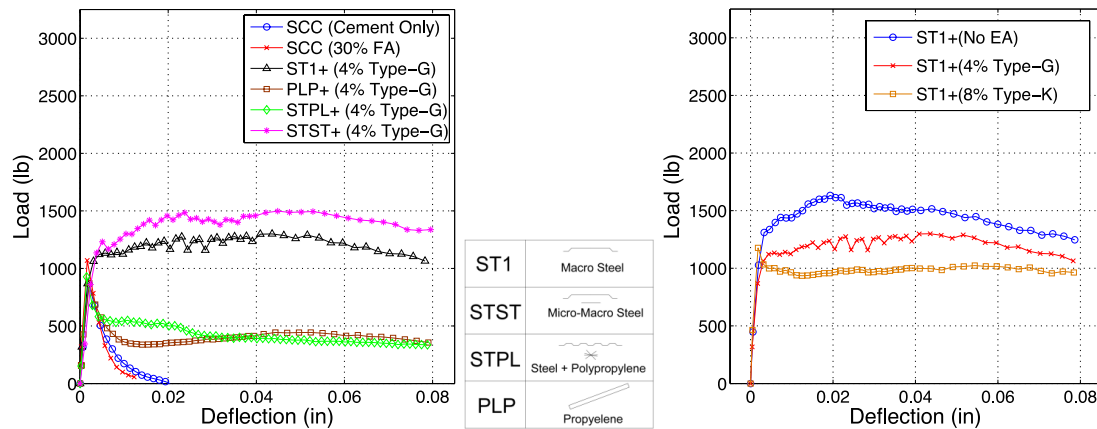


Figure 4-10: 56-day flexural strength and flexural toughness for SCCs and FR-SCCs

The incorporation of fibers had great impact on the ductility of SWC. Figure 4-11 shows the load deflection curves of (3* 3* 16in.) Beams of different FR-SWCs loaded at the first and the second thirds of the span with two point loads. The 56-day toughness of

SWC increased to 17 times in case of addition 0.5% fiber volume of steel fibers (ST1). While combination between 30 mm hooked end steel fibers and micro steel fibers (STST) increased the toughness about 21 times at 0.5% V_f and by 20 at 0.75% V_f . 5D fibers at 0.5% V_f increased the toughness of SWC 17 times and by 30 times at V_f of 0.75%. In case of the 4D and 3D steel fibers at V_f of 0.5% the toughness of SWC increased 16 times and by 4 times in case of 0.5% V_f of STPL.

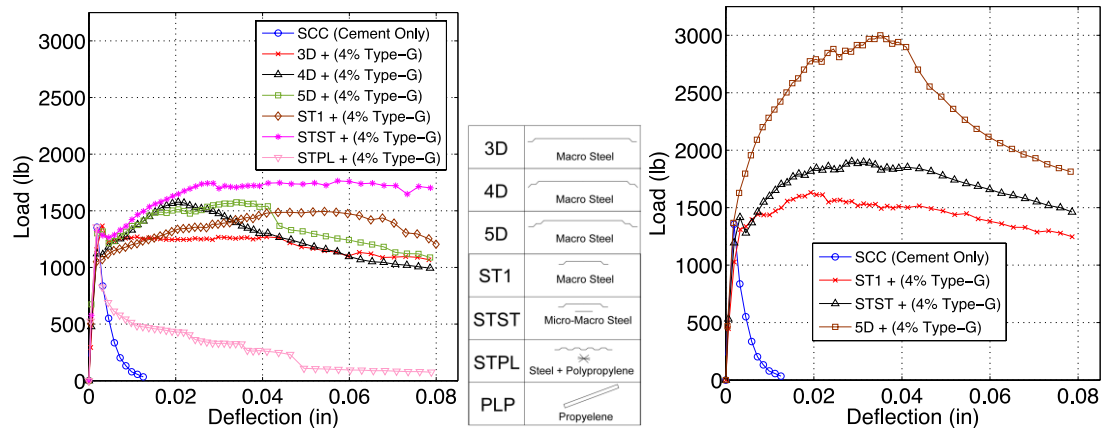


Figure 4-11: 56-day flexural strength and flexural toughness for FR-SWC (left $V_f=0.5\%$, right $V_f=0.75\%$)

4.3.2 Crack resistance

Figure 4-12 shows the load vs. crack mouth opening displacement (CMOD) of the notched beams made with different FR-SCCs loaded at mid span with a single point loading. In the case of 0.5% fiber volume of 30 mm steel fibers (ST1) with 4% Type-G EA, the residual stress at 0.14-in. crack width was 246 psi, which is 42% of the peak stress. On the other hand, the use of 8% Type-K EA increased the residual stresses at 0.14-inch crack width to 488 psi, which is 91% of the peak stress. The combination of 30 mm hooked end steel fibers and micro steel fibers (STS) resulted in residual stresses of 385 psi, which is 67% of the peak stress. In the case of the 40 mm propylene fibers (PLP)

with 4% G-type EA, the residual stress was 166 psi, which is 42% of the peak stress. In the case of hybrid of 50 mm crimped steel fibers and polypropylene fibers (STPL) with 4% G-type EA, the residual stress was 166 psi, which is 50% of the peak stresses.

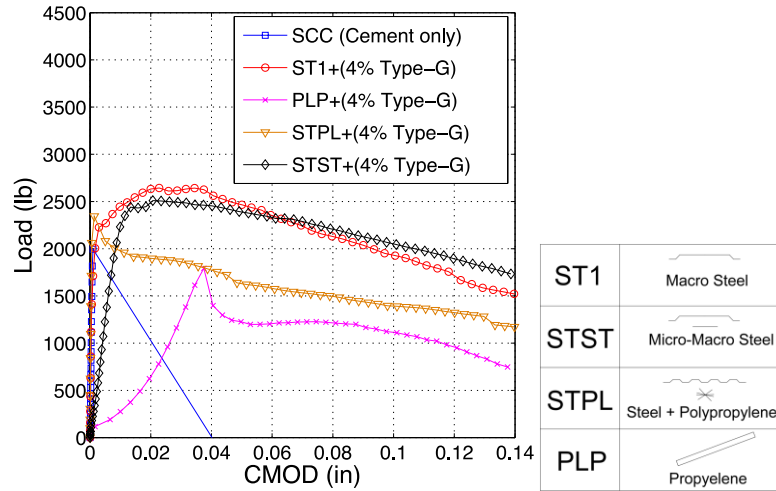


Figure 4-12: 56-day flexural crack resistance for different SCCs and FR-SCCs

Figure 4-13 shows the load Vs the crack mouth opening displacement (CMOD) curves of (6*6*22in.) notched beams (larger beams different from standard flexural beams were used for the RILEM T-162 test) FR-SWCs loaded at the mid span with a single point load. Fibers can change completely the flexural behavior of concrete, where FR-SCC can sustain cracking up to 0.14-inch crack width and more. In case of 0.5% fiber volume of 30 mm steel fibers (ST1) with 4% Type-G EA the residual stresses at 0.14-inch crack width were 545 psi which, is 92% of the peak stresses, while at 0.75% V_f the residual stresses were 54%. In case of 5D fibers at 0.5% V_f the residual stresses were 999 psi, which is 67% of the peak stresses and were 725 psi, which is 74%. In case of STPL fibers

at 0.5% the residual stresses were 72 psi, which is 14% of the peak stresses. In case of 4D fibers at 0.5% the residual stresses were 645 psi which is 72% of the peak stresses and the stresses were 699 psi, which is 80% of the peak stresses in case of 0.5% of 5D steel fibers.

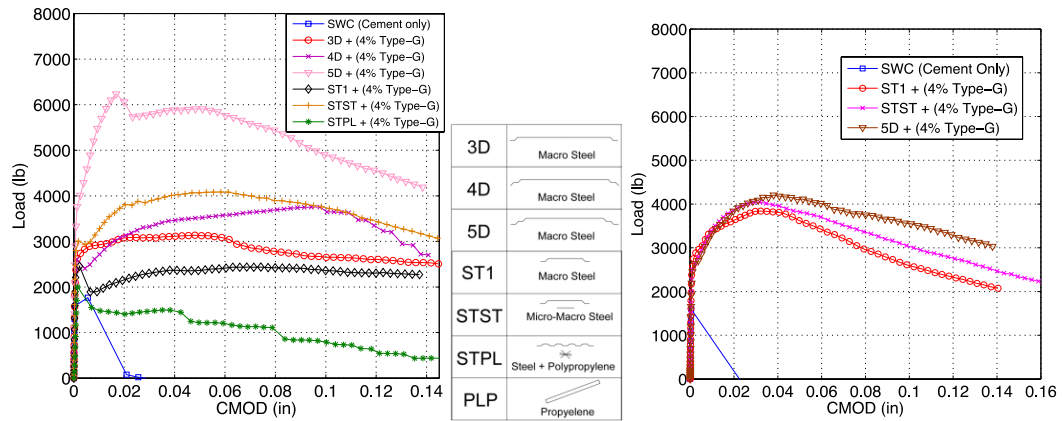


Figure 4-13: 56-day flexural crack resistance for SWC and FR-SWCs

4.3.3 Elastic modulus

Figure 4-14 shows the load vs. strain for a cylinder specimen of FR-SCC. The slope of each curve was calculated separately. Then the average of the three slopes was taken as the static modulus of elasticity.

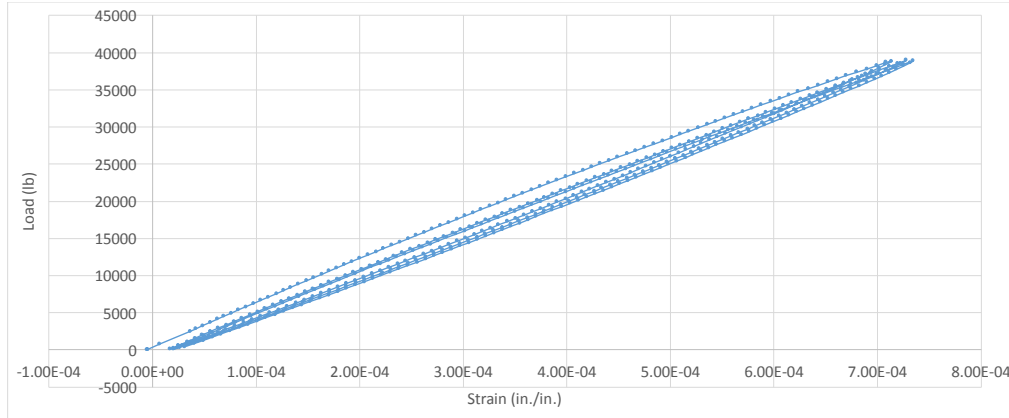


Figure 4-14: Load vs. strain for a cylinder specimen of FR-SCC

Figure 4-15 compares the static modulus of elasticity for SCC and FR-SCC mixtures. Fibers decreased the elastic modulus of FR-SCC. The decrease in case of syntactic fibers was higher than that with steel fibers, where PLP fibers decreased the 56-day elastic modulus by 23% and by 11% in case of steel fibers.

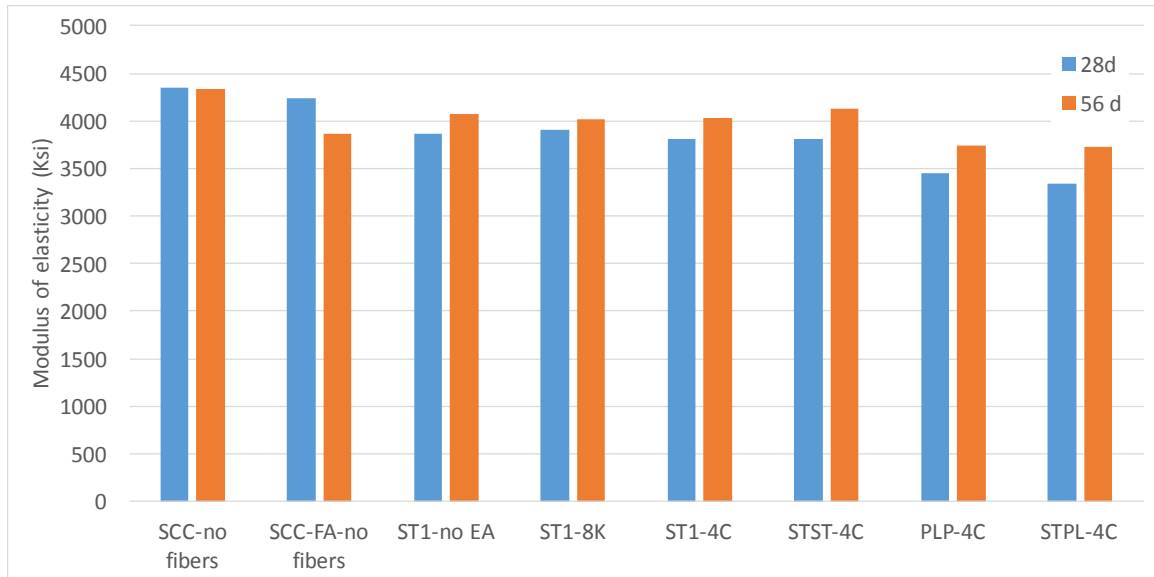


Figure 4-15: 28-day and 56-day elastic modulus for SCC and FR-SCCs

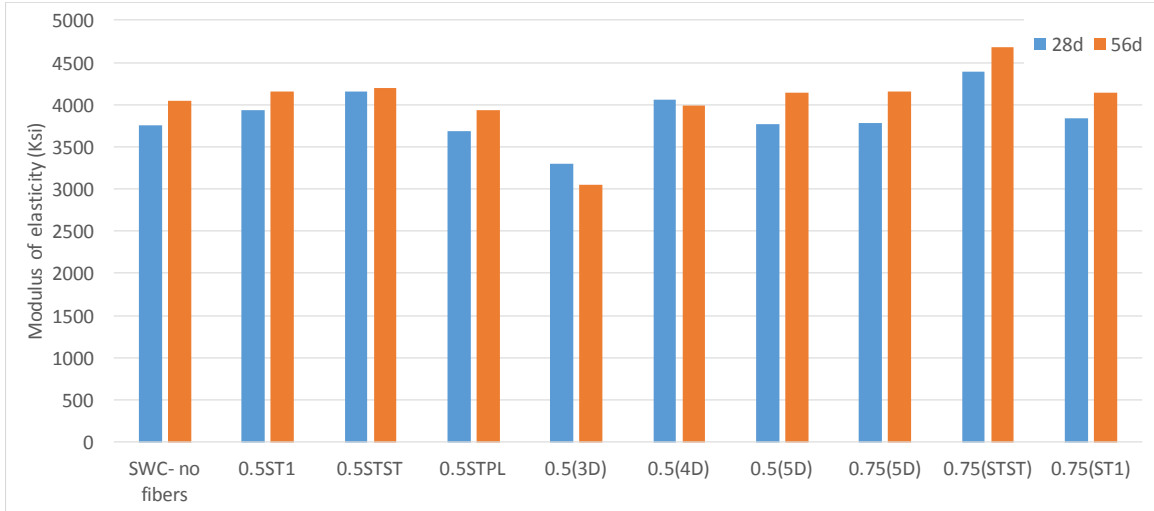


Figure 4-16: 28-day and 56-day elastic modulus for SWC and FR-SWCs

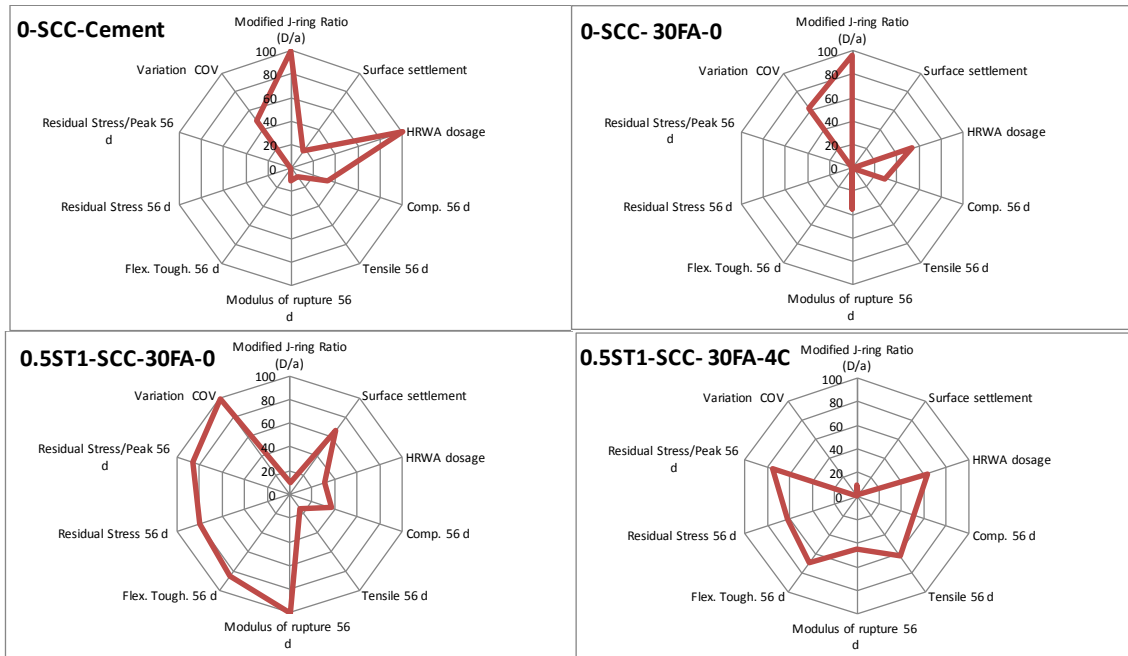
Figure 4-16 compares the static modulus of elasticity for SWC and FR-SWC mixtures. 3D, 4D and STPL fibers decreased the 56-day elastic modulus by 25%, 25% and 3%, respectively, while the rest of the fibers increased the 56-day elastic modulus, where STST fibers increased the elastic modulus by 4% and 16% at fiber volumes of 0.5% and 0.75%, respectively.

4.3.4 Overall performance

The overall performance was determined using the area of star diagram. The passing ability, stability and the HRWRA dosage to secure the required flowability were included in the performance evaluation of fresh properties. The mechanical properties of the optimized FR-SCC and FR-SWC mixtures included compressive strength, splitting tensile strength, flexural strength (ASTM C78), flexural toughness (ASTM C1609), crack resistance (RILEM TC-162) were included in the overall evaluation. The average

coefficient of variation (COV) for all the properties was taken as a factor in this evaluation.

Three FR-SCC mixtures were selected in addition to the references. These are the mixtures having 30% fly ash 4% G-Type expansive agents with three different types of fibers (ST1, STST and STPL) added at fiber volume of 0.5%. Four FR-SWC mixtures were selected besides the reference. These mixtures having 30% fly ash 4% Conex expansive agent with three different types of fibers; 0.5% and 0.75% 5D steel fiber, 0.5% ST1 steel fiber and 0.5% STST micro macro steel fibers. The selected FR-SCC mixtures and FR-SWC mixtures will be evaluated in next tasks, which include resistance to shrinkage cracking, frost durability, and structural performance.



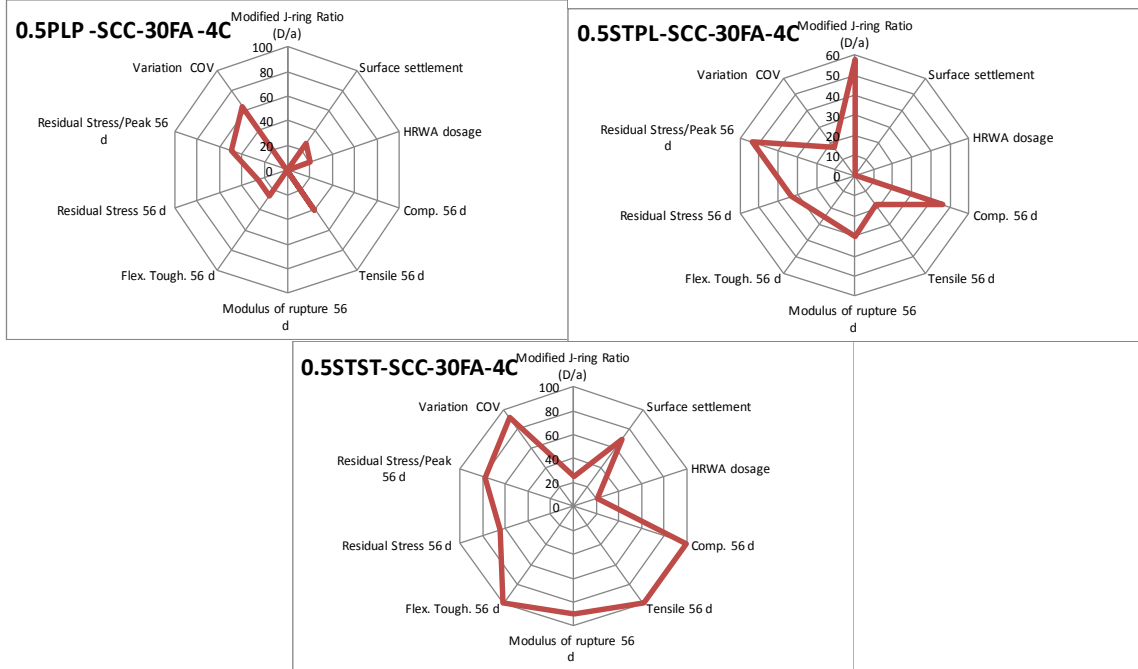


Figure 4-17: Star diagrams for all the SCC and FR-SCC mixtures

Figure 4-17 shows the star diagram for all the SCC and FR-SCC mixtures that showed acceptable workability. Figure 4-18 shows the comparison between areas inside the star diagram for all the SCC and FR-SCC mixtures. FR-SCC made with STST fibers showed the best overall performance.

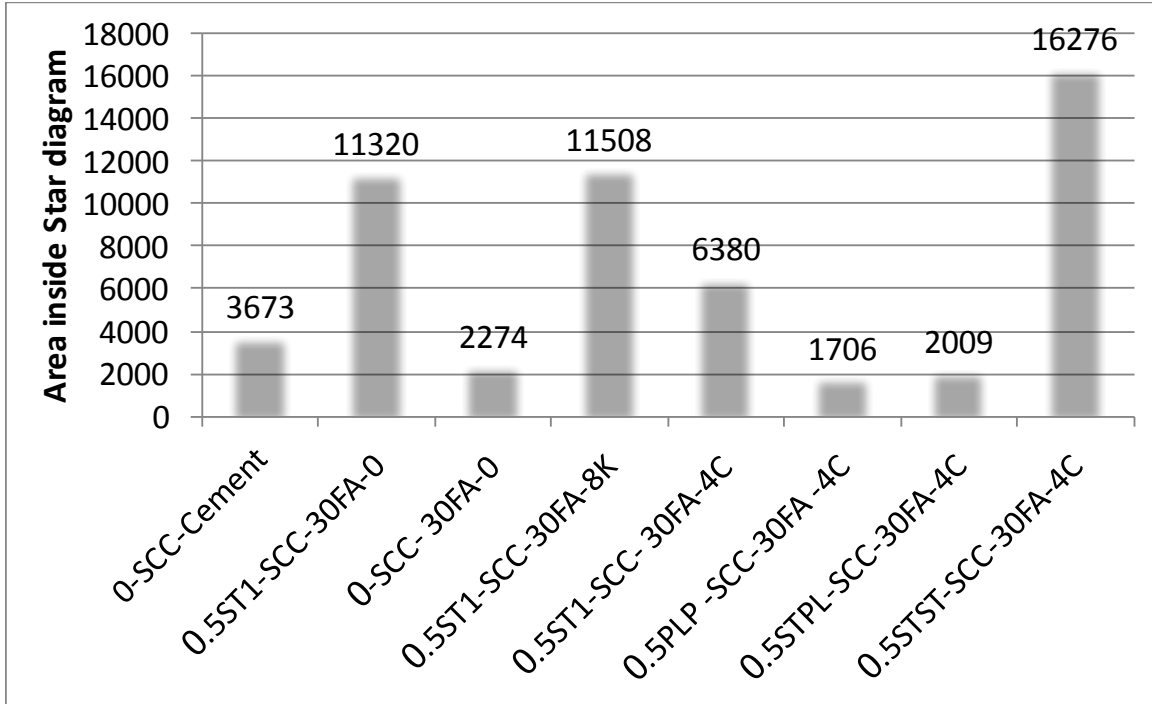


Figure 4-18: Area inside the star diagram for all the SCC and FR-SCC mixtures

Figure 4-19 shows the star diagram for all the SWC and FR-SWC mixtures that showed acceptable workability. Figure 4-20 shows the comparison between areas inside the star diagram for all the SWC and FR-SWC mixtures. FR-SWC made with 0.75% 5D fibers had the best overall performance, then 0.5% 5D, then 0.5% STST, then 0.75% ST1 and finally 0.5% STPL. The last five FR-SWC were selected as the best five FR-SWC mixtures.

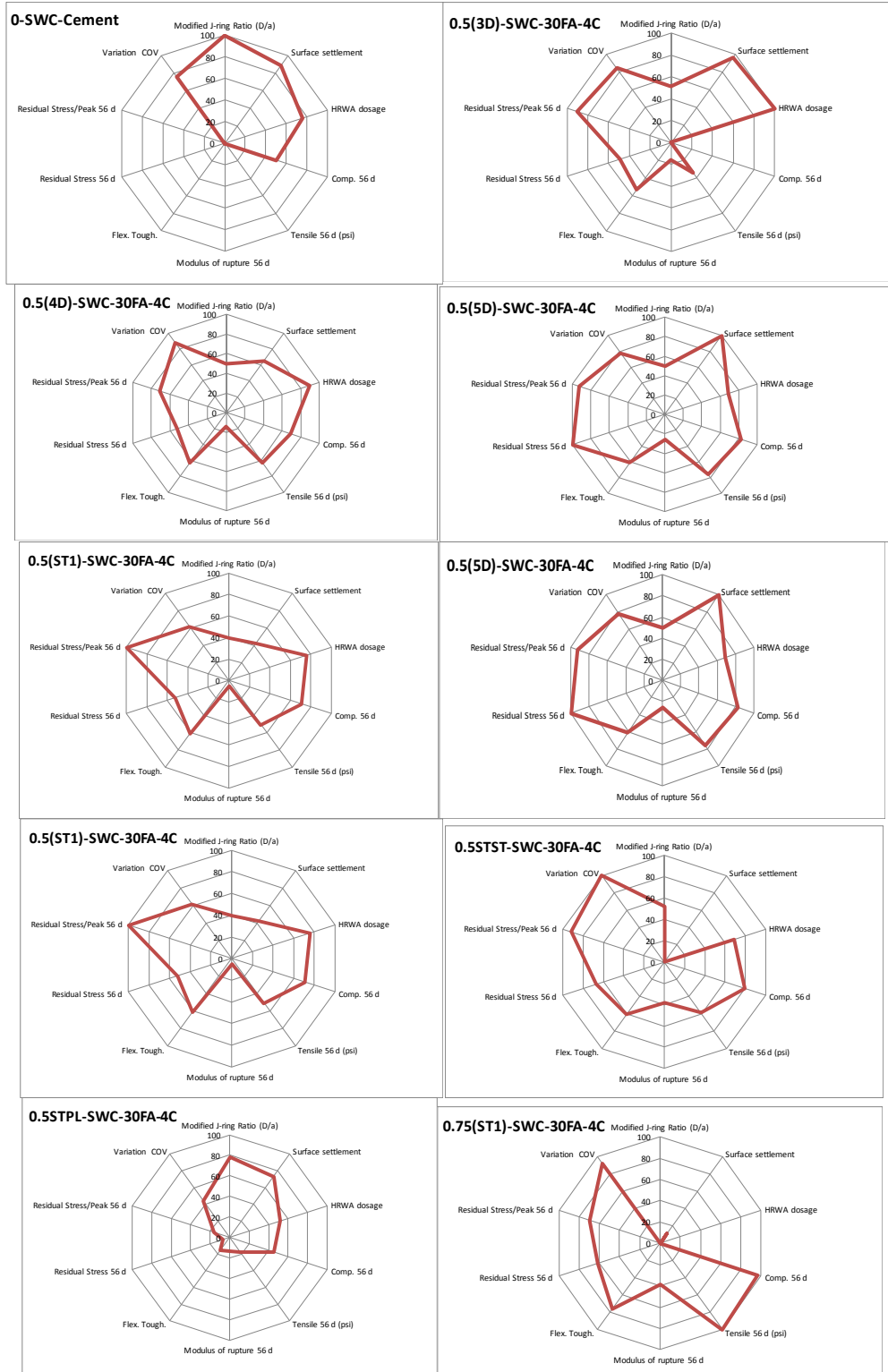


Figure 4-19: Star diagrams for SWC and FR-SWC mixtures

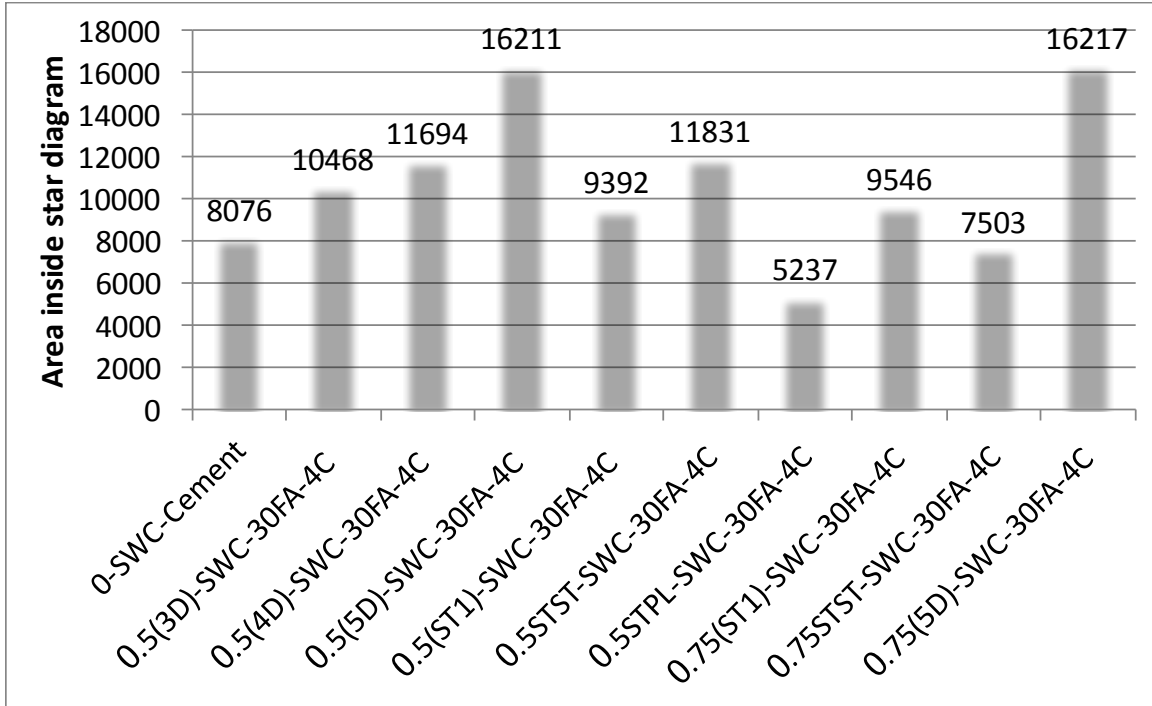


Figure 4-20: Area inside the star diagram for SWC and FR-SWC mixtures

4.4 Test results of Task 2D

The selected FR-SCC mixtures and FR-SWC mixtures from Task 2A and Task 2B were evaluated in this task which included measurement of drying shrinkage, resistance to shrinkage cracking, frost durability.

4.4.1 Shrinkage

Four FR-SCC mixtures and four FR-SWC mixtures beside SCC and SWC references were evaluated for drying shrinkage. Shrinkage measurements were recorded up to 365 days. Restrained shrinkage was evaluated in accordance to ASTM C1581. A ring-type test was performed. Twelve rings were cast using six different mixtures; one SWC, one SCC and four different FR-SCCs.

4.4.1.1 Drying shrinkage

The samples were cured for seven days then transferred and stored in a temperature and humidity controlled room of temperature 23 °C and relative humidity of 50% RH. Shrinkage was measured up to 365 days. Figure 4-21 shows the drying shrinkage for SCC, FR-SCC, SWC and FR-SWC. The 1-year shrinkage of SWC was 700 micro strain vs. 785 micro strain in case of SCC. Incorporation of ST1 steel fibers with EA to SCC decreased the 1-year shrinkage by 50%, while incorporation of ST1 steel fibers without EA to SCC decreased the 1-year shrinkage by 25%. The FR-SWC samples were tested only up to 120 days and the shrinkage will be monitored until 1 year as well. FR-SWC made with 0.5% ST1 and 4% EA reduced the 120-day shrinkage by 38% compared to STST fibers which reduced it by 22%. Increasing the fiber volume of 5D in FR-SWC

from 0.5% to 0.75% did not have a significant effect on 120-day shrinkage, where both of the mixtures had around 450 micro strain, which is 77% of the 120-day shrinkage of the reference SWC mixture.

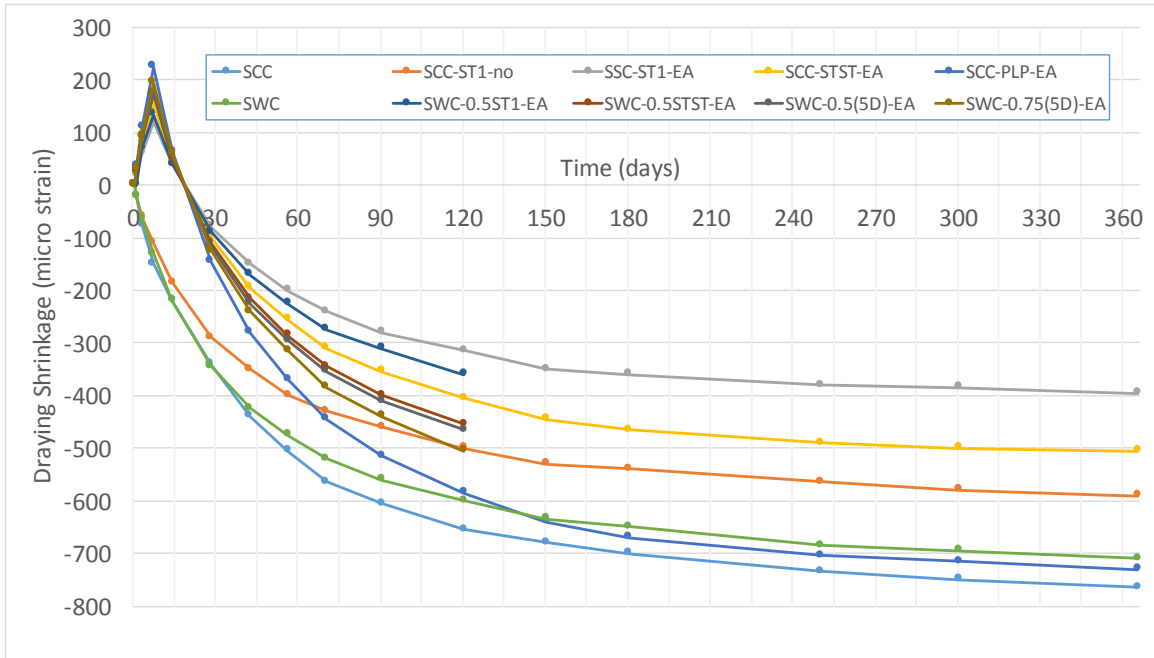


Figure 4-21: Drying shrinkage of FR-SCC and FR-SWC

4.4.1.2 Restrained shrinkage

Figure 4-22 shows the average strain in the inner steel rings for three different mixtures, SCC, FR-SCC made with 0.5% ST1 and 4% G-Type EA, and FR-SCC made with 0.5% ST1 without EA. Incorporation of 0.5% ST1 fibers to FR-SCC with 4% Type-G EA increased the restrained shrinkage resistance (FR-SCC rings cracked after 20 days) vs. FR-SCC made with 0.5% ST1 fibers without EA (FR-SCC ring cracked after 16 days).

Figure 4-22 shows the average strain in the inner steel rings for one plain SCC, and three different FR-SCC mixtures made with 4% Type-G EA. Incorporation of 0.5% STST

fibers to FR-SCC with 4% Type-G EA increased the restrained shrinkage resistance (FR-SCC rings cracked after 40 days) vs. SCC without fibers and EA (SCC rings cracked after 12 days). In case of PLP fibers rings cracked after 14 days.

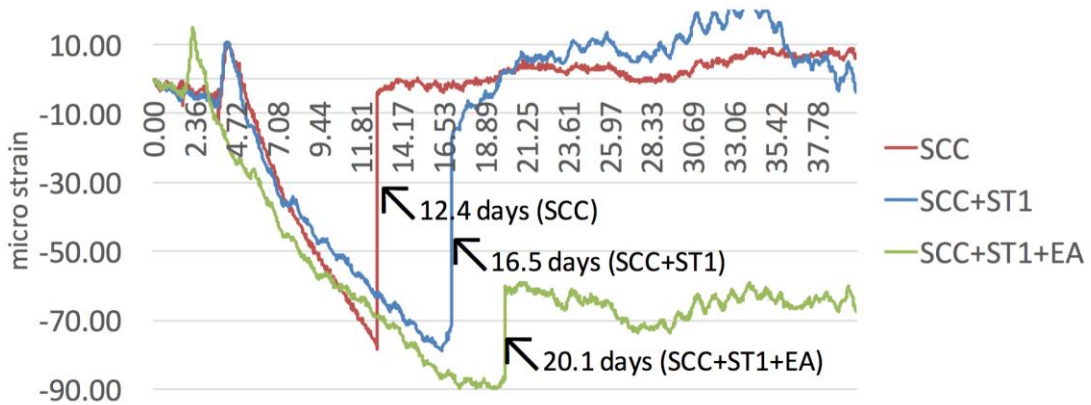


Figure 4-22: Strain in steel ring for SCC and FR-SCC with or without EA

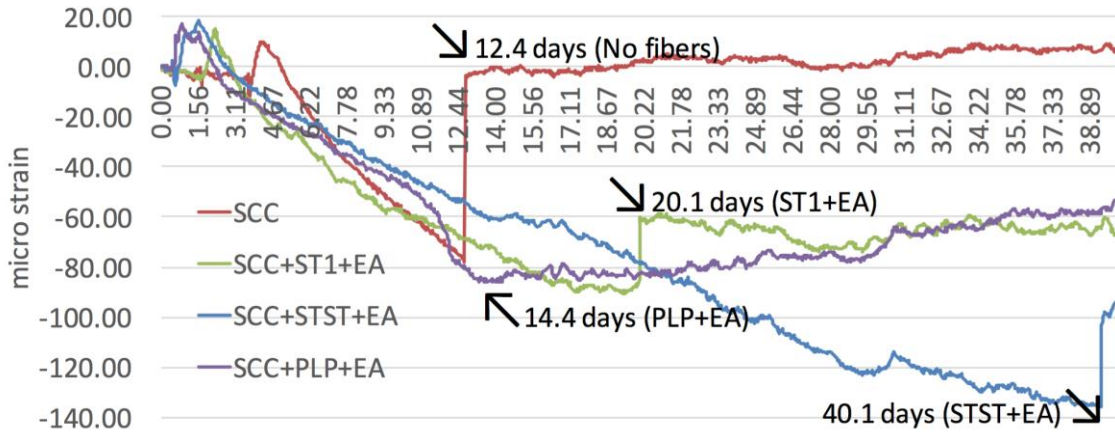


Figure 4-23: Strain in steel steel ring for SCC and FR-SCC with different types of fibers

4.4.2 Freeze/thaw Durability

The concrete prisms were cured first for 28 days before moving to the freeze-thaw chamber for testing. Specimens were subjected to 300 freeze-thaw cycles. After every 30 cycles, the mass loss and transverse frequency of concrete specimens were determined. The variation in durability factor of SCC mixtures up to 300 freeze-thaw cycles is shown in Figure 4-24. Mixture with durability factor greater than 80% after 300 freeze-thaw cycles (ASTM C 666, Proc. A) can be considered to exhibit adequate frost durability. The ultrasonic pulse velocity test was used to calculate the dynamic modulus of elasticity of the specimens. All FR-SCC and FR-SWC mixtures had a durability factor above 80% after 300 freeze-thaw cycles except for FR-SCC made with PLP fibers and FR-SWC made with 5D fibers, which fail after 90 cycles. Further investigation regarding air void system for these two mixtures will be done.

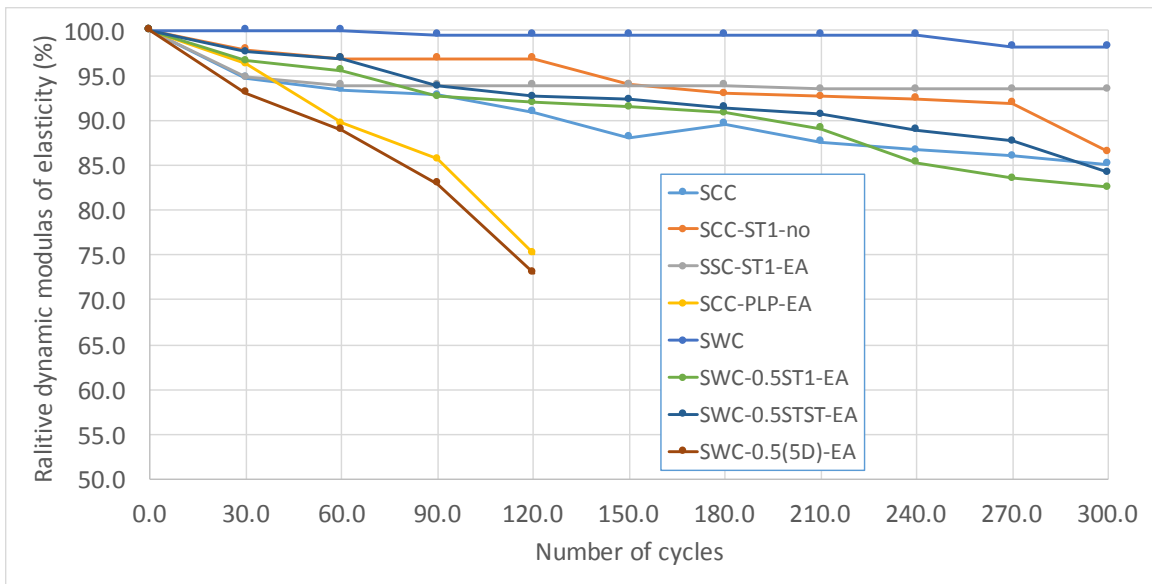


Figure 4-24: Relative dynamic modulus of elasticity for SCC, SWC, FR-SCC and FR-SWC

5 Structural Performance

This part of the study was aiming to evaluate the influence of different types of fibers on the flexural response and to develop FR-SCC mixtures targeted for the use in repair applications and FR-SWC for construction application. The optimized FR-SCC mixtures were used in the repair of full-scale reinforced concrete beams, while the optimized FR-SWC and FR-SCC mixtures were used in casting monolithic full-scale reinforced concrete beams. The validation of structural performance was carried out on the full-scale beam elements using four-point bending test. These beams include monolithic beams and repaired beams, those cast in two layers to simulate repaired structural elements. The mixtures used for casting the monolithic beam elements covered various types of concretes, including CVC, FR-CVC, SCC, FR-SCC, SWC, FR-SWC, while the concrete used for casting the repaired part was either SCC or FR-SCC. The parameters taken into account in this part of the study were:

- Concrete types: SCC, FR-SCC, SWC, FR-SWC vs. CVC, FR-CVC;
- Fiber type: one synthetic, one hybrid, and three steel fiber types;
- Fiber volume: 0, 0.5%, 0.75%, for FR-SWC mixtures, and 0 and 0.5% for FR-SCC and FR-CVC;
- Expansive agent: 0%, 4% G-Type
- Slump flow consistency (FR-SCC, FR-SWC and FR-CVC);

In total, 20 monolithic and 10 repaired beams measuring $12 \times 8 \times 96$ in. (b×h×L) were prepared. Two full-scale beams were cast from each mixture, 10 mixtures for monolithic beams and 5 mixtures for repaired beams. The main measurements that were carried out

on the investigated beams were ultimate load, toughness, concrete and reinforcement strains. The properties to be predicted were crack load, ultimate load, crack width, and deflection.

5.1 Beam design

Typical monolithic and repaired beams measuring 8 in. in width, 12 in. in height, and 96 in. in length were prepared to assess their structural performance using four-point bending test. The beams were designed to have a flexural failure not a shear failure. The beams were designed as an under reinforced section to undergo yielding in steel rebar before compression failure take place in the compression block part.

All of the prepared beams had a typical configuration of reinforcement, as shown in Figure 5-1. The beams were reinforced with three longitudinal #4 bars for tension, two longitudinal #3 bars for compression, and steel stirrups of #3 spaced 5 in. The side and vertical clear covers were kept constant at 1 in. for all the beams.

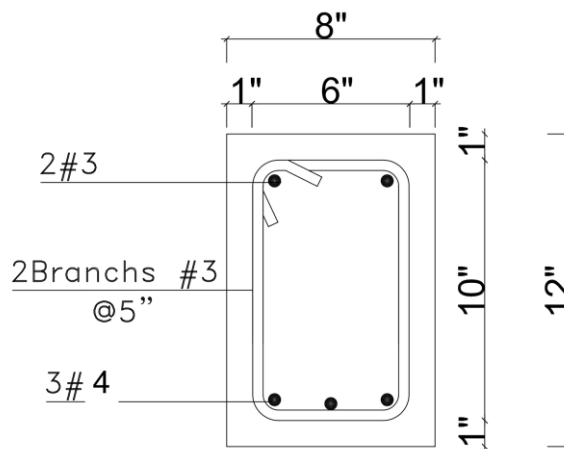


Figure 5-1: Typical configuration of reinforcement

Thickness of the repair layer

Thickness of the repair should cover three requirements:

- Ease of concrete placement
- Ensure sufficient bond with rebar
- Limit the thickness of repair section for economical considerations

Generally, the codes regulate the removal of concrete behind the steel bars to a minimum distance of 1 in. In this study, the minimum repair thickness (T_h), including the 1 in. of removed section, is expressed as follows:

$$T_h (\text{in.}) \geq [e + \Phi_1 + \Phi_2 + 1] = 2.9 \text{ in.}$$

where:

e : steel cover to the exterior face of the transversal stirrups ($e = 1 \text{ in.}$);

Φ_1 : diameter of the longitudinal steel bars, #4 ($\Phi_1 = 0.5 \text{ in.}$);

Φ_2 : diameter of the transversal steel stirrups, #3 ($\Phi_2 = 0.4 \text{ in.}$).

A repair thickness of 4 in., which is equivalent to one third of total height of beam, was decided.

5.2 Preparation of beams and instrumentation

Figure 5-2 shows procedure of tying rebar cages, where all of the stirrups were bent first then all of the longitudinal rebar and finally the cage was built by attaching the steel rebar and the stirrups using tying wires.

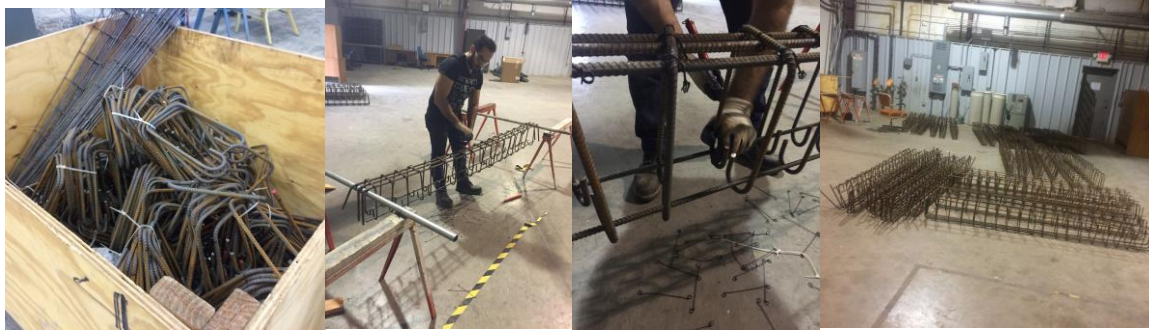


Figure 5-2: Tying rebar cages

After the assembling of the reinforcement cage, three strain gauges were glued to the middle of the three longitudinal #4 bars (mid-span of the beams) as shown in (Figure 5-3) using Catalyst-C, M-Bond 200 adhesive, and M- Coat B of Vishay Micro-Measurements. Two Concrete surface attached strain gages were glued to the mid-span top surface of each beam as shown in Figure 5-4. One LVDT was attached to the mid span of the beam as shown in Figure 5-5 to monitor deflection of the beam at the mid-span.



Figure 5-3: Attaching of the strain gages to steel rebar



Figure 5-4: Concrete surface attached strain gages

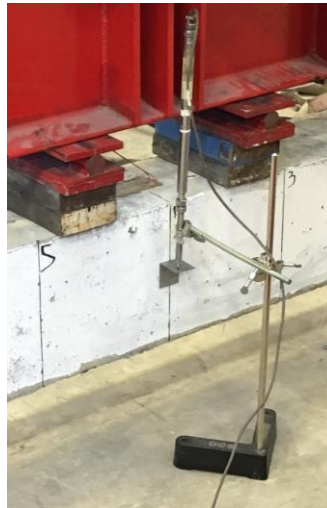


Figure 5-5: LVDT to monitor deflection of the beam

5.3 Casting, sampling and curing of monolithic beams

For CVC and FR-CVC mixtures, monolithic beams were cast in two layers and were internally vibrated using a 1-in. diameter vibrator. On the other side, for SCC and FR-SCC monolithic beams, the casting operation was done without mechanical consolidation

at a constant casting rate from the one end to flow along the length of the beam until the other end.

In the case of the FR-SWC mixtures, approximately one third of the mechanical consolidation energy applied on the CVC and FR-CVC mixtures was applied for each layer of casting. The barrel was lowered near the formwork to minimize the height of casting and thus to reduce segregation and loss of entrained-air bubbles. For the air volume, and slump flow tests, concrete was poured in one layer and consolidated by 10 internal strikes using a 16 mm steel rod. Three samples were taken from each mixture to estimate the compressive strength after 42 days.

The sampled cylinders were kept in their molds and covered with plastic sheets and then, stored in the laboratory conditions (normal temperature and humidity) during 24 hours after casting according to ASTM C 192. After de-molding at 24 hours, these samples underwent the same laboratory conditions as their beams until the age of testing. The beams and the samples were cured using a wet burlaps and plastic sheets (as shown in Figure5-6) that was water sprayed every 24 hours up to 42 days.



Figure 5-6: Curing of the beams and cylinder specimens using wet burlaps

5.4 Casting, sampling and curing of repaired beams

The repaired beams were designed so that the load points and the supports do not fall through the holes used for casting and air evacuation (Figure 5-7). Four holes were placed vertically at equidistance of 2.4 ft between the longitudinal #3 bars and the stirrups (Figure 5-8). One external hole was used for the repair casting and the other three holes for air evacuation during the casting. Flexible and low-stiff PVC holes measuring 4 in. in diameter and 8 in. in length, made basically as cylinder molds were used as holes for repair casting and air evacuation during the casting. These cylinder molds were placed into the reinforcement cage, which were inverted into the formwork (Figure 5-8).

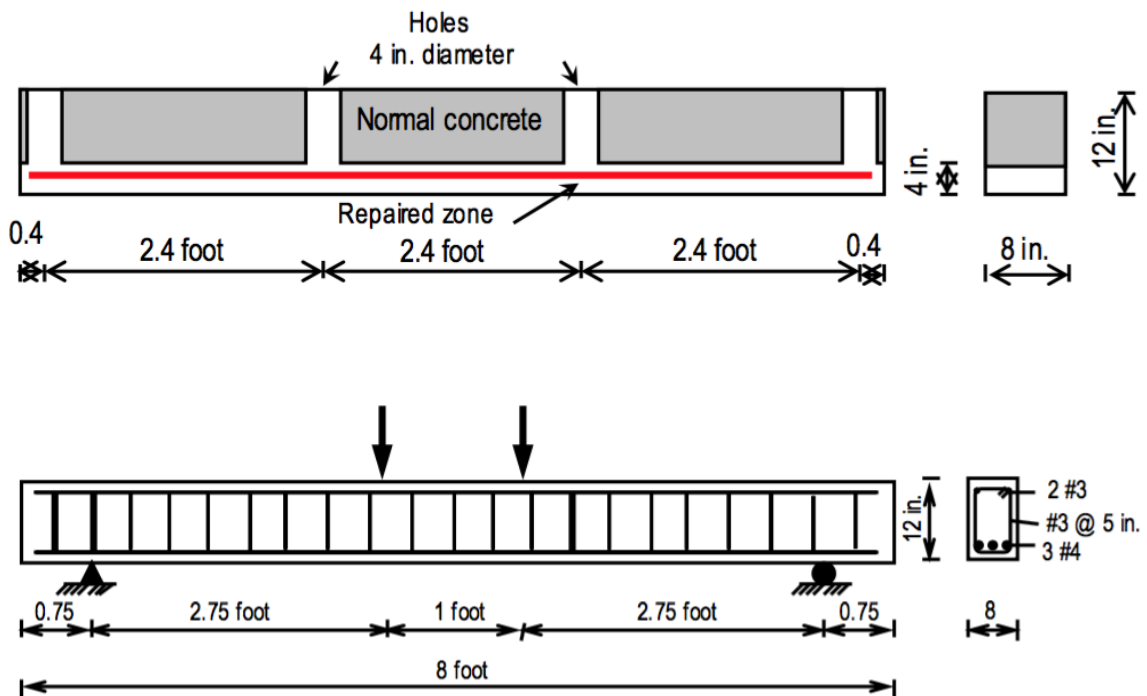


Figure 5-7: Casting points vs. supporting and loading points for repaired beams



Figure 5-8: PVC holes

5.4.1 Casting of substrate

The repaired beams were cast in one layer into the inverted position with CVC as substrate material, except for the bottom section of 4 in. to be repaired. This thickness represented the repaired area in the tension zone along the total length of the beam. The substrate was then compacted (Figure 5-9) and surfaced to have a height of 8 in.



Figure 5-9: Substrate casting (of the 2/3 upper beam height) in inverted position

5.4.2 Preparation of the intermediate surface, de-molding and curing of substrate

To ensure adequate bond and interlocking between the existing and new concrete and to simulate the surface preparation of the old concrete, the surface of the latter was simply sprayed with surface set retardant liquid (commercially known as Rugasol-S) as soon as the CVC substrate was cast as shown in Figure 5-10. Then the substrate and corresponding sampled specimens underwent the same curing conditions as in the case of monolithic beams. After the removal of lateral sides of the formwork at 24 hours, the concrete surface (representing interface between the existing and new concretes) was cleaned by removing the retarded surface mortar using a water flush to roughen the surface by exposing coarse aggregate and thus enhance bond to the repair concrete.

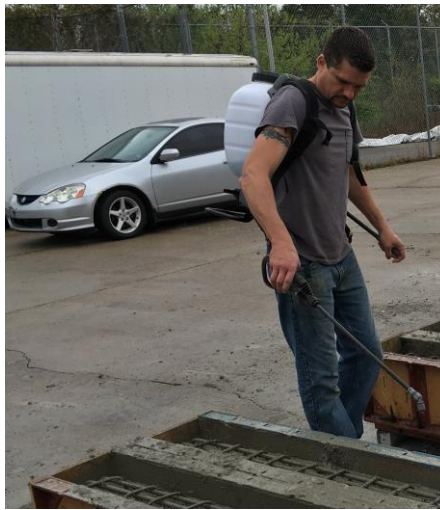


Figure 5-10: Spraying the substrate with set retardant

5.4.3 Casting of the repair

Figure 5-11 shows the steps followed to cast the repair part. The repair section was cast with the optimized repair mixtures using a half cubic yard hopper continuously through a funnel from one end allowing the concrete to go out from the next three holes.



Figure 5-11: Repairing of CVC Beams using FR-SCC

5.5 Testing of the beams

A loading system with hydraulic jacks and a load cell of 500 kip (maximum capacity) closed- loop MTS actuator was used to test beams under four-point bending, as shown in Figure 5-12 and 5-13. The actuator was supported by a steel frame and the load was transferred from the actuator to the tested beam through a steel spreader I-beam applied on the full width of the beam. The beam supported at two points 9 in. from the both ends and loaded in the middle using two point loads separated by 12 in. as shown in Figure 5-14.



Figure 5-12: Testing of monolithic beams



Figure 5-13: Testing of Repaired beams

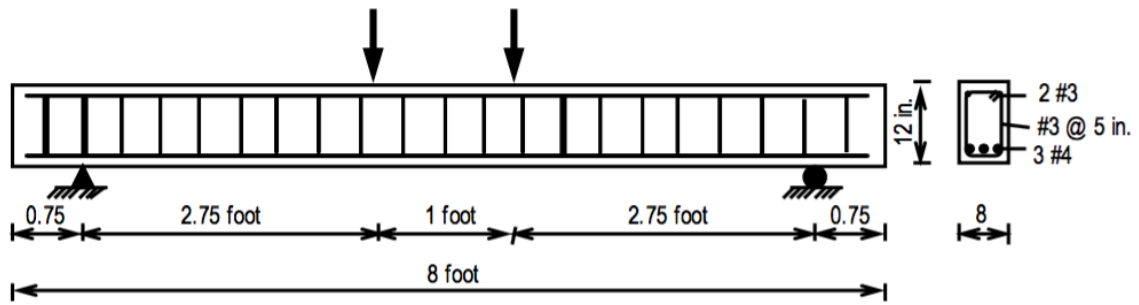


Figure 5-14: Loading points and supporting points

An automatic data acquisition system wired to a computer was used to read and record electronically the loads as a function of different strains (deflection, strains of compressive concrete and tension steel reinforcement). The beams were monolithically loaded at a controlled displacement of 0.5 in./min up to the failure. The applied load was measured by the internal load cell on the actuator and the beams were instrumented with linear variable displacement transducers (LVDT) and strain gauges for steel reinforcement and concrete as mentioned before.

5.6 Experimental program

5.6.1 Task 3A: Monolithic beam flexural tests for SCC, FR-SCC, SWC and FR-SWC

This sub-task evaluated the flexural behavior of beam elements in order to compare those of FR-CVC to fibrous mixtures of greater fluidity that necessitated low vibration energy (FR-SWC) or no mechanical consolidation (FR-SCC). 20 monolithic full scale beams were cast using conventional vibrated concrete (CVC), fiber reinforced conventional

vibrated concrete (FR-CVC), SCC, FR-SCC, SWC and FR-SWC. The beams were tested using four-point flexural load frame. The beams were loaded up to 3 in. deflection or a drop in the peak load by 20%. Strain in steel rebar vs. strain in concrete surface was measured using strain gauges, also the actuator load was monitored vs. deflection for the tested beams. Table 5-1 shows the different CVC, FR-CVC, SCC, FR-SCC, SWC, and FR-SWC that were used to cast monolithic beams.

Table 5-1: Mixture matrix for testing monolithic beams

SWC and FR-SWC					CVC and FR-CVC				
	Mix	Fly Ash (%)	EA Dosage (%)	Fiber Volume (%)		Mix	Fly Ash (%)	EA Dosage (%)	Fiber Vol. (%)
1	SWC	30%	4% Conex	0	9	CVC	30%	4% Conex	0
2	5D-SWC			0.5%	10	ST1-CVC			0.5%
3	5D-SWC			0.75%					
4	ST1-SWC			0.5%					
5	STST-SWC			0.5%					
SCC and FR-SCC									
6	SCC	30%	4% Conex	0					
7	ST1-SCC			0.5%					
8	STST-SCC			0.5%					

Task 3B: Repaired beam flexural tests for SCC and FR-SCC

This sub-task evaluated the flexural behavior of CVC beam elements repaired with either SCC or FR-SCC. Ten Beams were cast using CVC to the two thirds and then the bottom third of each was cast using different FR-SCCs. The beams were tested using four-point flexural load frame. The beams were loaded up to 3 in. deflection, a drop in the peak load by 20% or significant delamination of the repair material, if any. Strain in steel rebar vs. strain in concrete surface was measured using strain gauges, also the actuator load was

monitored vs. deflection for the tested beams. Table 5-2 shows the different SCC, and FR-SCC that were used to cast the repair part.

Table 5-2: Mixture matrix for testing repaired beams

SCC & FR-SCC						
	Mixture	Fly Ash (%)	EA Dosage (%)	Fiber Volume (%)	Casting Technique	Thickness of repair zone
1	SCC	0%	0	0	Beam	4 in.
2	ST1-SCC	30%	4% Conex	0.5	Beam	
3	ST1-SCC		0%		Beam	
4	STST-SCC		4% Conex		Beam	
5	STPL-SCC		4% Conex		Beam	

5.7 Results and discussion

5.7.1 Task 3A: Monolithic beams

Figure 5-15 shows load deflection curve of SCC vs. FR-SCC made with two different types of fibers; 30 mm hooked end steel fibers (ST1) and macro-micro steel fibers (STST) incorporated at 0.5% fiber volume. Incorporation of ST1 fibers increased the peak load by 14% and toughness by 90%, while in case of STST fibers the peak load was increased by 6% and toughness by 110%.

Figure 5-16 shows load deflection curve of SWC vs. FR-SWC made with three different types of fibers; 30 mm hooked end steel fibers (ST1) and macro-micro steel fibers (STST), 65 mm hooked end steel fibers (5D). Both ST1 and STST fibers were incorporated at 0.5% fiber volume, while (5D) fiber was incorporated at 0.5% and 0.75%

fiber volumes. Incorporation of 0.5% ST1 fibers increased the peak load by 14% and toughness by 55%, while in case of 0.5% STST fibers the peak load was increased by 19% and toughness by 95%. Incorporation of 5D fibers at a fiber volume of 0.5% had better effect on enhancing the flexural performance of FR-SWC compared to 0.75% fiber volume, where in case of 0.5% fiber volume the toughness increased by 50% vs. 86% in case of 0.75% fiber volume and the peak load increased by 18% in case of 0.5% fiber volume vs. 10% fiber volume in case of 0.75% fiber volume.

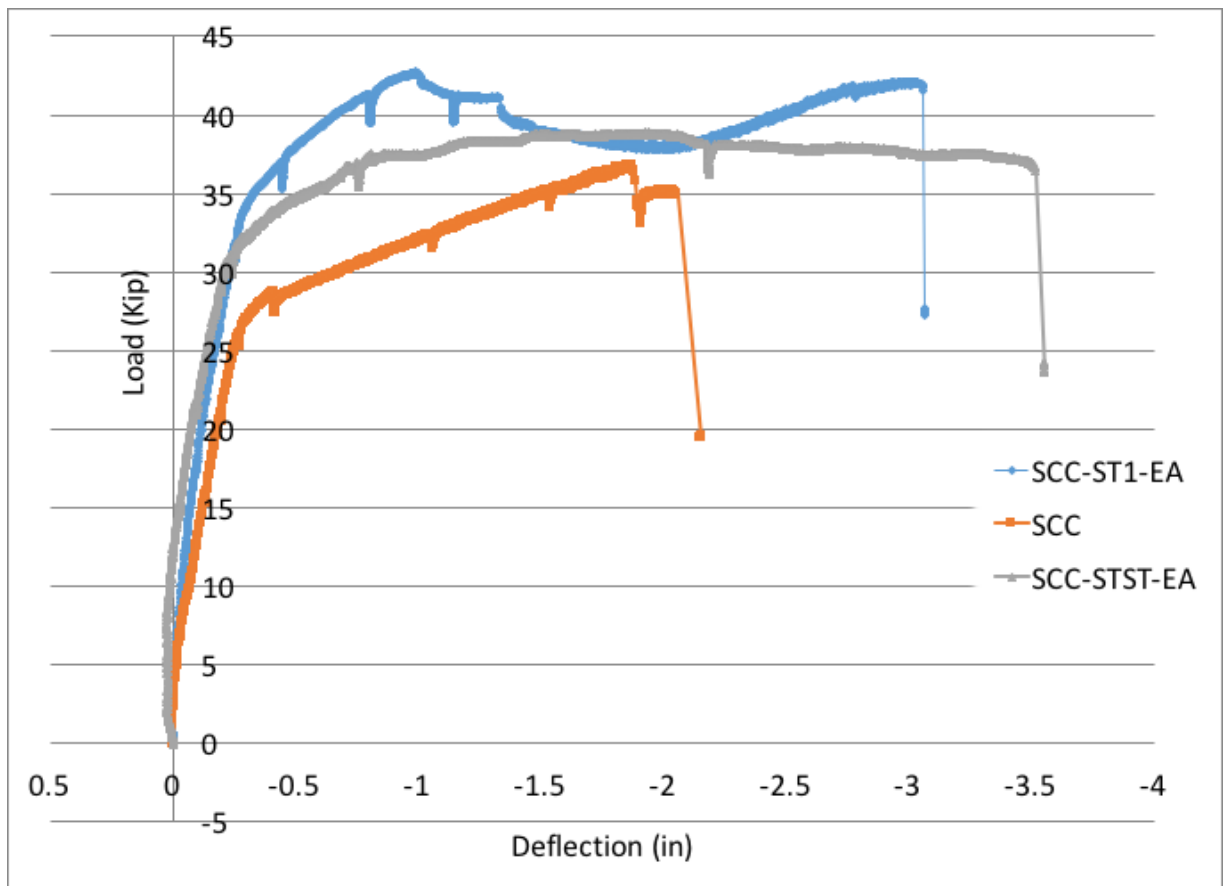


Figure 5-15: Effect of different fibers on SCC monolithic beams

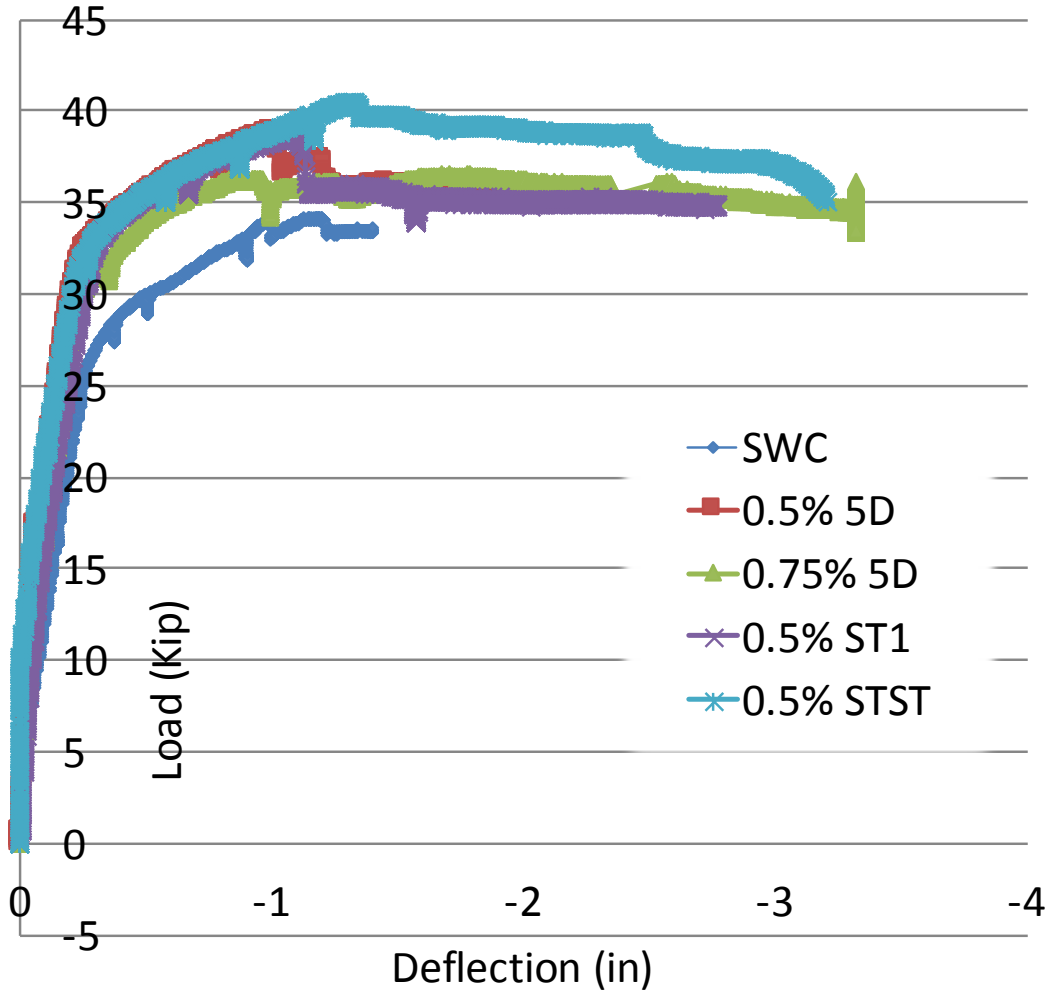


Figure 5-16: Effect of different fibers on SWC monolithic beams

Figure 5-17 shows load deflection curve for three different fiber-reinforced concrete, FR-CVC, FR-SCC, and FR-SWC. Three types of concretes made with 0.5% ST1 steel fibers and 4% G-Type EA. Incorporation of ST1 steel fibers to FR-CVC increased the toughness by 140% and the peak load by 9%, while incorporation of ST1 steel fibers to FR-SCCC increased the peak load by 14% and toughness by 90%, and incorporation of ST1 steel fibers to FR-SWC increased the peak load by 14% and toughness by 55%.

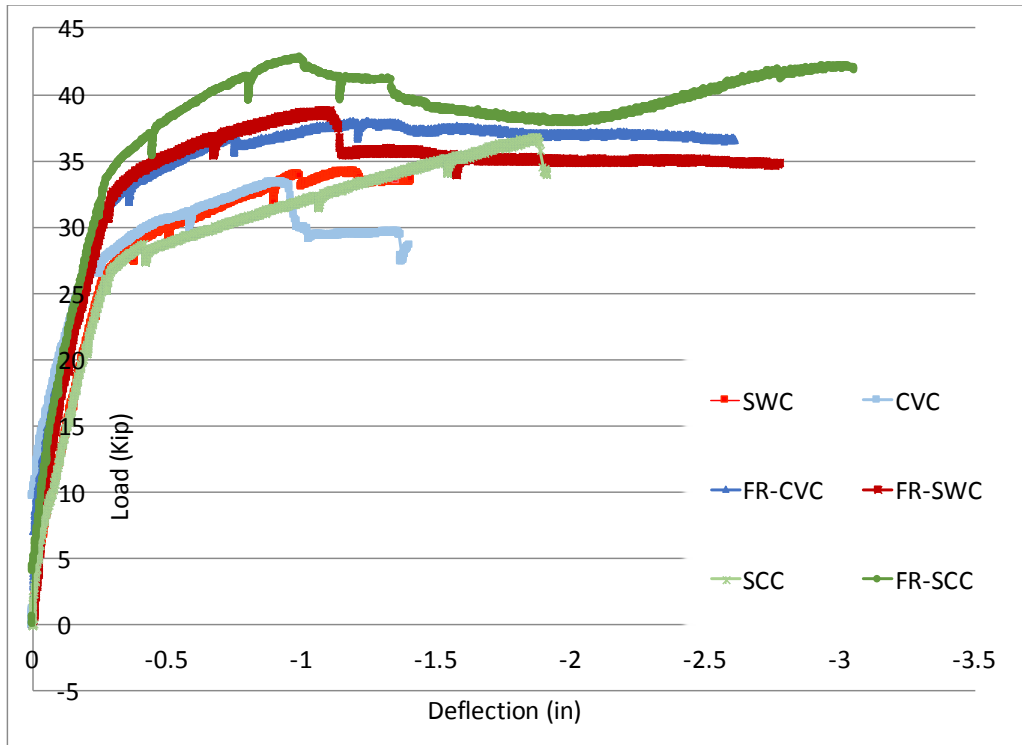


Figure 5-17: Effect of adding fibers to CVC, SWC and SCC monolithic beams

Fibers acted as an additional reinforcement for concrete to the rebar, where the fibers delayed yielding of steel rebars compared to case of concrete made without fibers. Figure 5-18 shows strain in steel rebar vs. strain in concrete for a monolithic beam made with SCC with no fibers compared to those strains in case of a monolithic FR-SCC beam made with 0.5% ST1 steel fibers. Steel fibers had a higher contribution in delaying steel rebar yielding compared to Syntactic fibers.

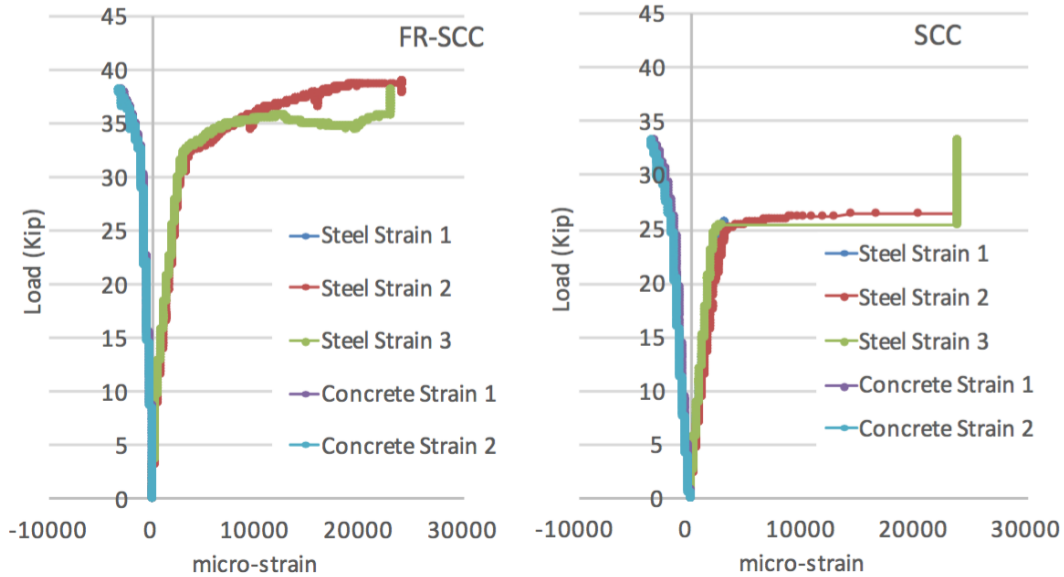


Figure 5-18: Strain in steel rebar vs. strain in concrete for SCC and FR-SCC

5.7.2 Task 3A: Monolithic beams

The investigated fiber-reinforced self-consolidating mixtures were found to be suitable for repair applications. FR-SCC were able to flow horizontally under their own weight along the length of 96 in. beams and achieve good compaction in the absence of vibration without exhibiting defects due to segregation and blockage. Figure 5-19 shows a Repaired beam loaded in flexural up to failure, where only flexural cracks can be observed propagating through the FR-SCC repair and continuing straight to the CVC substrate without any de-molding or pre-mature failure of the repair layer.



Figure 5-19: Repaired beam after loading up to failure

Figure 5-20 shows load deflection curve for three different beams, monolithic CVC beam, monolithic FR-SCC, and a CVC beam repaired using FR-SCC. The same FR-SCC was used for the monolithic beams and in the repair of the repaired beam. The FR-SCC was made using ST1 steel fibers at a fiber volume of 0.5% and with 4% G-Type EA. The repaired beam had an intermediate performance between monolithic CVC beam and FR-SCC monolithic beams, where FR-SCC monolithic beam peak load was 42.5 Kips vs. 36 Kips in case of the repaired beam and in case of the monolithic CVC beam the peak load was 34 Kips.

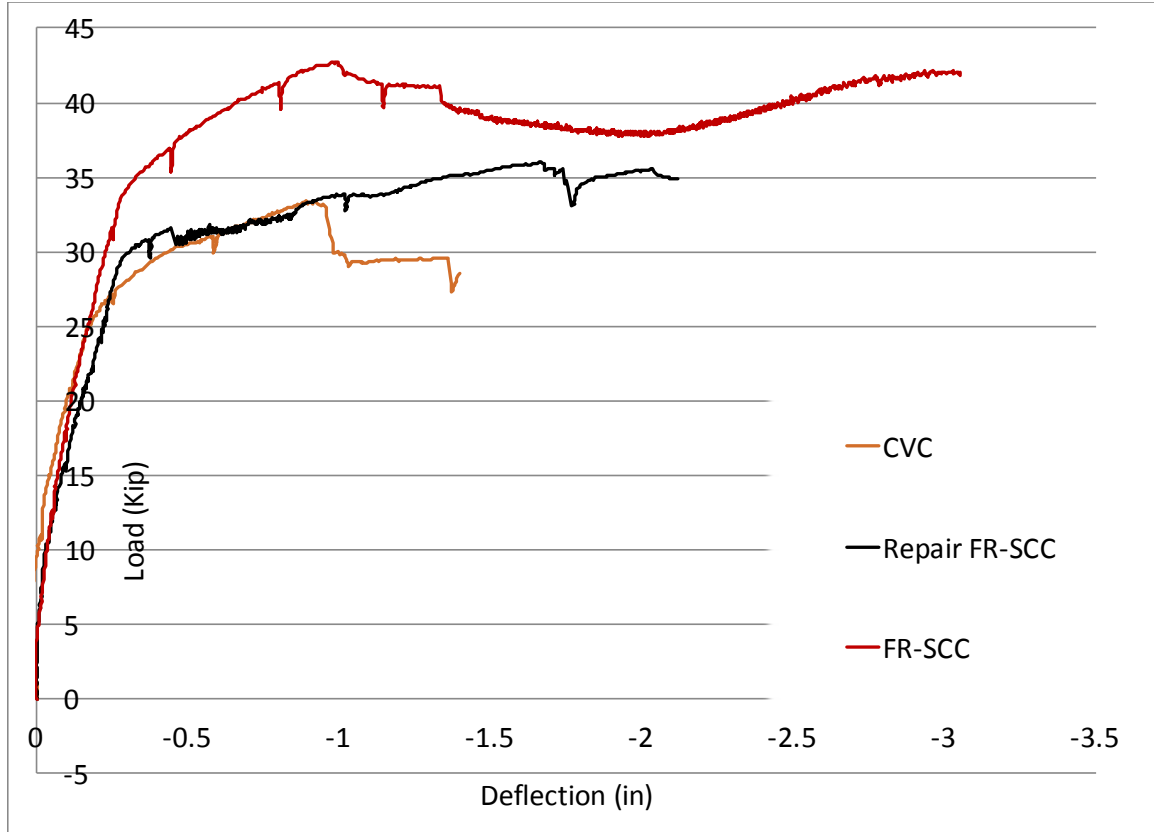


Figure 5-20: Monolithic CVC, monolithic FR-SCC and repaired beam using FR

Figure 5-21 shows load deflection curve for CVC monolithic beam vs. several CVC beams repaired using different FR-SCC mixtures. Repair of conventional vibrated concrete (CVC) beams using FR-SCC increased the flexural capacity of the beam by 6% and the toughness by 110% in case of using 0.5% ST1 fibers with 4% Type-G EA, while repair of the beams using FR-SCC made with 0.5% ST1 fibers without EA restored 90% of the original CVC beam capacity and increased toughness by 22%. Repair of CVC beams using plain SCC restored 88% of the original CVC beam capacity and increased toughness by 21%. In case of FR-SCC made with 0.5% STST fibers the restored strength

was 97%, while the toughness increased by 110% vs. 94% restored peak load and 80% increase in toughness in case of the repair material was FR-SCC made with 0.5% STPL fibers.

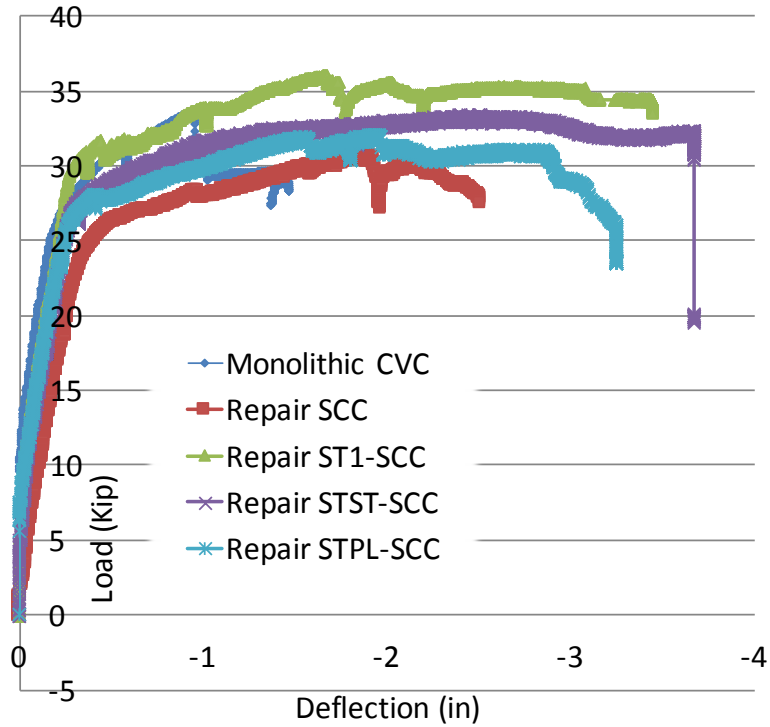


Figure 5-21: Monolithic CVC beam vs. repaired CVC beam using SCC and different FR-SCCs

6 Conclusions

Based on the results presented in this report, the following conclusions can be warranted:

1. Macro fibers can be used with FR-SCC designated for repair with fiber length \leq 50 mm at 0.5% fiber volume
2. Incorporation of fibers with 4% Type-G EA in FR-SCC can increase 56-day flexural strength by up to 32%, flexural toughness by up to 23 times, and 42% crack resistance at 0.14 in. crack width vs. vs. SCC without fibers and EA
3. Incorporation of fibers without EA in FR-SCC can increase 56-day flexural strength by up to 45%, flexural toughness by up to 24 times, and 70% crack resistance vs. SCC without fibers and EA
4. Fibers decreased the elastic modulus of FR-SCC. The decrease in case of syntactic fibers was higher than that with steel fibers, where PLP fibers decreased the 56-day elastic modulus by 23%, while the decrease was by 11% in case of steel fibers.
5. Macro fibers can be used with FR-SWC designated for construction with fiber length \leq 65 mm at 0.75% fiber volume
6. Incorporation of fibers with 4% Type-G EA in FR-SWC can increase 56-day flexural strength by up to 114%, flexural toughness by up to 30 times, and 75% crack resistance at 0.14 in. crack width vs. SWC without fibers and EA
7. FR-SWC made with 0.75% fiber volume has higher overall performance compared to those made with 0.5% fiber volume in case of 5D and ST1 steel fibers

8. FR-SWC made with 3D, 4D and STPL fibers decreased the 56-day elastic modulus by 25%, 25% and 3%, respectively, while ST1, STST and 5D increased the 56-day elastic modulus, where STST fibers increased the elastic modulus by 4% and 16% at fiber volumes of 0.5% and 0.75%, respectively
9. FR-SWC made with 0.5% fiber volume has higher overall performance compared to those made with 0.75% fiber volume in case of STST steel fibers (combination between micro and macro steel fibers)
10. The 1-year shrinkage of SWC was 700 micro strain vs. 785 micro strain in case of SCC. Incorporation of ST1 steel fibers with EA to SCC decreased the 1-year shrinkage by 50%, while incorporation of ST1 steel fibers without EA to SCC decreased the 1-year shrinkage by 25%
11. FR-SWC made with 0.5% ST1 and 4% EA reduced the 120-day shrinkage by 38% compared to STST fibers which reduced it by 22%. Increasing the fiber volume of 5D in FR-SWC from 0.5% to 0.75% did not have a significant effect on 120-day shrinkage, where both of the mixtures had around 450 micro strain, which is 77% of the 120-day shrinkage of the reference SWC mixture
12. Incorporation of 0.5% ST1 fibers to FR-SCC with 4% Type-G EA increased the restrained shrinkage resistance (FR-SCC rings cracked after 20 days) vs. FR-SCC made with 0.5% ST1 fibers without EA (FR-SCC ring cracked after 16 days)
13. Incorporation of 0.5% STST fibers to FR-SCC with 4% Type-G EA increased the restrained shrinkage resistance (FR-SCC rings cracked after 40 days) vs. SCC without fibers and EA (SCC rings cracked after 12 days)

14. All FR-SCC and FR-SWC mixtures had a durability factor above 80% after 300 freeze-thaw cycles except for FR-SCC made with PLP fibers and FR-SWC made with 5D fibers, which fail after 90 cycles. Further investigation regarding air void system for these two mixtures will be done
15. Incorporation of fibers with 4% Type-G EA to SCC increased toughness of full scale concrete reinforced beams by 90% and 110% in case of ST1 fibers and STST fibers, respectively
16. Incorporation of ST1, STST, and 5D fibers with 4% Type-G EA in FR-SWC full scale beams increased flexural strength by 14%, 18% and 19%, respectively
17. Incorporation of fibers with 4% Type-G EA to FR-SCC full scale beams increased toughness by 95% in case of STST fibers
18. In case of FR-SWC full scale beams 0.5% fiber volume for 5D macro steel fibers was better than 0.75% in terms of toughness and peak load
19. Fibers acted as an additional reinforcement for concrete to the rebar, where the fibers delayed yielding of steel rebars compared to case of concrete made without fibers
20. Repair of conventional vibrated concrete (CVC) beams using FR-SCC increased the flexural capacity of the beam by 6% and the toughness by 110% in case of using 0.5% ST1 fibers with 4% Type-G EA, while repair of the beams using FR-SCC made with 0.5% ST1 fibers without EA restored 90% of the original CVC beam capacity and increased toughness by 22%

21. Repair of CVC beams using plain SCC restored 88% of the original CVC beam capacity and increased toughness by 21%
22. In case of FR-SCC made with 0.5% STST fibers the restored strength was 97%, while the toughness increased by 110% vs. 94% restored peak load and 80% increase in toughness in case of the repair material was FR-SCC made with 0.5% STPL fibers.

Future work

Test results presented and discussed in this investigation confirm the effectiveness of fibers on the ductility, crack resistance, tensile strength, and shrinkage on concrete. The study confirms the overall enhancement in flexural performance of full scale concrete beams when it is made with FR-SCC or FR-SWC. Further research is still required to quantify the amount of reduction in steel reinforcement when using FR-SCC or FR-SWC. In addition, field-oriented study to implement and validate the performance of such concrete for the use construction and repair of bridge elements is required.

As a follow-up project, the research team will investigate and validate the performance of FR-SCC as a repairing material for a deteriorated structural element as bridge girder, bridge beam, bridge column, bridge pier cap, or reinforced concrete wall then the mechanical properties, crack resistance and structural performance obtained from the concrete prepared in the field will be compared to those obtained in this study. FR-SWC is proposed to be used as a construction material for a structural element as a bridge girder, bridge beam, bridge column, bridge pier cap or reinforced concrete wall then the

mechanical properties, crack resistance and structural performance obtained from the concrete prepared in the field will be compared to those obtained from this study.

The performance improvement of such advanced materials will be compared with performance of MoDOT typical concrete mixtures designated for bridge Substructures.

References

- [1] Liberato Ferrara, Fiber Reinforced Self-Compacting Concrete (FR-SCC), RILEM TC-228 MPS Chapter 6, 2013.
- [2] JASS 5, Japanese Architectural Standard: Specification for reinforced concrete work (in Japanese), Tokyo, 1986.
- [3] Nan Su, Kung-Chung Hsu, His-Wen Chai, A simple mix design method for self-compacting concrete, *Cement and Concrete Research* 31 (2001) 1799–1807.
- [4] P.L. Domone, Self-compacting concrete: An analysis of 11 years of case studies, *Cement & Concrete Composites* 28 (2006) 197–208.
- [5] J.E. Funk, D.R. Dinger, *Predictive Control of Crowded Particulate Suspension Applied to Ceramic Manufacturing*, Kluwer Academic Press, 1994.
- [6] H.J.H. Brouwers, H.J. Radix, Self-compacting concrete: theoretical and experimental study, *Cement and Concrete Research* 35 (2005) 2116–2136.
- [7] Fuller, W.B., Thompson, S.E., The Law of Proportioning Concrete, *Journal of Transportation Division, American Society of Civil Engineering*, 59 (1907).
- [8] Liberato Ferrara, Yon-Dong Park, Surendra P. Shah, A method for mix-design of fiber-reinforced self-compacting concrete, *Cement and Concrete Research* 37 (2007) 957–971.
- [9] Viktória Sugár, Márton Takács, Standardized investigation methods of self compacting concrete and effect of sand content on properties in fresh state, *Materials Science Forum* Vol. 729 (2013) pp 278-283.

- [10] Pereira, E. N. B., Steel fibre reinforced self-compacting concrete: From material to mechanical behaviour, Pedagogical and Scientific Aptitude Proofs dissertation, Dept. Civil Engineering, Univ. of Minho (2006).
- [11] Okamura H, Ozawa K. Mix design for self-compacting concrete, *Concr Lib JSCE* 25 (1995) 107–20.
- [12] A.K.H. Kwan, P.L. Ng, K.Y. Huen, Effects of fines content on packing density of fine aggregate in concrete, *Construction and Building Materials* 61 (2014) 270–277.
- [13] Wanchai Yodsudjai, Kejin Wang, Chemical shrinkage behavior of pastes made with different types of cements, *Construction and Building Materials* 40 (2013) 854–862.
- [14] ASTM C 1608. Standard test method for chemical shrinkage of hydraulic cement paste. American society for testing and materials. West Conshohocken (PA): ASTM International; 2007.
- [15] ASTM C 150/C 150M. Standard specification for Portland cement. American society for testing and materials. West Conshohocken (PA): ASTM International; 2012.
- [16] ASTM C 595/C 595M. Standard specification for blended hydraulic cements. American society for testing and materials. West Conshohocken (PA): ASTM International; 2012.
- [17] Hassan El-Chabib and Adnan Syed, Properties of Self-Consolidating Concrete Made with High Volumes of Supplementary Cementitious Materials. American society for testing and materials. *J. Mater. Civ. Eng.* 2013.25:1579-1586.
- [18] J.M. Khatib, Performance of self-compacting concrete containing fly ash. *Construction and Building Materials* 22 (2008) 1963–1971.

- [19] He, X. and Yang, Q.: “Research on impact properties of flexible fiber reinforced self-compacting concrete in middle-low intensity”, in C. Shi et al., eds, Proceedings 2nd International Symposium on the Design Performance and Use of SCC, SCC2009, Beijing, 5-7 June 2009, RILEM Pubs., pp. 577-585.
- [20] Mazaheripour, H., Ghanbarpour, S., Mirmoradi, S.H., and Hosseinpour, I., “The effect of polypropylene fibers on the properties of fresh and hardened lightweight self-compacting concrete”, *Construction and Building Materials*, 25, 2011, pp. 351-358.
- [21] Thomas Voigt, Van K. Bui, and Surendra P. Shah, Drying Shrinkage of Concrete Reinforced with Fibers and Welded-Wire Fabric. *ACI Materials Journal*, Title no. 101-M26 (2004) 233–241.
- [22] ASTM C 29/C 29M, “Test Method for Unit Weight and Voids in Aggregate,” ASTM International, West Conshohocken, Pa., 1991, 4 pp.
- [23] Kamal H. Khayat, Fodhil Kassimi, and Parviz Ghoddousi “Mixture Design and Testing of Fiber-Reinforced Self-Consolidating Concrete” *ACI Materials Journal*, Title No. 111-M13 (2014) 143-151.
- [24] A.W. Saak, H.M. Jennings, S.P. Shah, New methodology for designing self-compacting concrete, *ACI Materials Journal* 98 (6) (2001) 429–439.
- [25] K. H. Khayat, Workability, Testing, and Performance of Self-Consolidating Concrete, *ACI Materials Journal* Title no. 96-M43 (1999) 346–353.
- [26] K. H. Khayat and Y. Roussel, Testing and performance of fiber-reinforced, self-consolidating concrete, *Materials and Structures*, Vol. 33, July 2000, pp 391-397.

- [27] ASTM C1621/C1621M-09b, “Standard Test Method for Passing Ability of Self-Consolidating Concrete by J-Ring,” ASTM International, West Conshohocken, PA, 2012, 5 pp.
- [28] PCI, “Interim Guidelines for the Use of Self-Consolidating Concrete in Precast/Prestressed Concrete Institute Member Plants,” TR-6-03, Precast/Prestressed Concrete Institute, Chicago, IL, 2003, 150 pp.
- [29] Liberato Ferrara and Alberto Meda” Relationships between fibre distribution, workability and the mechanical properties of SFRC applied to precast roof elements, *Materials and Structures* (2006) 39:411–420.
- [30] Ozyurt, N., Woo, L.Y., Mason, T.O. and Shah, S.P. “Monitoring fiber dispersion in fiber reinforced cementitious materials: comparison of AC Impedance Spectroscopy and Image Analysis”, *ACI Materials Journal* 103, 2006, pp. 340-347.
- [31] J.F. Lataste, M. Behloul, D. Breyse “Characterisation of fibers distribution in a steel fiber reinforced concrete with electrical resistivity measurements” *NDT & E International*, Volume 41(8), 2008, pp. 638-647
- [32] Liberato Ferrara “Fiber Reinforced Self-Compacting Concrete (FR-SCC)”, RILEM TC-228 MPS Chapter 6.
- [33] Van Damme, S.; Franchois, A.; De Zutter, D.; Taerwe, L.; “Nondestructive determination of the steel fiber content in concrete slabs with an open-ended coaxial probe”; *IEEE Transactions on Geoscience and Remote Sensing*, 42, 2004, pp. 2511 – 2521

- [34] Faifer, M., Ottoboni, R., Toscani, S., Ferrara, L.: "Non-destructive Testing of Steel Fiber Reinforced Concrete using a Magnetic Approach," IEEE Transactions on Instrumentation and Measurement, 60 (5), 2011, pp. 1709-1717.
- [35] Felicetti, R., Ferrara L.: "The effect of steel fiber on concrete conductivity and its connection to on-site material assessment", Proceedings of Befib 2008, 7th International RILEM Symposium on Fiber Reinforced Concrete, R. Gettu ed., Chennai, India, 17-19 September 2008, RILEM Pubs. pp. 525-536.
- [36] Stahli, P., Custer, R. and van Mier, J.G.M.: "On flow properties, fiber distribution, fiber orientation and flexural behaviour of FRC", Materials and Structures, 41, 2008, pp. 189-196.
- [37] Laetitia Martinie, Pierre Rossi, Nicolas Roussel "Rheology of fiber reinforced cementitious materials: classification and prediction", Materials and Structures, Cement and Concrete Research 40 (2010) 226–234.
- [38] Alireza Khaloo, Elias Molaei Raisi, Payam Hosseini and Hamidreza Tahsiri, Mechanical performance of self-compacting concrete reinforced with steel fibers. Construction and Building Materials 51 (2014) 179–186.
- [39] ASTM C1399/C1399M-10, "Test Method for Obtaining Average Residual-Strength of Fiber-Reinforced Concrete," ASTM International, West Conshohocken, PA, 2012, 5 pp.
- [40] ACI 209R-92 (2012) *Prediction of Creep, Shrinkage, and Temperature Effects in Concrete Structures*, ACI Committee 209, American Concrete Institute, Farmington Hills, Michigan, 47 p.

- [41] GOEL, R., KUMAR, R., PARKASH, S., PAUL, D.K. (Mar., 2006) *Prediction of Creep and Shrinkage Strains in Prestressed Concrete Bridges*, Advances in Bridge Engineering, p. 543- 554.
- [42] FANOURLAKIS, G.C., and BALLIM, Y. (2003) Predicting Creep Deformation of Concrete: a Comparison of Results from Different Investigations, Proceedings, 11th FIG Symposium on Deformation Measurements, Santorini, Greece, 8 p.
- [43] SCHINDLER, A., K., BARNES, R., W., ROBERTS, J., B., RODRIGUEZ, S. (Jan-Feb., 2007) Properties of Self-Consolidating Concrete for Prestressed Members, ACI Material Journal, vol. 104, n° 1, p. 53-61.
- [44] Fodhil Kassimi and Kamal H. Khayat, Drying Shrinkage Models for Fiber-Reinforced SCC, 6th International RILEM Symposium on Self-Compacting Concrete and 4th North American Conference on the Design and Use of SCC, Montreal, September 26-29, 2010.
- [45] AASHTO (2004) AASHTO LRFD Bridge Design Specifications, SI Units, 3rd edition, Interim Revisions, American Association of State Highway and Transportation Officials.
- [46] CEB-FIP MC 1990 (1993), Design code, Comité Euro-International du Béton, Fédération Internationale de la Précontrainte, Edit. TELFORD, T., 1st Edition, London, 437 p.
- [47] GARDNER, N. J. (2000) Design Provisions for Shrinkage and Creep of Concrete, The Adam Neville Symposium: Creep and Shrinkage – Structural Design Effects, SP-194, American Concrete Institute, Farmington Hills, Mich., p. 101-134.

[48] BAŽANT, Z.P. (May 1st, 2000) Criteria for Rational Prediction of Creep and Shrinkage of Concrete, ACI special publication, vol. 194, p. 215-236.

SAKATA, K., (Sep. 6-9, 1993) Prediction of Concrete Creep and Shrinkage, Creep and [49] Shrinkage of Concrete, Proceedings of the 5th International RILEM Symposium, Barcelona, Spain, p. 649- 654.

[50] KHAYAT, K.H., LONG, W. J. (May-Jun., 2010) Shrinkage of Precast, Prestressed Self- Consolidating Concrete, ACI Materials Journal, vol. 107, n° 3, p. 231-238.

[51] Fodhil Kassimi and Kamal H. Khayat, Effect of fiber and admixture types on restrained shrinkage cracking of self-consolidating concrete, ACMB SCC2013: Fifth North American Conference on the Design and Use of Self-Consolidating Concrete, May 12–15, 2013, Chicago, USA.

[52] A.E. Richardson, K.A. Coventry, S. Wilkinson, Freeze/thaw durability of concrete with synthetic fibre additions, Cold Regions Science and Technology 83–84 (2012) 49–56.

[53] ASTM C 666, 1997. Standard Test Method for Resistance of Concrete to Rapid Freezing and Thawing. ASTM International, West Conshohocken, PA, USA.

[54] Salih Taner Yildirim and Cevdet Emin Ekinici (2012). Effects on Freeze-Thaw Durability of Fibers in Concrete, Polypropylene, Dr. Fatih Dogan (Ed.), InTech, Available from:

<http://www.intechopen.com/books/polypropylene/effects-on-freeze-thaw-durability-of-fibers-in-concrete>

- [55] Youcef Fritih, Thierry Vidal, Anacllet Turatsinze, and Gérard Pons, Flexural and Shear Behavior of Steel Fiber Reinforced SCC Beams, *KSCE Journal of Civil Engineering* (2013) 17(6): 1383-1393.
- [56] Qiaoyan Guan, Peng Zhang and Xiaopeng Xie, Flexural Behavior of Steel Fiber Reinforced High-Strength Concrete Beams, *Research Journal of Applied Sciences, Engineering and Technology* 6(1): 1-6, 2013
- [57] G. Pons, M. Mouret, M. Alcantara, J. L. Granju, Mechanical behaviour of self-compacting concrete with hybrid fibre reinforcement, *Materials and Structures* (2007) 40:201–210
- [58] RILEM TC 162-TDF (2001) Test and design methods for steel fibre reinforced concrete-uni-axial tension test for steel fibre reinforced concrete. *Mater Struct* 34(1):3–6.
- [59] Fodhil Kassimi, Ahmed K. El-Sayed, and Kamal H. Khayat, Performance of Fiber-Reinforced Self-Consolidating Concrete for Repair of Reinforced Concrete Beams, *ACI Structural Journal* (2014), Title No. 111-S108, pp 1277-1286.
- [60] ACI Committee 318, “Building Code Requirements for Structural Concrete (ACI 318-05) and Commentary,” American Concrete Institute, Farmington Hills, MI, 2005, 430 pp.
- [61] ACI Committee 544, “Design Considerations for Steel Fiber Reinforced Concrete,” *ACI Structural Journal*, V. 85, No. 5, Sept.-Oct. 1988, pp. 563-580.